Multi-Omics Analysis of a Rat Model of Aerobic Exercise Capacity and Metabolic Fitness

by

Yangsu Ren

A dissertation submitted in partial fulfillment
of the requirements for the degree of
Doctor of Philosophy
(Human Genetics)
in The University of Michigan
2016

Doctoral Committee:

Associate Professor Jun Li, Chair
Professor Steven L. Britton
Professor David T. Burke
Assistant Professor Jeffery M. Kidd
Professor Kerby A. Shedden

DEDICATION

To my family and friends

ACKNOWLEDGEMENTS

First, I have to thank my mother for her unwavering support. I also have to acklowledge all of the friends I have made here at the University of Michigan, who have all been great sources of inspiration.

I also have to thank my advisor, Jun Li, who is the most important figure of my PhD. I cannot begin to express my appreciation for his support and dedication to my growth as an independent scientist. I must also thank the past and present members of the Li lab for their help and support.

Finally, I have to thank the members of my thesis committee, Dave Burke, Jeff Kidd, Steve Britton and Kerby Shedden for providing me with guidance and expertise on my dissertation project.

TABLE OF CONTENTS

LIST OF TABLES

LIST OF FIGURES

LIST OF ABBREVIATIONS

Abbreviation	Definition
AEC	Aerobic Running Capacity
AFS	Allele Frequency Spectrum
AMOVA	Analysis of Molecular Variance
ATP	Adenosine Triphosphate
BH-FDR	Benjamini-Hochberg False Discovery Rate
BWA	Burrows-Wheeler Alignment
CLR	Composite Likelihood Ratio
DAVID	Database for Annotation, Visualization and Integrated Discovery
DSC	Desmocollin
DSG	Desmoglein
EDL	Extensor Digitorum Longus
Fst	Fixation Index
G	Generation
GATK	Genome Analysis Toolkit
GO	Gene Ontology
h_0	Heterozygosity
h^2	Narrow-sense Heritability
HCR	High Capacity Runner
HS	Heterogeneous Stock
IBD	Identity-by-Descent
IBS	Identity-by-State
KEGG	Kyoto Encyclopaedia of Genes and Genomes
LCR	Low Capacity Runner
LD	Linkage Disequilibrium
MAD	Median Absolute Difference
MAF	Minor Allele Frequency
MDS	Multidimensional Scaling
PCA	Principal Component Analysis
QTL	Quantitative Trait Loci
REML	Restricted Maximum Likelihood
ROH	Run of Homozyogity
SNP	Single Nucleotide Polymorphism
SNV	Single Nucleotide Variant
TCA	Tricarboxylic Acid Cycle
WGS	Whole-Genome Sequencing

ABSTRACT

We have previously established two lines of rat for studying the functional of aerobic exercise capacity (AEC) and its impact on metabolic health. The two lines, high capacity runners (HCR) and low capacity runners (LCR), have been selectively bred for high and low intrinsic AEC, respectively. They were started from the same genetically heterogeneous population and have now diverged in both AEC and many other physiological measures, including weight, body composition, blood pressure, body mass index, lung capacity, lipid and glucose metabolism, and natural life span. In order to exploit this rat model to understand the biological basis of metabolic traits I conducted four related studies. First, I performed a genetic characterization of both pedigrees, with ~30 generations and >6,000 animals in each, showing that AEC has high heritability in both lines, and that the lines have diverged at expected rates. Second, I performed gene expression analysis in skeletal muscle with a 2-2-2 design to compare HCR and LCR, aged and young, and rest and exhaustion. I found that mitochondrial function is the primary differences between the lines; and extracellular matrix components underlie the aging effect. Third, I used SNP genotype and whole genome sequencing data to identify signatures of selection using three different statistics (runs of homozygosity, fixation index, and aberrant allele frequency spectrum), and developed a composite score that combined the three signals. I found several pathways (ATP transport and fatty acid metabolism) are enriched in regions under differential selection. Fourth, I complemented the selection signals with a direct analysis of genotype-phenotype relationship in an HCR-LCR intercross F2 cohort (n>600). We have completed breeding and phenotyping of F2s for running distance, body weight, percent body fat, muscle mass, etc., and have genotyped them for ~625K SNPs using a custom genotyping panel that I designed to utilize ancestral informative markers. My preliminary QTL results highlight a candidate region on chromosome 18 with three biologically relevant

genes, one of which is a potential candidate from the selection signature results. Ancestry haplotype-based fine mapping are ongoing and will be integrated with the expression results and the selection scan.

CHAPTER 1

Introduction

1.1 Importance of rat models in studying complex traits

Despite tremendous progress in medical genetics, our understanding of the genetic architecture of complex human diseases remains limited. Population-based association studies have led to the discovery of nearly 100 loci for blood lipids (Teslovich et al. 2010) and >60 loci for Type 2 diabetes (Voight et al. 2010, Morris et al. 2012, Deloukas et al. 2013). But together they have only explained 5-10% of observed heritability. Gene-environment and gene-gene interactions likely play an important role, but are difficult to study in humans. An animal model brings the key advantage of having a consistent and controlled environment, and in many cases can accelerate the mapping and interpretation of human disease genes (Peltonen and McKusick 2001).

In humans, intrinsic aerobic exercise capacity (AEC) is measured as maximal work performed on a standardized treadmill test; and many studies have shown that it is a strong predictor of disease risk, with higher capacities associated with better health and stronger resistance to metabolic diseases (Blair et al. 1989, Sandvik et al. 1993, Lakka et al. 1994, Blair et al. 1996, Myers et al. 2002, Gulati et al. 2003, Church et al. 2004, Sui et al. 2007, Kokkinos et al. 2008). Maximal AEC is also a better predictor of all-cause mortality than other established risk factors including hypertension, smoking, and diabetes (Myers et al. 2002, Leeper et al. 2012). This epidemiological association

suggests a causal connection. However, the biological basis for this connection remains largely unknown (Pedersen and Saltin 2006, Bray et al. 2009). Aerobic capacity is a complex phenotype, affected by both genetic and environmental factors, including diet and exercise. However, in studies involving human subjects it is often difficult to resolve the relative effects of innate endurance from those due to aerobic training (Kaprio et al. 1981, Prud'homme et al. 1984, Simoneau et al. 1986, Perusse et al. 1989, Bouchard et al. 2000, Bray 2000). To overcome this limitation, an animal model is needed that allows in-depth analyses of AEC.

The rat is an excellent model organism for many reasons. The laboratory rat (*Rattus norvegicus*) has been a key system in basic biological and pharmacological research. A large body of literature exists concerning diverse phenotypes of rats, covering its cardiovascular, neural, and other physiological functions (Jacob and Kwitek 2002). Rat is evolutionally close to human; thus almost all known genes associated with human diseases have orthologues in the rat genome (Gibbs et al. 2004). Over 200 inbred strains of rats have been produced, many were first selectively bred for ‘‘disease’’ alleles (Hedrich et al. 1990). However, inbred lines of rats have the drawback of idiosyncratic breeding history, and lack the genetic diversity that characterizes natural populations. My Ph.D. research focuses on an outbred rat model, as it mimics the complexity of human traits more realistically.

1.2 Artificial selection for high and low aerobic capacity rats

Wild rats or heterogeneous stocks (HS) are outbred rat models frequently used in research. The HCR-LCR lines described below have an additional advantage in that they are derived from eight founder strains, and artificial selection has enriched for

functionally relevant and potentially higher-effect alleles in genetically divergent backgrounds, making available stronger signals to facilitate gene mapping. The HCR-LCR model was started with the goal of understanding the genetic and functional basis of aerobic exercise capacity (AEC) so that we have an animal model that allows in-depth analyses of the biology and health impact of intrinsic AEC that are not possible with human subjects. In 1996 Drs. Britton and Koch (both currently at U-M) initiated a long-term experiment to create two lines of rats through divergent selection for higher or lower intrinsic AEC (Koch and Britton 2001). Maximal AEC on a speed-ramped treadmill running test was adopted as the selection criterion because it provides a strong signal corresponding to whole-body energy management and can be measured efficiently in many rats, and more objectively than behavioral or emotional traits. The two lines, termed high capacity runners (HCR) and low capacity runners (LCR), were started from the same founder cohort (N=186) of genetically heterogeneous rats (N:NIH stock) originally derived from outcrossing 8 inbred strains (Hansen and Spuhler 1984). The highest- (for HCR) or lowest- (for LCR) performing male and female in each family were selected as breeders for the next generation, and bred in a rotational pattern to minimize inbreeding (details in Chapter 2).

1.3 Phenotypic Divergence Between HCR and LCR

One of the original aims for establishing the HCR-LCR lines was to test the hypothesis that artificial selection based on intrinsic aerobic capacity would yield models that also exhibit contrasts in disease risks. This hypothesis has been proven correct: after 28 generations of selection, the HCR and LCR diverged not only for running capacity, but also in other physiological measures, including blood pressure, body mass

index, lung capacity, lipid and glucose metabolism (reviewed in Koch et al. 2012). The LCR, relative to the HCR, manifest numerous clinically relevant conditions, including increased susceptibility to cardiac ventricular fibrillation (Lujan et al. 2006) and hepatic steatosis (Thyfault et al. 2009). At the behavioral level the LCR score higher for dysfunctional sleep (Muncey et al. 2010), diminished behavioral strategies for coping with stress (Burghardt et al. 2011), and impaired memory and learning (Wikgren et al. 2012). In contrast, the HCR have reduced weight gain (Wisloff et al. 2005), increased resistance to the deleterious effects of a high fat diet (Noland et al. 2007, Novak et al. 2010), increased capacity for fatty acid oxidation in skeletal muscle (Lessard et al. 2009) and liver (Thyfault et al. 2009), and an 28-45% higher lifespan (Koch et al. 2011).

At generation 10 of selection, HCR and LCR were phenotyped across several physiological measures to test if disease features had segregated differentially between the lines. Wisloff et al. discovered that adult LCR rats develop cardiovascular risks consistent with the metabolic syndrome, including large gains in visceral adiposity, increased blood pressure, dyslipidemia, endothelial dysfunction occurring within carotid arteries, and insulin resistance (Wisloff et al. 2005). Using HCR and LCR rats from generation-18 Kivela et al. (2010) found that gene expression differences related to oxidative phosphorylation and fatty acid metabolism in skeletal muscle correlated significantly with disease risk phenotypes such as physical activity levels, serum high density lipoproteins, and mitochondrial structure.

1.4 My contribution, using the HCR-LCR model for gene mapping

In my research, I combined this unique animal model with the latest high-throughput technologies to perform genetic and genomic analyses of the metabolic

phenotypes. My overall goal is to advance our understanding of the biological mechanisms that link AEC to metabolic fitness and related diseases, and I undertook four separate projects to accomplish this**.** The following chapters of this dissertation describe four related projects.

First, I used available pedigree data to assess the heritability of the AEC trait, as well as related metabolic and physiological traits. In addition, I used a panel of 10K SNP genotype data to show the genomic divergence between the HCR and LCR lines that may underlie the phenotypic divergence. Taken as a whole, my results suggest that the HCR-LCR system is a novel model system suitable for studying genome evolution under sustained selection, and for dissecting the functional and genetic basis of polygenic traits. This work was published as an article in *PLoS One*.

In the next project, I used transcriptomics data from the HCR and LCR in a 3-factor design to study the effects of, and interplay among, genetic background, exercise, and age, and found that each of the three factors--line, age, and exercise--has a main effect at the global level, and that the main effects are comparable in magnitude. My results support previous reports that HCRs show higher expression than LCRs for genes involved in mitochondria function, and my data further show that this difference is consistent whether after strenuous exercise and at rest. Further, aging-effect in LCRs show more significant enrichment for the extracellular, collagen, and adhesion pathways compared to HCRs, suggesting that LCRs' lower innate aerobic capacity underlies their faster aging. This work has been submitted for publication in *Physiological Genomics*.

For my third project, I genotyped a group of HCR and LCR rats from two different times of selection using a custom 800K SNP array and pooled sequencing data, to

identify genomic regions under selection. In order to capture different but related selection signals, I used scan statistics corresponding to three different local genomic properties (ROH, F_{st}, and AFS) to identify both between-line and temporal signals. I further implemented a composite score method that combines the three statistics into one score for every gene, and found interesting candidate genes and pathways under selection. This work has been posted as a preprint in *bioRxiv*.

Last, I designed a 625K SNP array using the Affymetrix Axiom platform specifically for our lines in order to genotype the most informative SNPs in our F2 intercross population for QTL mapping. I combined WGS data from the 8 founder inbred lines, and pooled WGS from our own HCR-LCR animals to create the panel of SNPs. This platform benefits not only our gene mapping efforts, but also the entire rat community. My preliminary QTL analysis on the >600 F2 animals uncovered a ~1 Mb QTL region on Chromosome 18 with three genes that have biological relevance, which also showed potential importance in the transcriptomic and WGS data of the HCR-LCR lines. The manuscript describing this work is under preparation.

CHAPTER 2

Genetic Analysis of the Rat Pedigrees

2.1 Introduction

Major advantages of the HCR-LCR system include the fact that the pedigree and running phenotype data (n = 11,422) are completely known; and tissue samples for most breeding members (n > 1,500) have been archived. This combination of existing data and reagents, combined with over 70 published physiological studies of the two lines, represents a valuable resource that allows comprehensive analyses of the effects of selection on genomic and phenotypic evolution.

In this study, I carried out a systematic analysis of the running phenotype and related traits over the known pedigree of 28 generations. I also collected a genome-wide 10K SNP dataset for a subset of breeding members from three generations (G) (n=142 over G5, G14, and G26), and used these data to examine patterns of genomic evolution in the two lines as they underwent selection. These analyses provided new insights into the genealogical structure, inbreeding patterns, and genetic variability of the two lines, and characterized the intercross animals to assess their suitability as a mapping population for identifying quantitative trait loci (QTL).

2.2 Materials and Methods

2.2.1 Ethics Statement

This study was approved by the University Committee on Use and Care of Animals, Ann Arbor, Michigan (Approval Numbers: #08905 and #03797). The proposed animal use procedures are in compliance with University guidelines, and State and Federal regulations.

2.2.2 Rotational Breeding Scheme

In practice, each line contains at least 13 mating pairs through all generations. From each of the produced families, one male and one female are selected as breeders for the subsequent generation. For HCR, the male and female with the greatest running distance are selected, whereas in LCR, those with the lowest distance are selected. The breeders are paired between different families to avoid brother-sister mating, and the pairings rotate in successive generations to minimize inbreeding (Nomura and Yonezawa 1996). When the 13th rotation is reached, same-family mating is skipped and the pairings are reiterated starting again in the same way as rotation 1. Sometimes, if a particular mating fails, or if a family lacks animal of one sex, substitute mating is attempted involving a male from another family. In some cases, one male is mated to two females. After G12, female HCR with body weights less than 160 grams were not selected to be breeders in order to ensure that fecundity does not diminish as a result of selection for better runners. G9-G13 in HCR included three cross-generation matings, whose offspring were incorporated into subsequent generations. Further, occasionally additional pairs are bred to generate experimental cohorts for study by us or for sharing with collaborators, and the progenies in these "analytical families" are not used for maintaining the lines, and are not counted in our calculation of the expected inbreeding

levels. They are, however, used to calculate heritability and the distribution of trait values.

One inevitable consequence of this breeding scheme is the mating of first-cousins at every half interval. For example, at G7, every breeding pair, such as 1M-7F (a male from Family 1 and a female from Family 7) involves first cousins, because they are from 1F-7M and 7F-13M matings respectively, in G6, in which 7M and 7F are siblings. This results in a 6% spike in inbreeding values in G8 (Figure 2.1), and such a cyclic pattern continues in subsequent generations, resulting in spikes at G14, G20, and G26. The actual pedigree deviates from a perfectly executed breeding scheme due to the inclusion of substitute breeders, and the calculated inbreeding coefficient from the actual pedigree depart slightly from expectations (Figure 2.1). As some breeding pairs were assembled to generate offspring for research use rather than line propagation, the "effective breeders" are those that contribute offspring who are also used as breeders, and do not include those whose offspring were used only for research but not as breeders themselves (Table 2.1).

2.2.3 Running Phenotype

Eleven week old animals are subjected to run-to-exhaustion tests without prior training, except for brief sessions of treadmill education during the week prior to the tests. The purpose of such education sessions is to familiarize the rats to the experimenters and the testing equipment and to ensure that each rat has the ability to achieve a minimal level of continual running for 5 minutes at least once, which constitutes the threshold performance necessary for inclusion in the actual running tests the following week. During education, the rats learn to keep running in order to avoid a

mild shock (1.2 mA of current at 3 Hz) induced by the electrified grid located at the back of the treadmill. For all sessions the treadmill is set at a 15-degree upward slope.

During the run-to-exhaustion test, each rat was evaluated on five consecutive days (Mon-Fri) for G0-G16 and on three alternating days (Mon-Wed-Fri) for G17-28. Each trial starts at a velocity of 10 m/min, which increases by 1 m/min every 2 min until the rat reaches exhaustion. Exhaustion point is defined as the third time a rat can no longer keep pace with the treadmill and remains on the shock grid for two seconds rather than resuming running. At this point the rat is removed from the treadmill and weighed. For each rat, the best distance out of the multiple trials is taken as the best estimate of its intrinsic capacity, and used as the criterion for breeder selection. The vertical work during each trial is estimated using the equation:

$$work = (running\ distance) \times (body\ weight) \times (\sin[15^{o}]) \times (9.8 m/s^{2})/1000$$

in which the unit for work is joule ($J=kg \bullet m^2/s^2$). The units for running distance and body weight are meter and gram, respectively.

2.2.4 Phenotype Distribution

To display the phenotype distribution I produced violin plots (as shown in Figures 2.1, 2.2, and 2.3) using the *vioplot* function from the *Vioplot* package in R. To calculate the Spearman's rank correlation coefficient (ρ) between maximal running distance and average body weight, separately for two sexes within each line, I used the *cor* and *cor.test* functions in R. The ρ values were calculated for each generation, and averaged over G1-G28.

2.2.5 Inbreeding Coefficient and Heritability

I calculated the inbreeding coefficient (F) for each animal in the pedigree using the *calcInbreeding* function from the *pedigree* package in R (Bastiaansen et al. 2012). The pedigree for earlier generations of NIH:H animals, i.e., those that preceded the founders of our lines, was not available. We are therefore limited to calculate the *increase* of inbreeding coefficients from those of the founders, effectively assuming they were unrelated, while in fact they were related according to the (unknown) breeding patterns in the preceding generations. To calculate the expected F under random mating, I used the equation $F_{n+1} = F_n+(N_f+N_m)/(8*N_f*N_m)-F_n(N_f+N_m)/(8*N_f*N_m)$, where the F_n and F_{n+1} are the inbreeding coefficients at the n-th and (n+1)-th generation, respectively, and N_f and N_m are the numbers of male and female breeders at the n-th generation ($N_f = N_m = 13$ in every generation for a 13 family breeding scheme). To calculate the expected F under perfect adherence to the rotational scheme, I generated an idealized pedigree of 13 mating pairs of exact mating patterns as intended, and used the *pedigree* package to calculate F for every member of the pedigree.

To calculate the narrow-sense heritability (h^2), I applied the variance and covariance component models as implemented in *SOLAR* version 4.3.1 (Almasy and Blangero 1998). I estimated h^2 for maximal running distance both over the entire pedigree and for four-generation intervals (with one and three generation overlap) to assess the h^2 variation over time. I also estimated h^2 for average body weight and work for the G0-G28 pedigree, and for additional traits for the F2 intercross. For the G0-G28 analysis, I included sex and operator as covariates; and for the F2 intercross I included sex and batch because the breeding was performed in two batches, containing 154 and 491 F2 animals, respectively.

2.2.6 Genotyping and Data Processing

DNA from 22-25 breeders from both lines in three non-adjacent generations (G5, G14, and G26, n=142) was extracted from frozen liver tissue, and genotyped across 10,846 SNP loci using the Affymetrix Rat Mapping 10K GeneChip. Attempts to extract DNA from generations earlier than G5 revealed that many samples in G0 and G4 were degraded. I therefore chose G5 as the earliest generation in our analysis due to its assured DNA quality. In assessing the quality of SNP markers I removed 28 duplicate SNPs, 496 SNPs with genotype missing rate >10%, and 137 SNPs with Hardy-Weinberg Equilibrium test $p < 0.001$. These steps led to 10,185 SNPs that formed the "Panel-1" markers. As some analyses require a reduced set of SNPs without rare variants and without strong linkage disequilibrium, I removed from Panel-1 an addition set of 7,284 SNPs selected by trimming SNP pairs in linkage disequilibrium with r^2 value >0.05 (in windows of 10 SNPs, sliding by 2 SNPs each time), and 572 SNPs with minor allele frequency (MAF) <5%. After these steps, 2,518 SNPs remained and formed the "Panel-2" markers. The Panel-2 markers were used in calculations of IBD, AMOVA, and genome-wide average heterozygosity. The pairwise Identity-by-State (IBS) matrix was estimated in *PLINK* (Purcell et al. 2007) using the *-genome* command and Panel-2 markers. Multidimensional scaling analysis of the IBS matrix was performed in R (R Development Core Team 2010). Analysis of molecular variance (AMOVA), as implemented in the program *Arlequin*, was used to calculate the within- and among-group differentiation (Excoffier et al. 2005).

I assessed the accuracy of recorded sex for each genotyped animal by calculating the average heterozygosity of the X chromosome SNPs. Male and female animals are

confirmed by non-overlapping distributions of ChrX heterozygosity values. I confirmed known sibling pairs among the genotyped animals by plotting pairwise Z0 vs Z1 values in R. Z0 and Z1 values were determined in *PLINK* using the *-genome* command.

2.2.7 Runs of Homozygosity

Using the 10,185 Panel-1 markers, I identified long runs of homozygosity (ROH), in *PLINK* using the *-homozyg* command. I defined ROHs as genomic segments with at least 4 homozygous markers and having a density of at least 1 SNP per 500Kb. Total ROH length in each animal was obtained by summing over all ROH and also reported as the fraction of the rat genome (2.75 Gb).

2.2.8 Genomewide Average Heterozygosity

Using the Panel-2 markers, I calculated the average heterozygosity in PLINK using the *-hardy* command, and compared across genotyped lines and generations using boxplots. The expected heterozygosity values were calculated using the equation $H_{n+1} = H_n(1-((N_f+N_m)/(8*N_f*N_m)))$, where the H_n and H_{n+1} are the heterozygosity at the n-th and (n+1)-th generation, respectively, and N_f and N_m are the numbers of male and female breeders at the n-th generation, respectively ($N_f = N_m = 13$ in every generation for a 13 family breeding scheme) (Table 2.1).

2.2.9 LD calculation

Pairwise measurements of LD (r^2) were calculated for marker pairs within 5 Mb on Chromosome 1 using Haploview (Barrett et al. 2005). To show the relationship between r^2 and inter-marker distance, I calculated average r^2 values for groups of marker pairs falling in discrete bins of inter-marker distance, in 500Kb increments, and plotted the values for G5, G14, and G26 in both HCR and LCR.

2.3 Results

2.3.1 Rotational Breeding and Inbreeding Coefficients

The protocols of animal maintenance, phenotyping, and rotational breeding have been described previously (Koch and Britton 2001) (see also Methods). I analyzed the pedigree data for generations 1-28, involving 5,976 HCRs and 5,446 LCRs. For each animal, I calculated its expected inbreeding coefficient (F) by tracing its parental lineage and documenting inbreeding loops. As expected, such pedigree-based estimates of F started to rise at G4-G5 and continued to increase over successive generations (Figure 2.1). The breeding history included occasional out-of-schedule pairings due to the lack of offspring of a certain sex in a given family or the need to substitute for unproductive mating pairs (see Methods for more details). Despite this, the pattern of F increase in the actual pedigree largely agrees with the expectation assuming perfect adherence to the planned rotation schedule (shown in solid lines in Figure 2.1). The cyclic rise of inbreeding coefficient every six generations is expected for 13 breeding pairs, due to the inevitable first-cousin paring every half cycle of the rotation (Farid et al. 1987, Windig and Kaal 2008) (further explained in Methods). Importantly, the average increase of estimated F is 0.94% and 0.95% per generation for HCR and LCR, respectively. These predictions are slower than the rate expected under random mating (shown in dotted lines in Figure 2.1), which increase at 1.51 per generation for both HCR and LCR, starting from the first generation.

2.3.2 Phenotypic Response to Selection and Heritability

For each animal, I collected phenotype data that include maximal running distance, body weight at the time of running trial, and vertical work performed during each run. All

animals were tested at 11-12 weeks of age. While both lines were derived from the same base population (indicated in yellow in Figure 2.2), their running performance gradually diverged over time. After 28 generations, the HCRs and LCRs differ by about 8.3-fold in running distance (9 times of the average within-line standard deviation), compared to ~2.8 fold (range of 298 to 840 meters) among eleven inbred lines commonly used in research (Barbato et al. 1998). The HCR continue to respond to selection (Figure 2.2, Tables 2.2-2.3), with maximal running distance reaching >2000 m, ~2.4 fold higher than the best recorded performance among the inbred lines (Barbato et al. 1998). The pattern of increase is consistent in both males and females. Across generations, body weight did not diverge significantly between the two lines, with a sex-averaged weight of 268 g and 215 g in LCR and HCR, respectively, or a 0.8-fold difference after 28 generations (Figure 2.3, Tables 2.2-2.3). In general, females are of lighter weight than males. However, as females tend to run longer, the overall vertical work is near-equivalent between males and females (1.3-fold difference in HCR, 1.1-fold difference in LCR) and larger in HCR than LCR by 6.8 fold.

The narrow-sense heritability (h^2) for the logarithm of running distance, which measures the proportion of total phenotypic variance explained by additive effects of genes, was calculated for each line separately, and was 0.47 ± 0.02 in HCRs and 0.43 ± 0.03 in LCRs when all 28 generations were considered. To evaluate potential change in heritability over time, I also calculated h^2 over four-generation, partially overlapping, intervals and found that while h^2 was variable across intervals, it maintained positive values, with no sign of abatement in later generations. The within-line h^2 for bodyweight and vertical work are 0.45 ± 0.06 and 0.37 ± 0.02, respectively, for HCRs, and 0.17 ±

0.03 and 0.58 ± 0.02 for LCRs. These results indicate that although LCRs did not show a decrease of running capacity as dramatically as the increase in HCRs, the heritability of running performance was comparable in the two lines. Lower body weight is associated with better running capacity, as shown by the negative correlations between the two phenotypes for both sexes within each line. For HCRs, the spearman correlation is -0.41 ± 0.15 and -0.17 ± 0.16 for males and females, respectively. For LCRs, the correlation is -0.19 ± 0.16 and -0.12 ± 0.13 for males and females, respectively. The fact that HCRs continued to respond to selection and that both lines maintained within-line heritability suggest that all causal genetic variants have not been fixed in either line, rather they continue to segregate in both pedigrees.

2.3.3 Increased Genomic Differentiation Between Lines

As an initial genetic characterization of the HCR-LCR system, I collected genotype data over a genome-wide panel of ~10K single nucleotide polymorphism (SNP) loci for 142 animals, consisting of 22-25 animals in each of three non-adjacent generations (G5, G14, and G26) in both lines (see Methods). I used the average heterozygosity of 61 X chromosome markers to infer sex, and found no disagreement with the recorded sex of the 142 animals. Documented relatedness was also confirmed by plotting the pairwise proportion of not sharing DNA segments due to identity by descent (P(IBD) = 0, or Z0) against the proportion of sharing one copy IBD (Z1) using the 2,518 SNPs (SNP Panel-2, see Methods). Siblings and non-sibling relatives are separated into distinct clusters, indicating that the sample identities reflected in the genotype data are consistent with the recorded pedigree. Multidimensional Scaling (MDS) analysis showed that at G5, HCRs and LCRs formed two readily separable clusters (Figure 2.4). From

G5 to G14 and from G14 to G26, between-lines separation increased, indicating a progressively greater differentiation between LCR and HCR.

To measure the apportionment of total genetic variance into between-line and within-line components I performed an Analysis of Molecular Variance (AMOVA) (Excoffier et al. 1992). The proportion of variance explained by among population difference, as a weighted average over all loci, is increasing over time, from 6.5% at G5, to 15.6% at G14, and to 26.5% at G26.

2.3.4 Decreased Genomic Diversity Within Lines

I analyzed genetic diversity at the individual level by calculating the average heterozygosity (H_0) across the 2,518 Panel-2 markers for each animal, and averaging within each of the six groups (two lines, at three time points) (Figure 2.5). At G5, H_0 averaged 0.379 in HCR and 0.372 in LCR. At G14 it decreased to 0.338 (-10.8%) in HCR and 0.327 (-12.1%) in LCR. At G26 it decreased further to 0.303 (-10.2% from G14) in HCR and to 0.296 (-9.4%) in LCR. Note that the absolute values of H_0 are influenced by the allele frequencies of the genotyped SNP markers, and it is the relative changes of H_0 that reflect the altered genomic diversity. The observed rates of decrease are slower than in random mating populations. Using the known numbers of effective breeders at each generation I calculated the expected H_0 at each generation assuming random mating, and found that the expected rate of decrease in H_0 is on average 1.53 per generation for both HCR and LCR,. The observed rate of decrease, 0.95% and 0.97% per generation for HCR and LCR, respectively, is lower by 37-38%, consistent with the pedigree-based predictions (Figure 2.1) and confirming that the rotational

breeding scheme has successfully reduced inbreeding as predicted (Nomura and Yonezawa 1996).

As the reduction of H_0 over time primarily reflects higher levels of inbreeding, a majority of the increase of homozygote genotypes should be accounted for by the emergence or expansion of long runs of homozygosity (ROH). Using 10,185 SNPs in SNP Panel-1 (see Methods), I found that for HCR, ROH covered an average of 46% of the genome in G5 animals, and this rate increased to 54.8% in G26. For LCR, ROH covered 46.8% of the genome in G5, and 55% in G26. Thus the non-ROH regions shrink by 0.73-0.77% per generation in the two lines, accounting for most of the decrease of H_0.

2.3.5 Linkage Disequilibrium

I examined linkage disequilibrium (LD) patterns using the Panel-1 SNPs on Chromosome 1 (n = 978). The LD index r^2 decays to 0.3 at ~3 Mb in both HCR and LCR (Figure 2.6). The level of LD is similar between HCR and LCR, showing slightly higher r^2 in later generations, and is consistent with those reported for the NIH Heterogeneous Stock (Johannesson et al. 2009). These results also suggest that the resolution of QTL mapping using HCR-LCR can be as high as 2-3 cM, considerably higher than the 20-40 cM resolution of F2 intercross of inbred lines (Flint et al. 2005).

2.4 Discussion

The HCR-LCR system was initiated in 1996 (Koch and Britton 2001) and reached G28 in 2011. During this time, the two lines have diverged in innate endurance running capacity and showed marked differences in body type and metabolic traits. The HCR

animals show a lower weight gain than LCR, in both young and adult rat, and this can be partly accounted for by higher spontaneous activity and lower fuel economy during activity in HCRs (Novak et al. 2010). The two lines also diverged for many health indicators, with HCR showing a relative resistance to obesity, higher insulin sensitivity, lower blood pressure, improved lipid parameters, and enhanced longevity (Wisloff et al. 2005, Noland et al. 2007, Koch et al. 2011). These phenotypes are of immense public health interest, as prevalence of diabetes, cardiovascular disorders, obesity, and metabolic syndrome is rising at an alarming rate and account for a major portion of disease burden worldwide (James et al. 2004). The model system used in this study is ideally suited for elucidating the fundamental biology of metabolic health. Understanding the genetic architecture and molecular underpinnings of the remarkable HCR-LCR differences has the potential to provide new insights into the relationship between exercise capacity and metabolic health in humans.

While previous studies have focused on functional, physiological comparisons between HCR and LCR rats, here I conducted the first in-depth pedigree and molecular genetic analysis of the two lines. Phenotypic data over the 28-generation pedigree not only revealed substantial heritability for the running capacity trait, but also showed that the heritability is maintained in later generations, suggesting continued selection.

I observed continued response to selection in HCR during generations 20-28. This observation is notable because it can be interpreted in two possible scenarios. The first is that the aerobic running capacity may be influenced by many interacting QTLs, and as variants in some loci become fixed under selection, the previously hidden phenotypic effects of other variants can be "released" and come under selection, thereby fueling

prolonged responsiveness. This agrees with previous observations in similar systems that long-term selection did not exhaust the genetic variation for the selected trait due to the gradual shifts in the capacitors of cryptic genetic variation (Queitsch et al. 2002, Dworkin et al. 2003). The second scenario is that the trait may be governed by many QTL of small effect, hence the strength of selection (~20% of animals become breeders in each generation (see Table 3)) may not have effectively driven the rapid changes of allele frequencies. These scenarios are not mutually exclusive, and the observation means that not all causal alleles have been differentially fixed in the two lines. Therefore we need to consider the possibility that the causal variants may be segregating *within* one or both lines.

HCRs exhibited accelerated improvement of running capacity during G12-G15 (Figure 2.2). To identify the cause(s) of this acceleration I examined factors such as diet, running protocols, the breeding schedule, and "Operator", i.e., the experimenter or a team of experimenters assessing the running phenotype. The average litter size (i.e., fecundity) in the recorded HCR pedigree was not changed significantly during this period, hence there was no noticeable change in fertility or the strength of selection (i.e., the fraction of animals chosen as breeders). There was no systematic correlation between litter size and inbreeding coefficient of the offspring (not shown); and there was no documented change in diet, running apparatus, or running protocol. The two lines were closely synchronized across all 28 generations. The pedigree-based prediction of F was increasing in both HCR and LCR as expected (Figure 2.1). However, a more detailed retrospective analysis of the breeding records found three factors having changes overlapping the G12-G15 period. The first is Operator: a team supervised by

Operator #3 performed the running tests during G7-G13, while a team supervised by Operator #4 performed the tests during G14-G15. The second factor is the number of animals in the pedigree with no entries for running data which accrued mostly from rats that "refused" to run. The number of non-compliant rats in both lines gradually increased during G7-G13 in both lines, dropped immediately at G14, and remained low for most of subsequent generations. Despite presumed standardization of the running protocol, the loss of running data may be Operator dependent in the sense that "refusal to run" is a subjective measure. Third, the fraction of mating pairs that were out-of-schedule increased in G12-G14 in HCR, and dropped after G15. The simplest interpretation of these co-occurrences is that Operator 3 subjectively determined that a large number of animals refused to run. Those who did run showed no improvement over G6-G13. With Operator 4, nearly all animals were able to run, and ran better than previous generations. While plausible, this simple scenario does not explain all the observations. First, despite being kept and tested under the same conditions as the HCRs, the LCRs exhibited no comparable acceleration or deceleration in running capacity. Second, the acceleration in HCRs began in G12-G13 with the unexplained emergence in some families of one or two exceptional runners, whose running distance were often more than twice as long as that of their siblings. The performance of these runners could not be easily explained by Operator. Partly because the exceptional runners tended to be selected as breeders, such improved performance spread wider across the cohort in G14-G15 and gradually became the norm after G16. However, there was not a clear-cut Mendelian segregation pattern in these generations: the pairing of two exceptional runners often still produced mediocre offspring. Among HCR mating pairs in G12-G15

there were 13 out-of-schedule pairs, which did not produce more exceptional runners than on-schedule pairs (not shown). The location of animal facility changed between G15 and G16 for both lines, but this change took place after the acceleration had started. Despite these complications, heritability estimates for HCR, calculated for each three-generation section of the pedigree and shifted by one generation, did not show dramatic changes over the generations.

The accelerated improvement of running capacity in HCRs during G12-G15 could also reflect genetic changes. However, emergence of a single high-impact *de novo* mutation is unlikely, as prodigious running capacity arose in multiple families concurrently. Such a pattern, however, is compatible with a scenario in which causal "high" alleles in multiple genes interact in a non-linear fashion. Various combinations of the high alleles could have undergone gradual enrichment and in G12-G15, began to manifest as improved phenotype when the most favored combinations were formed. Future studies, including linkage analysis of these intermediate generations, are needed to characterize the genetic changes accompanying the apparent varying tempo of trait evolution.

Taken as a whole, the results presented above suggest that the HCR-LCR system is well-suited to serve as a novel model system for studying genome evolution under sustained selection and for dissecting the functional and genetic basis of polygenic traits. The model exhibits large phenotypic divergence, sustained heritability for a wide range of cardiovascular and metabolic traits, and maintained outbred character. The complete pedigree is known, with running phenotype for all animals already collected, and tissue sample for most breeders archived. Our system has maintained genetic

diversity through rotational breeding, such that networks of interacting QTLs may have evolved jointly under selection, making the system particularly suitable for detection of interaction QTL (Carlborg et al. 2006). Animals in both lines carry fine-grained genomic mosaics of eight "ancestral" inbred strains, with LD structure on the order of 3 Mb, allowing for greater resolution in association analysis (Mott et al. 2000, Valdar et al. 2003, Valdar et al. 2006). Combining QTL mapping with the wealth of existing knowledge of the HCR-LCR system is expected to allow the identification and prioritization of high quality candidate genes that will shed insight into the biology of oxidative capacity and metabolic fitness.

2.6 Figures

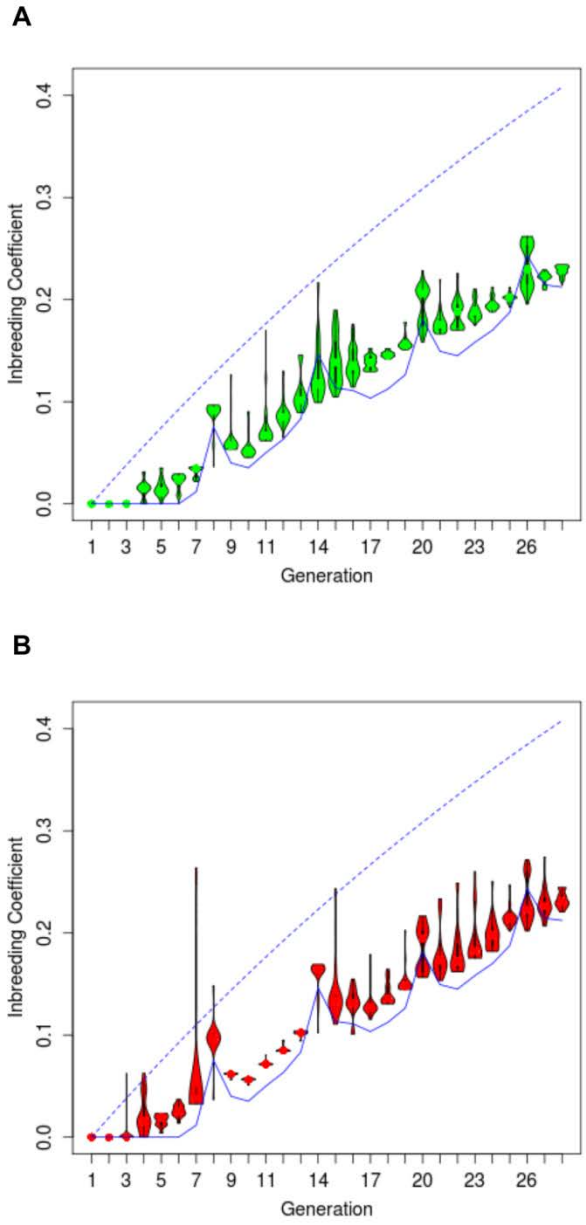

Figure 2.1: Distribution of predicted inbreeding coefficients (F) for G0 to G28.

Shown are "violin-plots" for individual generations for HCR (**A**) and LCR (**B**). The widths of the ovals indicate the probability density of the data values. The black dots and the thick black lines in the ovals denote the median and the 25-75 percentile range, respectively. The dotted blue line indicate the expected increase in F under random mating given the 13-family breeding scheme, and the solid blue lines indicate the expected F under perfect adherence to the rotational breeding scheme.

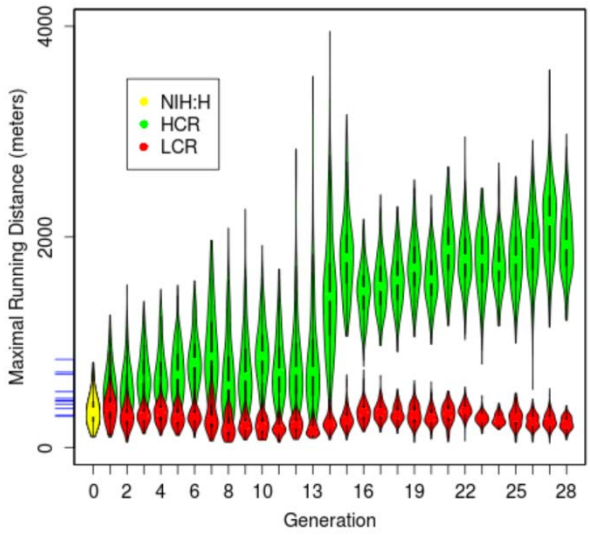

Figure 2.2: Distribution of maximal running distance for generations 0 to 28.

Shown are "violin-plots" for individual generations for females and males combined. The yellow oval to the left denotes the founder population (NIH:H, n=153 phenotyped, out of 186), while green and red ovals are for HCR and LCR, respectively. The blue tick marks on the y axis indicate the maximal running distance for eleven inbred lines, which are ordered, from top to bottom, as DA (840m), PVG (718m), AUG (699m), SR (533m), F344 (469m), ACI (450m), LEW (442m), WKY (414m), BUF (373m), MNS (308m) and COP (298m).

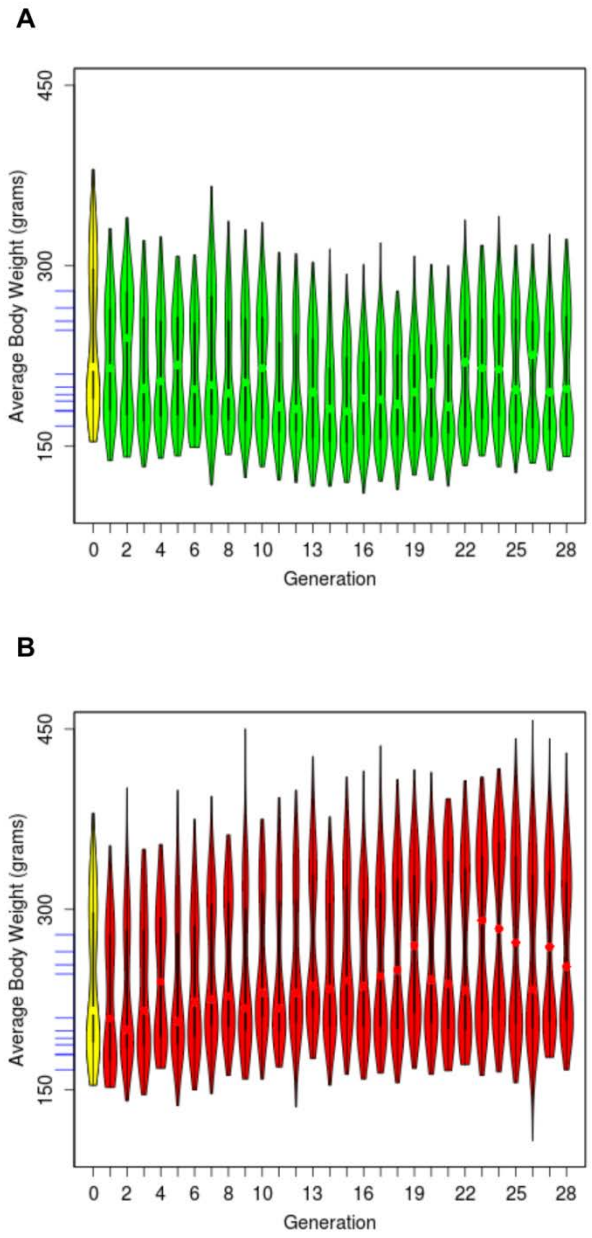

Figure 2.3: Distribution of body weight for generations 0 to 28 for HCRs (A) and LCRs (B).

The yellow oval denotes the founder population (NIH:H, n=153). Most distributions are bi-modal, as most females are of lower body weight than most males. The blue tick marks on the y axis indicate the body weight for eleven inbred lines. They are ordered, from top to bottom, as MNS (279g), LEW (265g), SR (254g), BUF (246g), WKY (210g), COP (199g), ACI (193g), F344 (188g), DA (180g), PVG (179g) and AUG (167g).

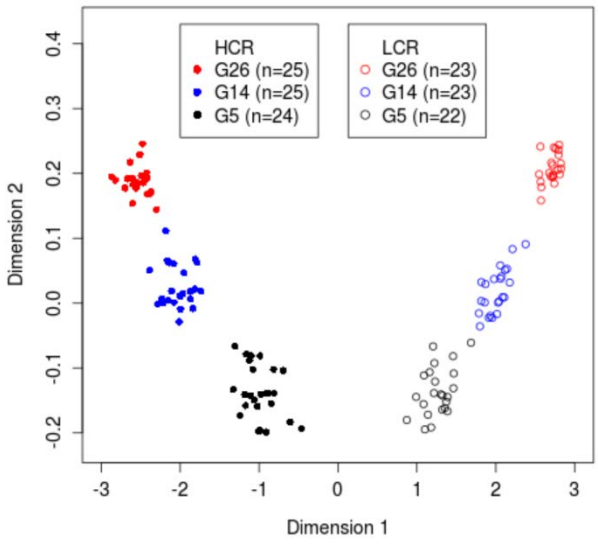

Figure 2.4: Progressive genetic differentiation revealed by 10K SNP genotyping data.

Shown is a multidimensional scaling plot (dimensions 1 vs. 2) for 142 genotyped animals in two lines and three generations, as indicated by different symbols, showing that the two lines formed separate clusters at G5, and diverged further in G14 and G26.

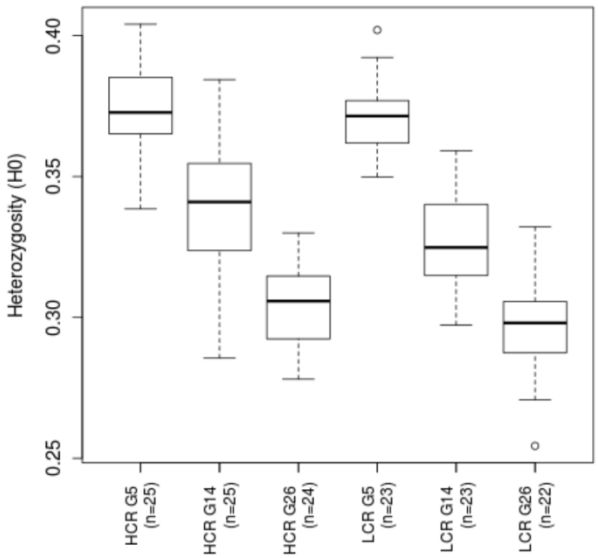

Figure 2.5: Decrease of average heterozygosity over time in both lines.

Shown is the boxplot of genomewide average heterozygosity for the genotyped animals in two lines and three non-adjacent generations.

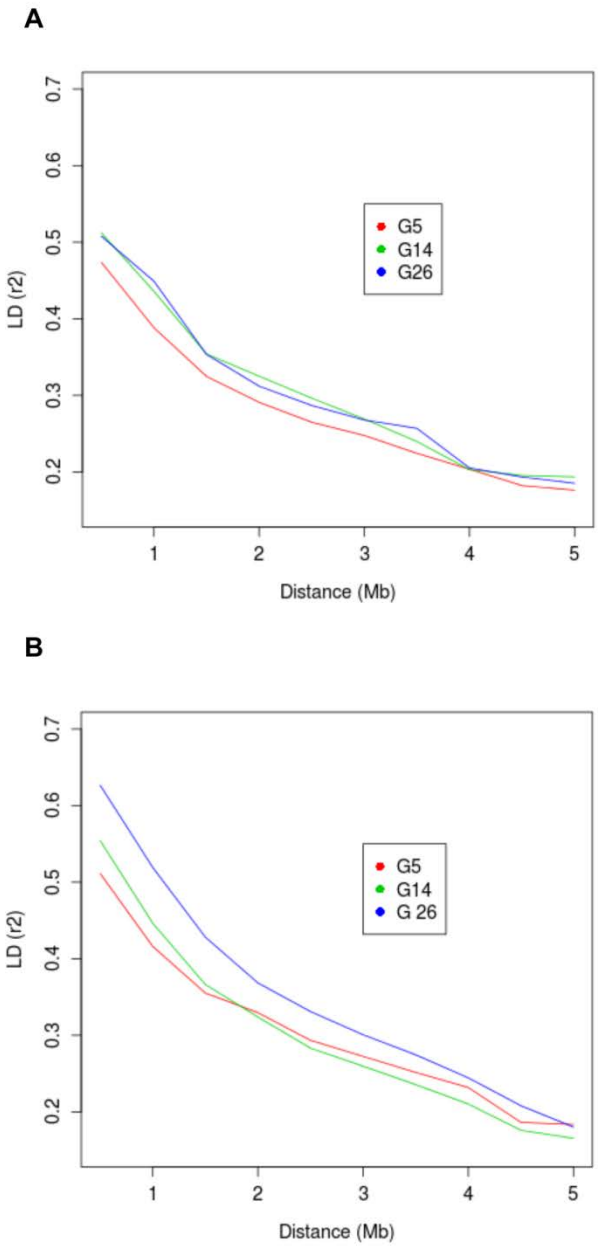

Figure 2.6: Linkage disequilibrium (LD) decay over distance in HCR (A) and LCR (B) for chromosome 1.

The LD index r^2, averaged for marker pairs falling in discrete distance bins, were plotted against the distance in Mb. LD decays to r=0.3 in about 3 Mb for both HCRs and LCRs.

2.7 Tables

			HCR				LCR	
Gen	**N^T**	**N_b**	**No. Male (N_m)**	**No. Female (N_f)**	**N^T**	**N_b**	**No. Male (N_m)**	**No. Female (N_f)**
0	-	26	13	13	-	26	13	13
1	116	28	14	14	125	26	13	13
2	137	28	14	14	126	26	13	13
3	160	28	14	14	167	30	15	15
4	131	26	13	13	138	26	13	13
5	151	28	14	14	150	26	13	13
6	151	30	15	15	155	26	13	13
7	133	30	15	15	141	26	13	13
8	185	28	13	15	143	28	14	14
9	234	30	14	16	198	27	14	13
10	238	29	13	16	150	27	13	14
11	202	34	16	18	245	28	14	14
12	195	30	14	16	202	26	13	13
13	240	34	16	18	216	28	14	14
14	222	30	15	15	209	28	14	14
15	232	32	16	16	231	30	15	15
16	210	38	19	19	141	30	15	15
17	283	42	21	21	254	38	19	19
18	270	46	23	23	246	38	19	19
19	227	42	20	22	238	45	22	23
20	248	44	22	22	233	50	25	25
21	235	50	25	25	226	39	19	20
22	258	48	24	24	204	50	25	25
23	227	48	24	24	191	52	26	26
24	215	44	22	22	172	50	25	25
25	264	50	25	25	225	44	22	22
26	297	44	22	22	240	50	25	25
27	290	-	-	-	254	-	-	-
28	225	-	-	-	226	-	-	-
Total	5976	967	476	491	5446	920	459	461

Table 2.1. Number of phenotyped animals (N) by line and generation, and the number of animals chosen as effective breeders (N_b), separately shown for male (N_m) and female (N_f).

	Male					Female				
		Best Running Distance (meters)		Body Weight (grams)			Best Running Distance (meters)		Body Weight (grams)	
Gen	n†	Mean	SD	Mean	SD	n†	Mean	SD	Mean	SD
1	57	529.0	244.3	265.7	27.5	59	564.7	224.3	181.2	20.7
2	82	495.3	201.9	271.3	29.0	55	652.2	263.0	174.2	16.7
3	74	630.4	215.1	258.2	29.3	86	721.9	248.5	175.0	18.3
4	64	611.3	190.2	261.4	25.4	67	784.3	270.4	176.0	15.9
5	86	661.6	218.0	252.9	26.2	65	812.9	270.0	171.9	14.2
6	79	769.9	220.0	250.6	28.2	72	916.5	271.1	169.7	13.4
7	67	722.6	305.7	274.5	34.5	66	1116.2	420.6	174.4	17.9
8	96	543.7	313.0	263.9	35.4	89	795.8	420.8	174.1	15.7
9	118	600.0	272.8	257.4	29.3	116	889.2	381.9	172.3	17.0
10	140	799.0	261.6	257.7	32.6	98	1018.7	308.0	172.3	17.5
11	92	641.2	281.3	246.2	30.5	110	849.3	314.0	164.5	17.6
12	90	756.1	348.6	251.3	27.1	105	883.5	528.5	166.4	16.0
13	134	729.4	386.5	236.8	28.6	106	1024.2	651.6	158.8	19.1
14	112	1243.2	443.2	220.9	32.2	110	1703.6	602.7	154.9	16.2
15	122	1667.0	284.5	221.0	28.5	110	2023.8	424.5	152.1	15.1
16	106	1476.0	253.0	224.1	25.1	104	1475.0	236.9	158.0	17.2
17	146	1509.2	248.9	227.4	28.1	137	1595.6	264.7	157.4	17.8
18	149	1540.9	241.1	220.8	29.4	121	1658.5	256.4	156.5	17.5
19	126	1669.0	271.8	225.7	26.2	101	1787.4	263.0	160.1	15.4
20	135	1579.2	246.0	233.7	26.0	113	1661.3	233.2	156.6	15.0
21	115	1834.0	306.7	233.1	27.1	120	1934.1	291.0	160.2	14.6
22	140	1729.6	250.1	254.2	28.2	118	1902.0	279.5	167.8	16.0
23	122	1697.3	279.0	254.0	31.0	105	1867.1	290.6	173.5	16.8
24	110	1649.4	226.5	258.0	25.7	105	1834.2	264.9	173.8	18.5
25	124	1657.0	279.2	257.7	25.2	140	1913.6	258.5	172.5	15.2
26	168	1834.9	277.7	251.8	23.1	129	2053.1	357.0	163.5	12.1
27	145	2000.7	364.3	246.3	26.3	145	2295.2	392.6	163.8	14.8
28	112	1810.4	269.6	261.4	26.1	113	2108.6	297.5	169.1	14.0

Table 2.2: Summary of cohort size, running distance, and body weight by gender and by generation for HCRs.

	Male					Female				
		Best Running Distance (meters)		Body Weight (grams)			Best Running Distance (meters)		Body Weight (grams)	
Gen	n†	Mean	SD	Mean	SD	n†	Mean	SD	Mean	SD
1	61	372.3	157.1	280.6	29.0	64	421.1	176.7	178.3	17.2
2	58	268.7	116.4	296.7	31.2	68	333.8	123.6	187.5	12.9
3	86	309.5	119.5	287.3	34.2	81	325.3	96.2	186.3	17.2
4	72	302.6	89.2	297.6	27.8	66	366.9	106.0	194.7	16.0
5	58	252.4	73.0	299.9	38.4	92	326.1	104.9	194.7	19.1
6	74	281.7	73.0	293.8	31.1	81	333.9	108.8	195.7	19.2
7	78	263.0	139.2	312.7	29.5	63	356.3	150.3	203.8	17.6
8	70	157.7	93.4	313.6	24.2	73	259.6	104.8	209.4	23.9
9	95	171.7	65.3	320.8	39.3	103	260.3	81.8	205.5	20.6
10	76	167.3	94.4	321.9	25.6	74	245.0	88.5	213.8	18.8
11	124	156.5	60.9	318.6	38.7	121	217.7	72.4	207.2	20.8
12	98	182.8	90.6	321.4	36.5	104	267.9	102.8	211.9	21.5
13	109	150.4	51.6	336.2	31.5	107	215.2	69.5	216.9	16.7
14	98	205.8	57.8	304.2	32.6	111	266.4	78.4	207.2	20.9
15	111	240.3	75.9	318.3	40.4	120	318.7	102.7	214.4	21.4
16	63	303.2	69.3	314.3	29.9	78	370.0	107.3	208.0	28.0
17	127	318.3	75.6	316.8	35.5	127	367.4	87.2	203.8	19.4
18	127	282.6	58.2	323.5	32.8	119	374.6	69.3	202.7	18.0
19	123	281.3	78.4	327.7	32.1	115	363.9	92.0	213.6	19.1
20	113	272.3	64.0	326.7	29.2	120	330.7	87.3	208.0	19.4
21	112	291.3	90.4	336.3	30.7	114	356.3	83.8	203.9	19.2
22	99	328.9	63.6	335.1	30.8	105	389.2	65.8	202.3	16.6
23	103	248.3	38.0	339.8	32.3	88	322.5	45.7	210.8	17.6
24	88	238.1	30.1	354.9	24.3	84	308.9	47.0	214.8	19.2
25	115	228.0	65.2	340.6	33.2	110	346.5	73.3	205.3	17.7
26	117	201.7	45.1	327.0	50.3	123	305.3	49.4	206.2	19.4
27	135	217.8	49.6	331.6	31.7	119	309.3	64.1	206.4	14.4
28	115	191.8	42.9	328.2	31.5	111	278.3	45.8	208.6	16.7

Table 2.3: Summary of cohort size, running distance, and body weight by gender and by generation for LCRs.

CHAPTER 3

Selection-, Age-, and Exercise-Dependence of Skeletal Muscle Gene Expression Patterns

3.1 Introduction

Researchers at the University of Michigan recently showed that an increased capacity for skeletal muscle fatty acid and branched chain amino acid oxidation underlies the higher oxidative capacity in these animals (Overmyer et al., 2014). As in humans, the enhanced oxidative capacity of the HCR compared to the LCR is paralleled by increases in lifespan, with the median age of death increasing from 23.5 months for LCR to 30.1 months for HCR rats, representing a 28% difference in life expectancy, with no significant difference for maximal lifespan between females and males within lines. In as early as Generation-7 of selection, HCR displayed significantly greater O_2 utilization in the skeletal muscles (Howlett et al. 2003). Continued selective breeding up to generation 15 resulted in further divergence in O_2 utilization as well as O_2 delivery in the skeletal muscle (Howlett et al. 2009). An initial gene expression analysis of the skeletal muscle from HCR and LCR at generation 18 revealed significant differences for genes in the pathways of oxidative energy metabolism, including fat metabolism, branched-chain amino acid metabolism, Krebs cycle, and oxidative phosphorylation (Kivelä et al. 2010). A subsequent study that looked at gene expression in skeletal muscle of HCR and LCR at generation 16 found that HCR up-regulated genes involved in lipid

metabolism and fatty acid elongation compared to LCR in exercise-trained rats, while the sedentary rats only showed minor differences in gene expression between the two lines (Bye et al. 2008). The differences in gene expression were found to be consistent with results from proteomic analysis of skeletal muscle mitochondria (Overmyer et al., 2014) which showed similar pathways enriched in HCR vs. HCR.

It has long been appreciated that biological regulation, in this case transcript levels, are affected by inherited genetic variation, naturally occurring aging process, as well as responses to immediate physiological stressors. These factors often act jointly but have not been analyzed simultaneously in a single study. Here I analyzed the transcriptomic profiles of both young and aged female rats from generations 29 and 32, and under both resting and exercise conditions, with the goal of identifying pathways that could explain the divergence in aerobic capacity, longevity, and adaptation to exercise.

3.2 Methods

3.2.1 Ethics statement

This study was approved by the University Committee on Use and Care of Animals, Ann Arbor, Michigan (Approval Numbers: #08905 and #03797). The proposed animal use procedures are in compliance with University guidelines, and State and Federal regulations.

3.2.2 Animals

I used old (~84-93 weeks of age) and young (~12-20 weeks of age) rats from HCR and LCR generations 29 and 32, respectively. The study included eight groups;

HCR-Old-Exhausted (H-O-E, n=6), HCR-Old-Rest (H-O-R, n=6), HCR-Young-Exhausted (H-Y-E, n=6), HCR- Young -Rest (H-Y-R, n=6), LCR-Old-Exhausted (L-O-E, n=6), LCR-Old-Rest (L-O-R, n=6), LCR-Young-Exhausted (L-Y-E, n=6), and LCR-Young -Rest (L-Y-R, n=6). For the exhausted rats, dissections were performed within 10 min after the maximal running distance was reached.

3.2.3 Tissue and RNA extraction

We extracted skeletal muscle RNA from a total of 48 female animals (n=6 in each of the 8 group). Skeletal muscle tissue was obtained from the *Extensor digitorum longus* (EDL). All rats were dissected immediately after sacrificing, and all tissue samples were immediately weighed, snap frozen in liquid nitrogen, and stored at -80C. Total RNA was extracted from frozen tissue with a Trizol reagent (Invitrogen) and purified with an RNAse kit (Ambion).

3.2.4 Gene expression microarray

We ran the skeletal muscle RNA on the Affymetrix Rat Gene ST 2.1 array. The microarray hybridizations were performed by the DNA sequencing core at the University of Michigan according to the manufacturer's instructions. We used the Affymetrix Expression Console^{TM} software to generate gene expression values from individual probe intensity (CEL) files. The microarray yielded a total of 19,607 transcript expression values.

3.2.5 Gene expression data analysis

Data analysis were performed with an R software environment for statistical computing (R Development Core Team 2010). The data were normalized with quantile normalization. Principal component analysis was performed using the *prcomp* function.

The Euclidean distance between clusters was calculated with the *dist* function using the median expression values of each gene. Statistically significant differences in gene expression between test groups were tested using multiple regression with the *lm* function.

For the main effect analyses, I implemented the regression models:

exp ~ line + age + exercise

exp ~ line (for old and exhausted; edge 2)

exp ~ line (for young and exhausted; edge 4)

exp ~ line (for old and rest; edge 6)

exp ~ line (for young and rest; edge 8)

exp ~ age (for HCR and exhausted; edge 1)

exp ~ age (for LCR and exhausted; edge 3)

exp ~ age (for HCR and rest; edge 5)

exp ~ age (for LCR and rest; edge 7)

exp ~ exercise (for HCR and old; edge 9)

exp ~ exercise (for HCR and young; edge10)

exp ~ exercise (for LCR and old; edge 11)

exp ~ exercise (for LCR and young; edge 12)

For the interaction effect analysis, I implemented the regression models:

exp ~ line + age + line*age (for exhausted; top)

exp ~ line + age + line*age (for rest; bottom)

exp ~ line + exercise + line*exercise (for old; left)

exp ~ line + exercise + line*exercise (for young; right)

exp ~ age + exercise + age*exercise (for HCR; back)

exp ~ age + exercise + age*exercise (for LCR; front)

3.2.6 Pathway analysis

Pathway enrichment tests were performed using *LRpath* (Sartor et al. 2009) for all ~20K genes, p-values, and fold-change levels for each of the 12 comparisons. I tested for enrichment of Gene Ontology (GO) terms and Kyoto Encyclopaedia of Genes and Genomes (KEGG) pathways for the rat. *LRpath* allows us to perform both unidirectional and directional analyses; for unidirectional analysis, *LRpath* tests for gene sets that have significantly higher significance values than expected at random given a set of genes and p-values; for directional analysis, *LRpath* tests up- and down-regulated genes simultaneously given a set of genes, p-values, and fold-change between test groups to distinguish between up and down regulated gene groups.

3.3 Results

Our study adopted a 2×2×2 full factorial design to simultaneously examine the effects of three factors: HCR-LCR, aging (Old-Young), exercise (Rest-Exhaustion), and their interactions. Here “Young" animals are of age 31.1 ± 2.6 weeks and “Old” are 99.4 ± 2.9 weeks. Among the young animals, HCRs and LCRs show 8.5-fold difference in their maximal running capacity. Compared to the young, running performance in old animals declined by ~50% in both lines, and the HCR-LCR difference remained at 8.9-fold. Within each age group in either line there was not a significant correlation between age and maximal running distance. For three factors and two levels each, there are eight experimental combinations. In each combination I measured the skeletal muscle

(extensor digitorum longus, EDL) samples of six animals as biological replicates. Tissues from "Exhaust" animals were obtained immediately (<10 mins) after the run-to-exhaustion test. In all, we measured 19,607 transcripts in 48 samples in a single batch of microarray experiments.

3.3.1 Global patterns

A principal component analysis (PCA) of the 19,607 measured transcripts separates the 48 samples into eight clusters in the PC1-PC2 space; and they correspond to the eight known groups, as marked by the colored ellipsoids (Figure 3.1). The eight clusters occupy mostly non-overlapping areas in the PC1-PC2 space. While a few of the clusters are close to each other, most are "coherent" and have gaps of varying sizes to the nearest cluster. Thus, at the global level there are observable transcriptional effects for all three factors. PC1 is mainly driven by the Old-Young differences, while both PC2 and PC3 are driven by HCR-LCR and exercise effects (Figure 3.1).

As a 2×2×2 design can be naturally displayed as a cube, I overlaid a hexahedron, i.e., an irregular, "stretched" cube, in Figure 3.1 to connect the median expression patterns of the eight groups. Note that this hexahedron is not a quantitative representation of the high-dimension gene expression profiles, nor the between-cluster distances in their reduced two-dimensional view, but only a geographic illustration of the relationships among the experiment groups. This representation has six quadrilateral faces (or planes) forming three opposing pairs, each representing the two levels of a given factor. For example, the left and right faces represent the Old and Young animals, respectively, whereas the top and bottom faces represent Exhaust and Rest

groups, respectively. The stretched cube has eight vertices, representing the centroid of the eight experimental groups; and its twelve edges represent the twelve two-way contrasts, each representing the main effect of a given factor in one of the four strata formed by the other two factors. In Figure 3.2, I used a three-letter shorthand to indicate the eight vertices, where "H" and "L" denote "HCR" and "LCR", respectively, "O" and "Y" denote "Old" and "Young", respectively, and "R" and "E" denote "Rest" and "Exhaust", respectively. For example, the upper left vertex of the front face, "L-O-E", is for the Old, LCR animals measured at Exhaustion. The set of four quasiparallel edges connecting a pair of opposing faces are shown as arrows of the same color: red for HCR-LCR, purple for Old-Young, and black for Rest-Exhaust. The twelve edges were also numbered 1-12 for ease of description. For example, Edge-2, from L-O-E to H-O-E, is the HCR-to-LCR difference for Old and Exhausted animals. This contrast is also written as (HCR-LCR|Old, Exhausted) in Figure 3, where "|" is the mathematical notation of "conditional on", indicating the specific strata in which the contrast in defined.

Globally, the eight clusters form a well-proportioned convex cube, indicating that each of the three factors has a main effect, that the effects are comparable among the line, age, and exercise factors, and that they jointly determine the observed gene expression pattern. Further, the effects are not strictly additive (or independent). If they were, i.e., if there was no interaction among the factors, all six faces would be parallelograms, i.e., formed by parallel edges of equal lengths, and the opposing faces would form parallel pairs of planes. If this were the case, with suitable rotation of the PC axes the six faces could all be transformed to rectangles. However, the observed hexahedron is not a cuboid: it contains unparalleled faces and unparalleled edges; and

in most faces, the opposing edges are of unequal length, indicating that the effect of any one factor depends on the specific combination of the levels of the other factors: the classic definition of statistical interaction. My simultaneous analyses of the three factors thus revealed both main effects and their interactions, as examined in more detail below.

I calculated the genomic distance along the twelve edges using all 19,607 transcripts, and in the cube display, varied the line widths to be proportional to the genomic distance (Figure 3.2). This way, a thicker line indicates a larger contrast (or distance), thus providing a different, but analogous, visual representation as the stretched cube shown in Figure 3.1, where it was the line lengths that represent the effect size along individual edges. Figure 3.2 used the Euclidean distance as line width; the numeric values were shown in Figures 3.3. Alternative distance measures, such as the median absolute difference (MAD) between pairs of group centroids, yield similar results: the Pearson's correlation coefficient (r) between MAD and Euclidean values is 0.91 across the 12 conditions. In the following I will describe the analysis of the three factors, one at a time, before describing the analysis of two-factor interactions.

3.3.2 Between-line differences (HCR vs. LCR)

For each gene I assessed the HCR-LCR main effect overall, corresponding to the transcriptomic differences between the two genetic lines, averaged over Old-Young and Rest-Exhaust conditions. In the geographic representation this corresponds to the distance between the center of the HCR face (the back plane of the cube) to the center of the LCR face (front plane). The effect size reflects the transcriptomic consequence after divergent selection for aerobic running capacity. In all, 2,838 transcripts are

significantly difference at Benjamini-Hochberg False Discovery Rate (BH-FDR) < 0.05. The pathway analysis of these genes will be described in a later section.

I next analyzed the HCR-LCR difference separately for each of the four age-exercise combinations. Across the four strata, Old-Rest has the largest line contrasts, while Young-Rest has the smallest. This can be interpreted from two perspectives. First, *the HCR-LCR effect at Rest is age-dependent*: the lengths of Edge-6 and Edge-8, defined as Euclidean distance over all measured genes, are 36.6 and 29.2, respectively, indicating a stronger between-line difference in the Old animals (Figure 3.3a). In contrast to Rest, this age dependence of line effect is much reduced at Exhaustion: the lengths of Edge-4 and Edge-2 are 32.9 and 33.4, respectively, nearly the same between the Old and Young animals. From the second but equivalent perspective, *the HCR-LCR difference for Young animals depends on the exercise state*: it is greater at Exhaustion (Edge-4 vs. Edge-8; 32.9 vs. 29.2), but conversely, for Old animals the HCR-LCR difference is greater at Rest (Edge-2 vs. Edge-6; 33.4 vs. 36.6).

3.3.3 Exercise effects (Exhaustion vs. Rest)

Next, I assessed the Exhausted-Rest main effect averaged over the HCR-LCR and Old-Young conditions. This corresponds to the distance between the center of the Exhausted face (top of the cube) to the center of the Rest face (bottom of the cube). The effect size reflects the transcriptomic adaptation after an endurance run. In all, 1,715 transcripts are significantly difference at BH-FDR < 0.05 (Supplementary Table 1). The pathway analysis of these genes will be described below.

I then analyzed the Exhausted-Rest difference separately for each of the four line-age combinations. Across the four strata, HCR-Young has the largest line contrasts

whereas LCR-Young has the smallest. At Young age, the Exhausted-Rest effect is line-dependent: the lengths of Edge-10 and Edge-12 are 38.0 and 28.4, respectively, indicating a stronger exercise difference in the HCR animals (Figure 3.3b), which may reflect the longer exercise-related stimulus in the HCR due to the enhanced running capacity in the HCRs compared to LCRs. This line-dependence of exercise effect is much reduced when measured in Old animals: the lengths of Edge-9 and Edge-11 are 33.1 and 32.5, respectively. In an alternative view, the age-dependence of exercise effect varies by line: in HCR it is greater for Young animals (Edge-10 vs. Edge-9; 38.0 vs. 33.1); but conversely, in LCR the exercise difference is greater for Old animals (Edge-11 vs. Edge-12; 32.5 vs. 28.4).

3.3.4 Aging effects (Old vs. Young)

The Old-Young main effect, averaged over HCR-LCR and Exhausted-Rest conditions, corresponds to the distance between the center of the Old face (left plane of the cube) to the center of the Young face (right plane). The effect size reflects the transcriptomic changes during the aging process. In all, 2,561 genes are significantly different at BH-FDR < 0.05 (Supplementary Table 1). The pathway analysis of these genes will be described below.

Again, I analyzed the Old-Young difference separately for each of the four line-exercise combinations. Across the four strata, LCR-Rest has the largest line contrasts whereas HCR-Rest has the smallest. At Rest, the Old-Young effect is line-dependent: the lengths of Edge-5 and Edge-7 are 31.0 and 39.1, respectively, indicating a stronger age difference in the LCR animals (Figure 3.3c). This line dependence of age effect is much reduced when measured at Exhaustion: the lengths of Edge-1 and Edge-3 are

32.4 and 33.8, respectively. In an alternative view, the Old-Young difference for HCR is slightly greater for Exhausted animals (Edge-1 vs. Edge-5; 32.4 vs. 31.0), but conversely, for LCR the age difference is greater for Rest animals (Edge-3 vs. Edge-7; 33.8 vs. 39.1).

3.3.5 Pathway analyses of the three factors

The three overall comparisons, for the main effects of line, age, and exercise, respectively, implicated many biological pathways, of which I focus on five most strongly affected. These non-overlapping Gene Ontology pathways are: *Mitochondria Part*, *Extracellular Matrix*, *Collagen Fibril Organization*, *Focal Adhesion*, and *Sequence-Specific DNA Binding Transcription Factor Activity* (Table 3,1). Stratified analysis of each of the three effects in the four combinations of the other two factors, as shown by the twelve edges in Figure 3.1, showed largely consistent patterns as the overall effects (Table 3.2 and Figure 3.4).

For the line effect, HCR consistently shows up-regulated *Mitochondria Part* pathway compared to LCR (Edges-2, 4, 6 and 8) (Figure 3.3a).

For the age effect, old rats consistently show down-regulation in *Extracellular Matrix*, *Collagen Fibril Organization*, and *Focal Adhesion* pathways compared to young (Edges-1, 3, 5, 7) (Figure 3.3b). Further, aging in LCR (sides 3 and 7) results in more significant enrichment for all three pathways compared to HCR (sides 1 and 5) (Table 3.2).

For the exercise effect, exhausted rats consistently show up-regulated *Sequence-Specific DNA Binding Transcription Factor Activity* pathway compared to rats at rest (Edges-9, 10, 11, 12) (Figure 3.3c).

3.3.6 Interaction effects

For each face of the cube, I assessed the interaction between two factors while keeping one factor constant (front=LCR; back=HCR; top=Exhausted; bottom=Rest; left=Old; right=Young), for a total of six analyses. At the threshold of $p < 0.001$, the number of significant genes are 15, 67, 141, 113, 79, and 60 genes for the top, bottom, left, right, front, and back analysis, respectively, with the middle two comparisons showing the largest effect. At the threshold of FDR < 0.1 the trend is similar, with 0, 2, 56, 64, 1, 1 genes in the six comparisons, again with the left-Old and right-Young showing the greatest number of significant interactions. I therefore focused on these two "planes" of the cube, asking: what are the patterns of the 141 (or 113) genes among the four groups? That is, what type of non-additive effects are driving the observed statistical interactions?

For the left plane, I extracted the expression data for the 141 genes with $p < 0.001$ for the 24 Old animals, and performed unsupervised hierarchical clustering of the 141-by-24 data matrix (Figure 3.4a). From left to right are the 24 animals: with the exception of animal #15, they are clustered into four known groups: LCR and HCR for Rest, and LCR and HCR for Exhaust. From top to bottom are the 141 genes that formed three clusters, with 32, 19, and 90 genes respectively. The dendrogram is built using the standardized data, i.e., each gene is centered across the 24 samples and scaled to have the same standard deviation. The unscaled data, showing in the heatmap in the middle panel, showed that some genes have much larger variance than other genes. I used *DAVID* to test if any pathways are enriched in the three gene clusters. As shown in the right panel, the first and second clusters are enriched for

Phosphatidate Phosphatase Activity (p-value=1.3E-2) and *Response to Toxin* (p-value =1.9E-3), respectively. The heatmap shows that they have higher expression for HCR at Exhaustion and, to a lesser extent, LCR at Rest, thus breaking the additive effects of Line and Exercise. It also suggests that for these pathways, the LCR animals at rest are "pre-exhausted". The third cluster, enriched for *Cytoskeletal protein binding I* (p-value = 5.5E-3), shows the opposite trend: higher expression in HCR at Rest and LCR at Exhaustion, as if the HCR animals have pre-activated these genes even at rest, while the LCR's do not activate them until exhausted.

Similarly, for the right plane, I extracted the data for the 113 genes with $p < 0.001$ for the 24 Young animals, and performed unsupervised hierarchical clustering (Figure 3.4b). Once again, the 24 animals are perfectly clustered into four known groups, and the 113 genes formed four clusters with, from top to bottom, 55, 20, 25, and 13 genes. The first and fourth clusters, enriched for *Response to protein stimulus* (p-value=1.5E-5) and *Plasma membrane* (p-value2.6E-3), respectively, show opposite patterns: with HCR at Exhaustion to be different from the other three groups, thus breaking the additive effects and driving the interaction. The second cluster show higher expression levels for HCR at rest and LCR at Exhaustion and is enriched for *Regulation of RNA metabolic process* (p-value=5.1E-4). The third cluster show the opposite pattern as Cluster 2, with lower expression levels for HCR at rest and LCR at Exhaustion. It does not have a clear pathway enrichment signal.

3.4 Discussion

The ability to evaluate three main effects (genetic background, exercise, aging) jointly and uncover interactions between them in a rat model is a novel contribution of this study. The HCR-LCR difference is driven by mitochondrial pathways during both exercise and rest (Table 3.1). According to both the GO Biological Processes and the KEGG Pathways, genes involved with mitochondria are associated with substrate metabolism and oxidative metabolism, including *Branched chain amino acid metabolism*, *Fatty Acid metabolism*, *Oxidative Phosphorylation* and *Tricarboxylic Acid cycle (TCA) metabolism*. These genes are expressed significantly higher in HCR muscle, as has been previously reported (Kivela et al. 2010). We have recently found that the up-regulation of these pathways increases the capacity for non-glucose fuel utilization in the HCR and LCR rats, delaying the 'lactate threshold' associated with glycolysis-mediated ATP production (Overmyer et al., 2014).

When at rest, the HCR-LCR difference is far greater for old rats than the young (Fig. 3.3a). This reflects a relative slowing of aging in HCR and is entirely consistent with the reported longevity difference between HCR and LCR (Koch et al. 2011). Interestingly, this age-dependent difference disappears for the exhausted rats. The difference between HCR-LCR is the strongest for young rats and at rest, perhaps due to their intrinsic expression differences for mitochondrial genes (Table 3.1). The larger HCR-LCR difference at exhaustion may be due to the up-regulation of the same exercise-related gene sets for both genetic backgrounds. The exhausted-rest difference is driven by the transcription activity pathway; with exhausted animals showing up-regulated transcription activity.

Between the exhaustion and rest rats, the difference is greatest for the young HCRs, and weakest for young LCRs (Fig. 3.3b). The associated genes are largely transcription factors and cofactors that are associated with muscle development or known to be responsive to exercise, and similar trends have previously been observed in trained human muscles (Cary and Guan 1999). These gene expression differences in HCR and LCR may simply be attributable to exercise duration, as HCRs run on average 9-fold longer that LCRs (Ren et al. 2013).

The old-young difference is driven by the extracellular matrix (ECM), collagen, and adhesion pathways in both HCRs and LCRs during both exercise and rest (Table 3.1). When at rest, the old-young difference is far more prominent for LCRs compared to HCRs (Fig. 3.3c). In addition, age-effects in the aging indicator pathways are more pronounced in the LCRs compared to the HCRs (Table 3.3). As mammals age, the amount of collagen in the muscle increases, which results in muscle stiffness and reduced muscle function (Haus et al. 2007). The collagen-related pathways are down-regulated in the old rats compared to the young rats. This finding is similar to those from a previous meta-analysis across humans and rodents for gene expression data among aging groups, in which the researchers also found collagen gene sets to be under-expressed with age, and explain it by reduced collagen deposition with aging (de Magalhaes et al. 2009).

3.6 Figures

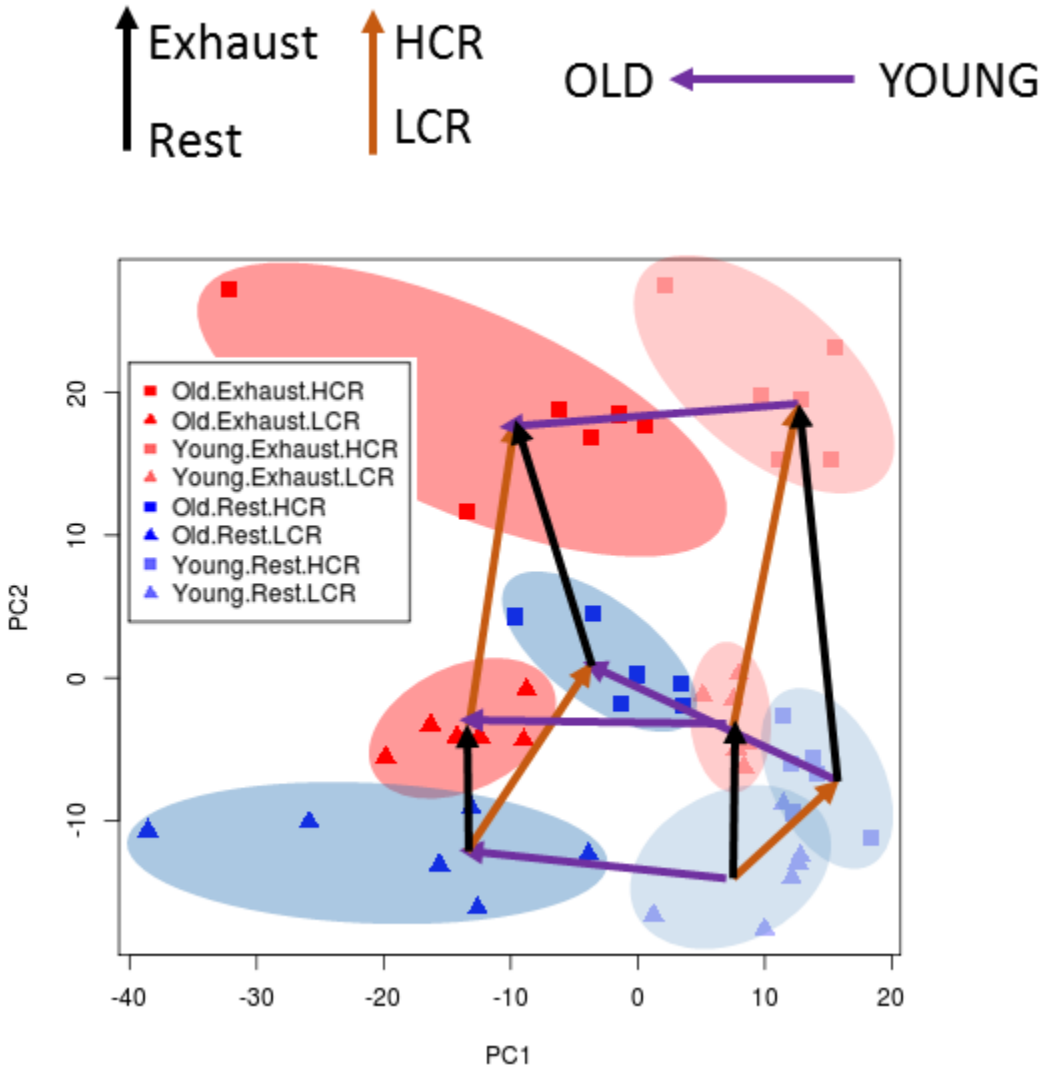

Figure 3.1: **Principal component analysis (PCA) plot (PC1 vs PC2) for 48 rats across the expression of ~20K transcripts**.

The samples are divided across 8 different groups in a 2×2×2 design to compare HCR and LCR, aged and young, and between rest and exhaustion (n=6 each). Groups are highlighted using different colored ovals to show clustering, and HCR-LCR are shown as squares and triangles, respectively. All of the exhausted animals are red, and animals at rest are blue. Old animals are shown as dark red/blue, and young animals are shown as light red/blue. Arrows are drawn from each cluster to show the direction of each group variable; purple arrows show direction of old-young animals; orange arrows show direction of HCR-LCR; black arrows show direction of exhaust-rest.

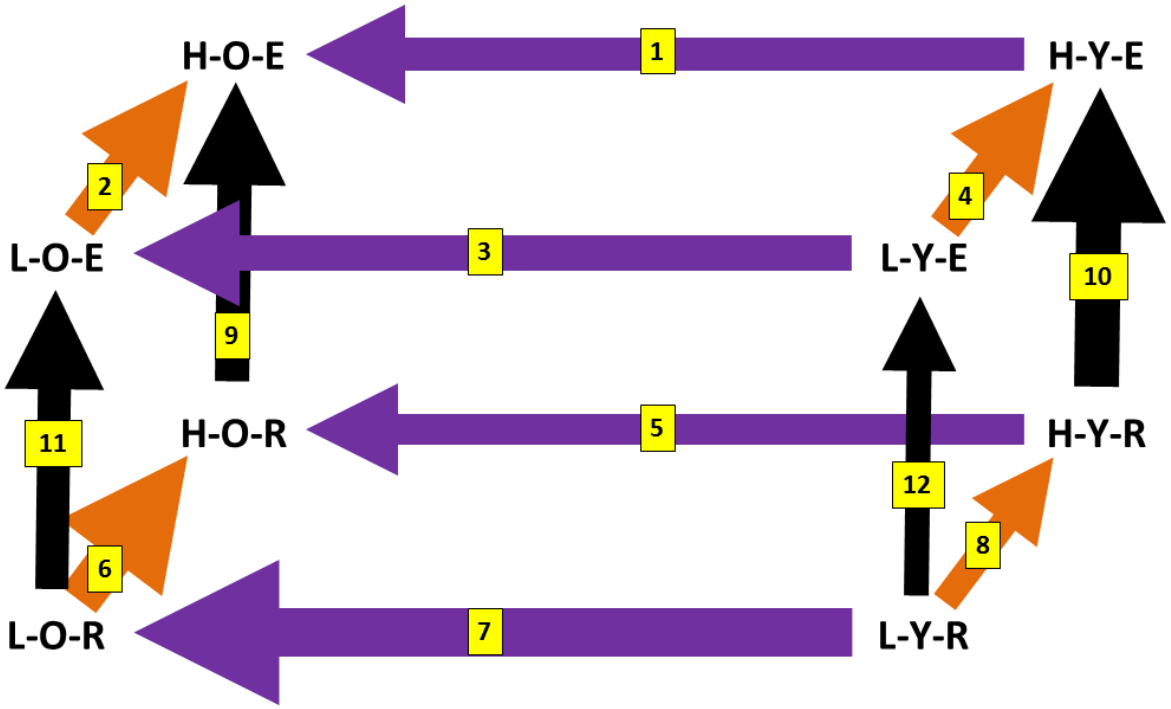

Figure 3.2: Cube depiction of the PCA plot in Figure 3.1.

Each group is represented by their abbreviated names (HCR/LCR = H/L, old/young = O/Y, exhaust/rest = E/R). The arrow color scheme is the same as Figure 1. (A) The numbers beside each arrow represents the Euclidean distance calculated using all ~20K transcripts, with larger numbers representing more distant groups in terms of skeletal muscle transcriptome. (B) The numbers on each arrow represent the denotation of the analysis (between 1-12) that will be referred to in the manuscript, and the thickness of each arrow represents the Euclidean distance for each side.

a

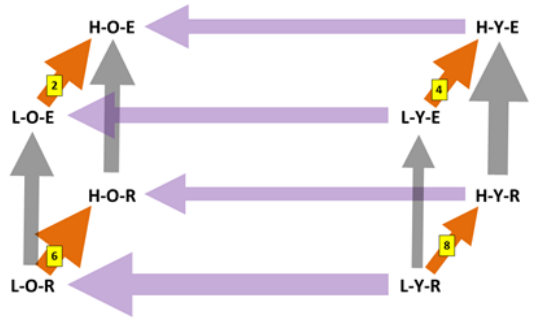

Side	Comparison	Euclidean Distance
2	HCR-LCR | Old,Exhausted	33.4
4	HCR-LCR | Young,Exhausted	32.9
6	HCR-LCR | Old,Rest	36.6
8	HCR-LCR | Young,Rest	29.2

b

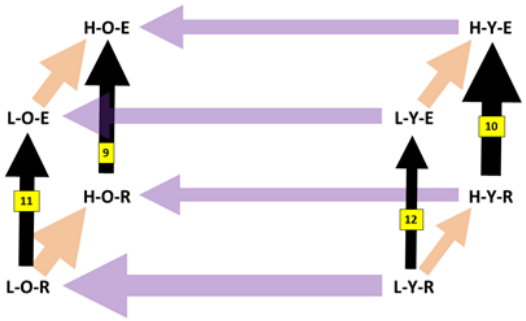

Side	Comparison	Euclidean Distance
9	Exhausted-Rest | HCR,Old	33.1
10	Exhausted-Rest | HCR,Young	38.1
11	Exhausted-Rest | LCR,Old	32.5
12	Exhausted-Rest | LCR,Young	28.4

c

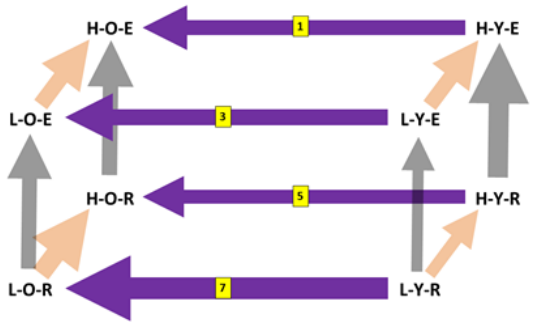

Side	Comparison	Euclidean Distance
1	Old-Young | HCR,Exhausted	32.4
3	Old-Young | LCR,Exhausted	33.8
5	Old-Young | HCR,Rest	31.0
7	Old-Young | LCR,Rest	39.1

Figure 3.3: **Euclidean distances between each sample group**.

(a) shown are the cube depiction and Euclidean distances focused on the effects of genetic background: differences between HCR and LCR (sides 2, 4, 6, and 8); (b) shown are the cube depiction and Euclidean distances focused on the effects of exercise: differences between exhaustion and rest (sides 9, 10, 11, and 12); (c) shown are the cube depiction and Euclidean distances focused on the effects of aging: old vs young (sides 1, 3, 5, and 7).

a

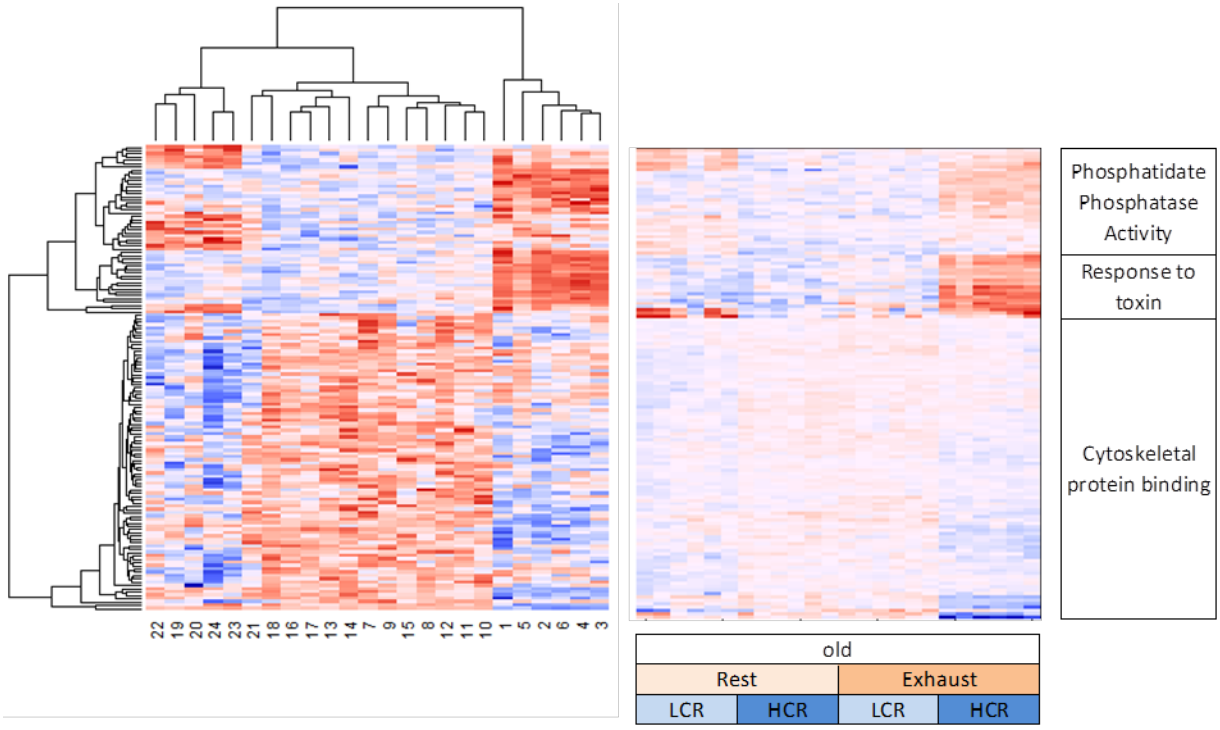
22 19 20 24 23 21 18 16 17 13 14 7 9 15 8 12 11 10 1 5 2 6 4 3
Phosphatidate Phosphatase Activity
Response to toxin
Cytoskeletal protein binding
old
Rest
Exhaust
LCR
HCR
LCR
HCR

b

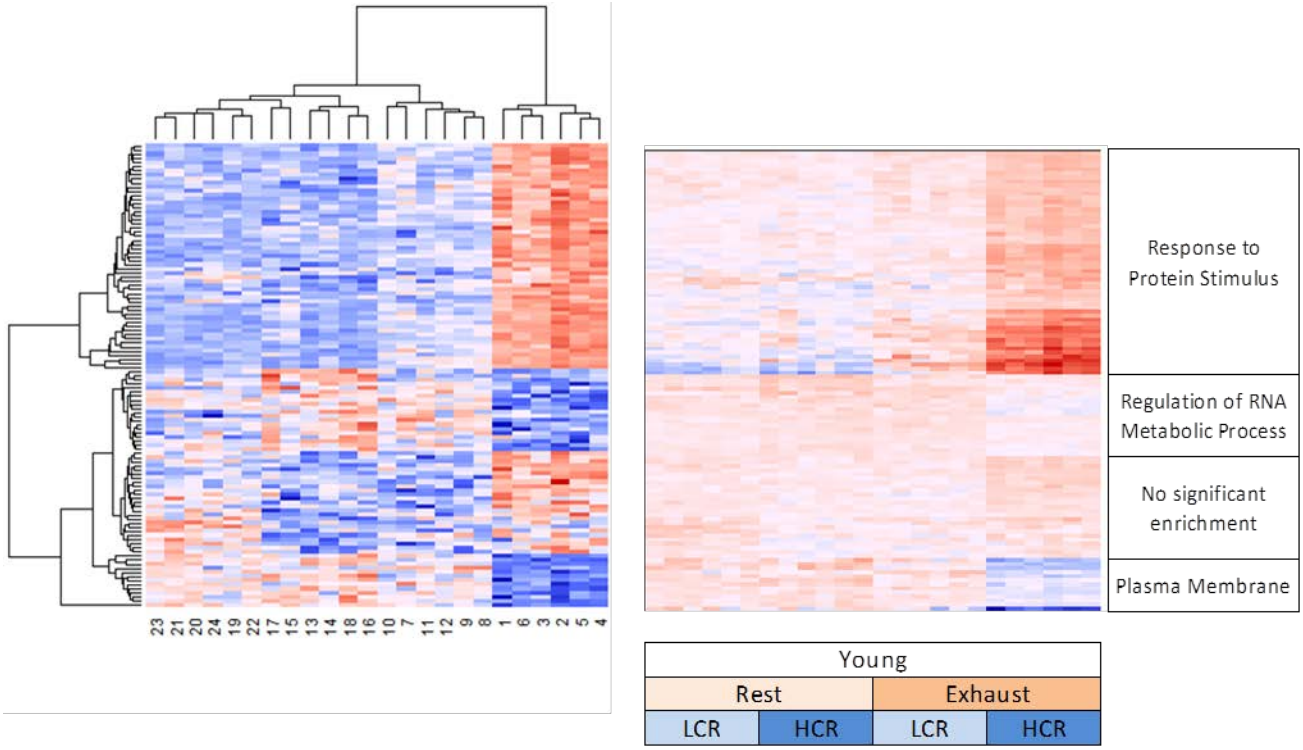
23 21 20 24 19 22 17 15 13 14 18 16 10 7 11 12 9 8 1 6 3 2 5 4
Response to Protein Stimulus
Regulation of RNA Metabolic Process
No significant enrichment
Plasma Membrane
Young
Rest
Exhaust
LCR
HCR
LCR
HCR

Figure 3.4: Heatmap of significantly (p<0.001) differentially expressed genes for for the interaction effects represented by the left and right faces of the cube from Figure 3.2

shown is the heatmap of the 141 significant genes for old animals on the left face of the cube (a) and the 113 significant genes for young animals on the right face of the cube. Each row shows the expression of a single gene across all samples, and the 24 samples for each face are ordered by group (shown at the bottom) across the columns. The genes are grouped into clusters based on hierarchical cluster. The heatmap is colored in a blue-red spectrum, with low expression shown in dark blue and high expression shown in dark red. The top enriched pathway of the sub-clusters of genes for each face are shown at the right.

3.7 Tables

Analysis	Comparison	Mitochondrial Part	Extracellular Matrix	Collagen Fibril Organization	Focal Adhesion	Sequence-Specific DNA Binding Transcription Factor Activity
Line	HCR-LCR	65.9	0.90	1.6	0.18	0.76
Age	Old-Young	0.07	55.1	25.0	16.9	6.9
Exercise	Exhaust-Rest	6.5	3.2	0.10	1.0	27.6

Table 3.1: -log(p-values) for the major pathway groups in the overall main effects of the three factors.

A heatmap is used to show the difference in significance levels; with green denoting greater significance and red denoting less significance.

Analysis	Comparison	Mitochondrial Part	Extracellular Matrix	Collagen Fibril Organization	Focal Adhesion	Sequence-Specific DNA Binding Transcription Factor Activity
Edge 2	HCR-LCR | Old,Exhausted	7.2	6.1	0.56	3.5	0.04
Edge 4	HCR-LCR | Young,Exhausted	34.4	1.3	1.0	3.7	0.10
Edge 6	HCR-LCR | Old,Rest	41.2	0.75	0.80	3.5	0.16
Edge 8	HCR-LCR | Young,Rest	58.9	17.2	8.7	0.42	2.7
Edge 1	Old-Young | HCR,Exhausted	4.1	27.1	13.1	4.6	2.0
Edge 3	Old-Young | LCR,Exhausted	4.7	50.5	20.2	20.1	1.4
Edge 5	Old-Young | HCR,Rest	0.86	18.0	12.5	2.9	11.1
Edge 7	Old-Young | LCR,Rest	1.1	33.9	19.5	14.8	4.5
Edge 9	Exhausted-Rest | HCR,Old	19.2	4.2	0.63	0.17	9.5
Edge 10	Exhausted-Rest | HCR,Young	7.0	7.7	1.1	0.10	17.3
Edge 11	Exhausted-Rest | LCR,Old	4.1	1.7	1.5	0.97	9.4
Edge 12	Exhausted-Rest | LCR,Young	4.0	0.56	0.26	3.6	24.0

Table 3.2: -log(p-values) for the major pathway groups in each main effect analysis.

A heatmap is used to show the difference in significance levels; with green denoting greater significance and red denoting less significance.

Edge	Comparison	Mitochondrial Part	Extracellular Matrix	Collagen Fibril Organization	Focal Adhesion	Sequence-Specific DNA Binding Transcription Factor Activity
2	HCR-LCR | Old,Exhausted					
4	HCR-LCR | Young,Exhausted					
6	HCR-LCR | Old,Rest					
8	HCR-LCR | Young,Rest					
1	Old-Young | HCR,Exhausted					
3	Old-Young | LCR,Exhausted					
5	Old-Young | HCR,Rest					
7	Old-Young | LCR,Rest					
9	Exhausted-Rest | HCR,Old					
10	Exhausted-Rest | HCR,Young					
11	Exhausted-Rest | LCR,Old					
12	Exhausted-Rest | LCR,Young					

Table 3.3: Directions of the major pathway groups.

Green arrows denote that the pathway was up-regulated for the control group compared to the test group in each analysis, and vice versa for red arrows (control groups are HCR, old, and exhaust; test groups are LCR, young, and rest). The thickness of the arrow indicates the significance of the pathway for the respective analysis; with a thicker arrow representing smaller p-values.

CHAPTER 4

High-Density SNP Array and Genome Sequencing Reveal Signatures of Selection in a Divergent Selection Rat Model for Aerobic Running Capacity

4.1 Introduction

After 32 generations of selection, the two lines differed by ~9-fold in AEC, and diverged in many other metabolic phenotypes and health indicators. Nearly 100 papers have been published on the "downstream" physiology of the HCR/LCR model, but the genetic basis of these remarkable phenotypic differences has not been established. I hypothesize that divergent trait selection in these two lines of rats may have resulted in selective sweeps with fixation/near fixation of variants that underlie the running capacity and associated metabolic and physiological traits. In this study, I used SNP genotyping and pooled whole-genome sequencing data from rats in both lines (HCR and LCR) and two non-adjacent generations (5 and 26) to identify signatures of selection. I implemented three different statistics as well as a composite score that combines the signals from the three statistics in an attempt to uncover swept genes/pathways. The test statistics I selected included 1) runs of homozygosity (ROH), which captures long stretches of homozygous variants that could be due to the "hitchhiking" effect near a region under positive selection; 2) fixation index (F_{st}), which captures increased genetic differentiation due to divergent selection (although it could also be due to random genetic drift); and 3) aberrant allele frequency spectrum (AFS), with which a region

under selection may show a local AFS that departs from the genome-wide AFS. Previous studies have proposed several methods of combining multiple selective sweep signals into a composite signal to improve the detection of true signatures of selection (Grossman et al. 2010, Utsunomiya et al. 2013, Randhawa et al. 2014). The basic rationale, as stated in Grossman et al., is that "*If each signature provides distinct information about selective sweeps, combining the signals should have greater power for localizing the source of selection than any single test.*" My method follows the same rationale.

Using the three related but unique test statistics, I identified gene sets and genomic windows that significantly diverged between time points during selection or between the two lines, and interpreted their potential roles in relation to the trait under selection as well as the other traits that diverged. The results therefore provide useful insight into the underlying genetic basis of intrinsic oxidative capacity and other metabolic and physiological phenotypes in our HCR-LCR rat model.

4.2 Methods

4.2.1 Study overview

The protocols of animal maintenance, phenotyping, and rotational breeding have been described previously (Koch and Britton 2001). The characterization of genetic structure, heritability, and linkage equilibrium using both pedigree and genotype data have also been published (Ren et al. 2013)(Chapter 2). This study was approved by the University Committee on Use and Care of Animals, Ann Arbor, Michigan (Approval

Numbers: #08905 and #03797). The proposed animal use procedures are in compliance with University guidelines, and State and Federal regulations.

4.2.2 Direction of comparisons

In this study, I focused on four sample groups, separated by line (HCR-LCR) and selection time (G5 and G26). Because I am interested in finding signatures of positive selection, the direction of comparisons is always HCR-minus-LCR and G26-minus-G5. Furthermore. HCR-LCR analyses will be referred to as ‘between-line’, while the G26-G5 analyses will be referred to as ‘temporal’. Given that our method is based on a two-tailed analysis, both directions have meaning. For example, strong positive selection signature in the HCR-LCR analysis would indicate positive selection that occurred in the HCR line, but not in the LCR. These would include the genomic regions under selective pressure as a consequence of the artificial selection for higher AEC. Inversely, strong negative selection signature in the HCR-LCR analysis would indicate positive selection that occurred uniquely in the LCR line. We currently do not know how to interpret these genomic regions, but it is possible that the LCR line experienced positive selection events not experienced by the HCR.

4.2.3 Genotyping data collection and quality control

I collected genotype data for four groups of rats, representing 10-12 breeders each from the two lines in two non-adjacent generations (G5 and G26, total n=45). Genomic DNA was extracted from frozen liver tissue, and genotyped across 803,484 SNP loci using a custom 800K rat SNP array (Baud et al. 2014). Attempts to extract DNA from generations earlier than G5 revealed that many samples in G0 and G4 were degraded. I therefore chose G5 as the earliest generation in our analysis due to its

assured DNA quality. During QC I removed 21,295 SNPs with genotype missing rate >10%. This step led to 782,189 “pass QC” SNPs, which were used in calculations of runs of homozygosity (ROH) and fixation index (F_{st}), described below.

4.2.4 Pooled whole-genome sequencing (WGS) and quality control

DNA for four sample groups, containing 10 female breeders each from the two lines and in two non-adjacent generations (G5 and G26, total n=40), was extracted from frozen liver tissue and sequenced for the whole-genome in four pools using the Illumina Hiseq system at the U-M DNA Sequencing Core. The reads were mapped to the rat reference genome RGSC-3.4 using the read alignment software *Burrows-Wheeler Alignment tool (BWA)* (Li and Durbin 2009). The average read depth for the four pools were 8.4 for HCR G5, 9.9 for HCR G26, 9.9 for LCR G5, and 9.2 for LCR G26. I made joint variant calls using Genome Analysis Toolkit (GATK) and obtained 8,909,190 single nucleotide variants (SNV) representing alternative alleles observed in at least one of the four pools (McKenna et al. 2010). I removed variants in each pool with read depth less than half of the pool-average. This step led to high-quality genotypes at 6,806,440 sites for HCR G5, 7,533,943 sites for HCR G26, 7,430,142 for LCR G5, and 7,218,598 for LCR G26. In all, there are 5,101,259 SNV sites with high-quality genotypes in all four pools, and these sites were used in the identification of genomic regions with aberrant allele frequency spectrum.

4.2.5 Identification of long runs of homozygosity (ROH)

ROHs for each group (HCR G5, HCR G26, LCR G5, LCR G26) were identified via *PLINK* using the pass-QC markers and the following parameters:

--homozyg-window-snp 50 --homozyg-window-missing 5 --homozyg-window-het 1 --homozyg-window-threshold .001 --homozyg-snp 25 --homozyg-kb 500

The first parameter means that the search is by sliding a moving window of 50 SNPs across the genome to detect long contiguous runs of homozygous genotypes. An occasional genotyping error or missing genotype occurring in an otherwise-unbroken homozygous segment could result in the under-calling of ROHs. To address this, I allowed five missing calls and one heterozygous call per window, as described by the second and third parameters. Each SNP is then assigned an ROH status (yes/no) based on the proportion of all the 50-SNP windows that overlap this SNP and that are called homozygous, which I have set to be 0.001. While the above parameters describe how to define sliding windows as ROH or not, the ROH windows are then merged into longer ROH segments, with the next two parameters used to set the thresholds for the minimum number of SNPs (25) and minimum length (500 kb) needed to be called an ROH segment. ROH windows that failed to meet these two thresholds would still be considered not an ROH. Note that given the SNP density of the array (about 290 SNPs per 1000 Kb), the 500 Kb threshold to be called an ROH is dominant over the 25 SNP threshold for all four groups.

After finding ROHs for each animal, I calculate the ROH frequency for each of the four groups across the entire genome , then I assigned an ROH score to each Refseq gene based on the average frequency of ROHs segments that overlapped its position for each group (a score of 1 indicates 100% of the individuals within that group have an ROH across that position). This is based on an un-weighted average of all ROH segments that overlap any part of the gene. I then calculated ΔROH for temporal

(G5 vs G26) and between-line (HCR vs LCR) comparisons, for a total of four analyses. The ΔROH value for every gene was ranked, and the fractional rank was transformed into a z-score via the inverse normal distribution. The z scores are used in constructing the composite scores described below.

4.2.6 Fixation index (F_{st})

F_{st} is a measure of genetic differentiation between two groups. It is constructed as the squared allele frequency difference between the two groups divided by a scaling factor, such that its range is from 0 (no differentiation) to 1 (complete differentiation, i.e., the two groups are fixed for different alleles). The formula for calculating F_{st} for each SNP is :

$$F_{st} = (x-y)^2/(4*avg*(1-avg))$$

where *x* and *y* are the allele frequencies of the two groups being compared, and *avg* is the average of *x* and *y* (Wright 1965). I calculated F_{st} for every SNP for temporal (G5 vs G26) and between-line (HCR vs LCR) comparisons , for a total of four analyses(an example is shown in Figure 4.1). I then assigned a score to each 1 Mb window as the 80^{th} percentile of the F_{st} values of the SNPs in that window (about 290 SNPs per window). I then assigned an F_{st} value to each gene based on the unweighted average F_{st} of the windows that overlapped its position. The per-gene F_{st} values are transformed as described below when constructing the composite scores.

4.2.7 Aberrant allele frequency spectrum (AFS)

AFS analysis requires fully ascertained variant sets; that is, all variants in a region as discovered by sequencing. For this reason, genotyping data that focus on pre-selected panels of SNPs are not suitable for characterizing AFS. To identify genomic

regions with aberrant AFS I collected pooled WGS data, and used the observed alternative allele fraction in the pool as the surrogate of the allele frequency in each of the four groups. The difference between a local AFS, in my case defined in 1 Mb windows, and the genomewide AFS, is quantified in a parametric test described by Nielsen and colleagues, implemented in the program *SweepFinder* (Nielsen et al. 2005). When a new beneficial mutation increases in frequency in a population because of positive selection, the standing genetic variation in its neighboring region on the same chromosome will also increase in frequency (i.e., selective sweep). The pattern of allele frequencies will be skewed. *Sweepfinder* tests whether a local AFS differs from the spectrum of the whole genome by calculating a maximum composite likelihood ratio (CLR) for each window. The CLR is the ratio of the likelihood of a selective sweep to the likelihood of no sweep given the observed AFS in a window and the genome-wide AFS. It outputs the CLR statistic as well as the parameter alpha (the strength of the sweep). After calculating the CLR for each of the four sequenced pools (an example is shown in Figure 4.1), I calculated ΔCLR for temporal (G5 vs G26) and between-line (HCR vs LCR) comparisons, for a total of four analyses, and then transformed the ΔCLR as described below when constructing the composite scores.

4.2.8 Composite score

The main challenge of detecting signatures of positive selection is that random genetic drift could also lead to apparent peaks in certain genomic regions in ΔROH, F_{st}, and ΔCLR values. As these statistics capture different aspects of the true signal, a composite score that combines the three statistics is more likely to highlight true signatures of selection above the background effects of genetic drift. In other words,

regions concordant across the three test statistics will show a high composite score, whereas those with conflicting signals may show reduced composite score that is closer to the genome-wide average. Several strategies for constructing such a composite score have been described previously in similar studies (Grossman et al. 2010, Utsunomiya et al. 2013). In my case, each of the constituent statistics had its distinct, non-normal distribution, I need to transform them individually to ensure that (1) the three statistics have comparable contributions to the composite score - if the variance of one statistics is far larger than those of the other two, it will dominate the final composite score, and (2) the specificity of a scan statistics, as reflected by how frequent and how strong the peaks are, should preferably be preserved as much as possible.

I developed a novel composite score that involves transforming the three statistics with different strategies.

- For ΔROH, the original scores are symmetrically distributed around 0, with a prominent peak in the middle (Figure 4.2a), and both tails are meaningful in that they capture the increase and decrease of ROH, respectively, in the comparison. I converted the fractional rank for every gene into a z-score based on the formula $z = \Phi^{-1}(r)$ where $\Phi^{-1}( )$ is the inverse normal cumulative distribution function and r is the fractional rank, defined as n/(N+1), where n is the rank of the gene and N is the total number of genes. The resulting z score is a standard normal distribution, N(0,1), as shown in Figure 4.2b. The directionality is preserved after the transformation as shown by the scatterplot (Figure 4.2c)
- For ΔCLR, the distribution is symmetrical around zero, with extremely strong outlier values(Figure 4.2d). To perform rank-based inverse normal

transformation as above would have dampened the contribution of these strong peaks. To allow the peaks to make suitably large contributions to the composite score I decided to apply a cubic-root ($x^{1/3}$) transformation. The resulting score, shown in Figure 4.2e, preserved the specificity of the strongest ΔCLRs. The directionality is preserved, and the majority of the observations fall near zero after the transformation (Figure 4.2f)

- For F_{st}, the original scores are all positive, where a larger score indicates a greater population differentiation, but it does not tell which population has experienced more changes. Further, the F_{st} 's fall in the range of (0, 0.33), and need to be scaled up to make comparable contributions as the other two scores (Figure 4.2g). To convert the one-tailed distribution into two-tailed, symmetrical distribution I attributed a sign to each F_{st} by borrowing information from the other statistics. Specifically, the assigned sign is equal to the sign of the summation of the other two transformed statistics: Z-score and $\Delta CLR^{1/3}$. I then scaled up the score by a factor of 10 in order to bring the three statistics to comparable scales of variability (Figure 4.2h). Given that about half of the F_{st} values flipped signs, the scatterplot between the raw and transformed values is mirrored on the y-axis (Figure 4.2i).

Finally, the composite score is the simple average of the three transformed scores. When a pseudo-p-value is needed in pathway analysis using *LRPath* (described below) I converted the composite score to the fractional rank.

4.2.9 Pathway analysis

Pathway enrichment analysis was performed using *LRpath* for all genes, using the composite scores and their associated pseudo p-values. I tested for enrichment of Gene Ontology (GO) terms (across 18,083 terms) and Kyoto Encyclopedia of Genes and Genomes (KEGG) pathways (across 225 terms). The analysis was done on September 30, 2015. (Note that around June 2015 the GO annotation was updated and the results became different. Future updates are expected to cause further changes of the pathway analysis results. The stability of gene annotation is a nuisance in this case, but also an opportunity for the same data to return new pathway results in the future.) For a moderate correction for testing thousands of pathways I reported those that satisfied the per-pathway p-value < 0.001 for both temporal and between-line analyses.

4.2.10 Visualization of enriched pathways

In many comparisons there are too many pathways that turn out to be apparently enriched and they become difficult to summarize. To facilitate the interpretation of the pathway analysis results in terms of the most salient biological signals, I needed to consolidate the top pathways into clusters of biologically related clusters, and this can be done by evaluating how any two pathways share more or fewer genes.

To visualize the clustering of significant pathways from *LRpath* in an organized manner while incorporating the overlap among gene sets, I used the *Cytoscape* plugin *EnrichmentMap (Merico et al. 2010)*. For each *LRPath* result I selected pathways passing the p-value threshold of 0.1 to build cluster maps, and defined two pathways as *connected* if they share >20% of genes between them (i.e., overlap coefficient > 0.2). In the cluster plots produced by *EnrichmentMap*, each node represents a pathway, and each green line links a pair of pathways with >20% overlap of their constituent genes.

Red nodes indicate pathways showing positive selection signatures, while blue nodes indicate negative selection. The map of all the pairwise connections often reveals heavily connected nodes – pathways that are connected to many other pathways, thus forming the center, or "hub", of the clusters. These clusters are highlighted by ovals; and by annotating the individual clusters we can capture the main biological signals in a given *LRPath* result file. Currently there is no formal method to summarize all the pathway terms represented by a cluster as they often include very diverse concepts. I decided to apply a *WordCloud* algorithm (Oesper et al. 2011) that returns the most commonly used words among the pathway names in each cluster, though the resultant phrases often do not have biological meaning.

4.3 Results

4.3.1 Runs of homozygosity (ROH)

Given that significant selective sweeps could result in long stretches of homozygous variants, I called ROH for the two lines and two distant generations (HCR-LCR, Generations (G) 5 and 26) in *PLINK* using the 782K pass-QC SNPs. Going from G5 to G26, the average number of ROH per animal did not change noticeably for HCR (383 to 382) or LCR (371 to 391); but the average length of ROH per animal increased from 3.4 to 4.3 Mb for HCR (by ~26%) and from 3.6 to 4.3 Mb for LCR (~20%) (Figure 4.3). In parallel, the average number of SNPs per ROH also increased by ~28% for HCR (981 to 1,252) and by ~19% for LCR (1,035 to 1,229) (Figure 4.4). Reflecting the lengthening of ROH runs, the average genome coverage by ROH per animal increased from 48% to 60% for HCR, and 49% to 60% for LCR; and the average gap length

between ROHs decreased by ~25% for HCR (3.2 to 2.4 Mb) and by ~27% for LCR (3.3 to 2.4 Mb) (Figure 4.5). I calculated ROH frequencies for each of the four groups of samples, and ΔROH for each of the four pairwise comparisons. Lastly, the ΔROH values were assigned to individual Refseq genes based on their genome coordinates.

4.3.2 Fixation index (F_{st})

Given that divergent selection often results in frequency divergence for functional alleles, I calculated F_{st} for every SNP to determine between-line allele frequency changes at both time points and within-line allele frequency change between time points, for 782K pass-QC SNPs. The average between-line F_{st} increased from 0.04 at G5 to 0.08 at G26, while the temporal F_{st} is ~0.05 in both lines (Figure 4.6). After calculating F_{st} for each of the four pairwise comparisons and summarize to 1 Mb windows I assigned F_{st} values to Refseq genes.

4.3.3 Aberrant allele frequency spectrum (AFS)

Given that the AFS in a region under selection may depart from that of the genomewide average, I calculated the composite likelihood ratio (CLR) for every 1Mb window across the genome to determine the likelihood of a selective sweep given the local AFS, using the high quality SNVs called from the whole-genome sequence data for the four DNA pools. The average CLR increased from G5 to G26 for both lines (9.9 to 23.7 for HCR and 9.1 to 19.9 for LCR), suggesting that more regions under selection became apparent in later generations (Figure 4.8). After calculating ΔCLR for each of the four pairwise comparisons for 1 Mb windows I assigned ΔCLR values to individual Refseq genes.

4.3.4 Correlations among the three scan statistics

I calculated the Spearman's rank correlation coefficient (ρ) between each pair of post-transformation test statistics using per-gene values to evaluate the level of concordance among the three signals. I repeated the calculation for each of the four pairwise analyses, using ~16,000 genes with non-missing values in all three statistics.

For HCR G26-G5, the correlations for ΔROH- F_{st}, ΔROH-ΔCLR, and F_{st} -ΔCLR are 0.61, 0.17, and 0.52, respectively (Figure 4.8). For LCR G26-G5, the correlations for ΔROH- F_{st}, ΔROH-ΔCLR, and F_{st} -ΔCLR are 0.65, 0.22, and 0.55, respectively (Figure 4.9). For G5 HCR-LCR, the correlations for ΔROH- F_{st}, ΔROH-ΔCLR, and F_{st} -ΔCLR are 0.59, 0.07, and 0.47, respectively (Figure 4.10). For G26 HCR-LCR, the correlations for ΔROH- F_{st}, ΔROH-ΔCLR, and F_{st} -ΔCLR are 0.66, 0.36, and 0.63, respectively (Figure 4.11). Thus the recurring trend is that ΔROH and F_{st} have consistently high levels of concordance, followed by ΔCLR and F_{st}. However, the concordance between ΔCLR and ΔROH is low. This confirms that the three statistics are related, but each also represents unique signatures of selection.

4.3.5 Overlap of top ranked genes among the three statistics

To examine the genes that are highlighted in more than one statistic, I extracted the top 10% of the genes from each of the statistics and looked for overlap. This resulted in 137 genes for HCR G26-G5, 67 genes for LCR G26-G5, 79 genes for G5 HCR-LCR, and 176 genes for G26 HCR-LCR. I then evaluated pathway signals in these gene sets by using *DAVID* (Huang et al. 2007), and observed no significant pathways. In an effort to improve the power of detecting significant pathways by integrating the three statistics systematically, I developed a composite score to represent concordant selection signatures.

4.3.6 Composite selection signature

I calculated the composite score to combine the three statistics described above. The composite scores for the four comparisons are shown in Figures 4.12. Because the tracks do not have a natural threshold for "significance", we do not have a cutoff threshold to determine candidate genes, but given the strong phenotypic response to selection at as early as G5 (Chapter 2), I expect that the genes with large HCR-LCR difference in G5 are also among the top ranked HCR-LCR genes in G26. Indeed, of the 100 genes with the highest HCR-LCR composite scores in G5, 12 also appeared among the 100 genes with the highest HCR-LCR composite scores in G26 (Table 4.3). These 12 genes fall under three shared top peaks between G5 and G26 between-line composite analyses on Chromosomes 9, 16, and 18 (Figures 4.12c & 4.12d). Of particular interest are *FN1* (Fibronectin 1), which functions in cellular adhesion and extracellular matrix stability and *PRELID2* (PRELI Domain Containing 2), which functions in phospholipid transport. These are of particular interest because I have previously found that cellular adhesion and extracellular matrix stability are two of the primary biological pathways differentially regulated in transcriptomic data between HCR-LCR as both lines age, with LCR showing greater down-regulation in both pathways as a consequence of aging (Chapter 3). Phospholipid transport is interesting because Overmyer et al. previously found that the HCR-LCR lines differ in their fuel preference and utilization, specifically in lipids and fatty acids (Overmyer et al. 2015).

I then applied the composite scores through pathway analysis. The *LRPath* algorithm returned enrichment p values for >4,000 pathways terms and I analyzed the results in two ways. First, I focused on the individual pathways passing $p < 0.001$. In

the H26-H5 temporal analyses, the top three most significantly pathways are related to muscle contraction, including *regulation of actin filament depolymerization*, *myosin filament*, and *actin filament depolymerization*. These are followed by other muscle-related pathways with slightly lower levels of significance, including *negative regulation of actin filament depolymerization*, *actin cytoskeleton*, and *actin filament capping*. In the L26-L5 temporal analysis there are six pathways satisfying $P < 0.001$ and with increased composite score at G26 (Table 4.2), implicating various "signaling" functions, such as *termination of signal transduction*, *apoptotic signaling*, and *G-protein coupled receptor signaling*. Further, the HCR-LCR comparison at G5 returned 13 pathways (Table 4.4), and at G26 returned 7 pathways (Table 4.5). As is often the case in this type of analysis, the names of the top 3-6 pathways may not converge on 1-2 coherent functional themes. In Table 4.4, for example, we noted that regions with higher composite scores in HCR than LCR are enriched for genes in the *homophilic cell adhesion* pathway, echoing the aging effects found in gene expression data (Chapter 3), but other pathways are difficult to interpret. Likewise, Table 4.5 showed that one of the top ranked pathways is for *regulation of glycogen metabolic process*, which seems relevant to the metabolic differences between the two lines (Overmyer et al. 2015). I would like to note that there are 7 significant pathways in G5 and 4 significant pathways in G26 that are down-direction, which indicate that these pathways show signatures of selection in LCR compared to HCR (Tables 4.4 & 4.5). Despite their significance, neither group of down-direction pathways appear to have any clear biological interpretation.

One of the difficulties in interpreting *LRpath* results is in choosing the level of interpretation: over four thousand pathways are provided in the output, each accompanied by significance levels and direction, and many of which are redundant pathways, i.e., they share the same genes with varying degrees of overlap. While in the above I examined the "significant" pathways defined at $P < 0.001$, my second approach is to visualize the relationship of a more relaxed set of "top" pathways, defined at $P < 0.1$, while taking into account the overlap of genes among the pathways. This is done by displaying the larger number of pathways meeting $P < 0.1$ using *EnrichmentMap* (see Methods).

For the temporal analysis in HCRs, there were 45 pathways and they formed many clusters (Figure 4.13). Two clusters on the upper right, shown in red, contain pathways that are enriched with genes with higher score in G26 than G5, with the most frequently observed words of *phospholipid-dephosphorylation* and *transport-acid-anion,* respectively (Figure 4.13). Note that these names attached to the clusters do not have inherent meaning as they come from the word frequency analysis (by the *WordCloud* algorithm), thus these names can only serve as provisional labels of the clusters. How to properly annotate the functional theme for a given cluster in a formal, automated way remains a challenge. By manual annotation I determined that the *phospholipid-dephosphorylation* cluster mainly contains the pathways involved in phospholipid and fatty acid metabolism, while the *transport-acid-anion* cluster contains pathways involved in amino acid transport and metabolism. The most significant pathways related to muscle function shown in Table 4.1 is no longer apparent in this analysis involving a larger number of less significant pathways. Several other clusters in Figure 4.13

showed opposite direction: they contain pathways enriched with genes with higher score in G5 than G26. Such *reduced* effect of selection in later generations is difficult to interpret.

For the temporal analysis of LCRs, there were 34 pathways at $P < 0.1$ and their clusters are shown in Figure 4.14. *Protein kinase* and *microtubule organization* are the major clusters enriched with genes with higher score in G26 than G5. Other clusters are difficult to interpret.

The HCR-LCR comparison at G5 revealed multiple clusters (in red) containing pathways enriched with genes with higher scores in HCR than LCR, showing frequently observed words as *cytoskeletal-protein-binding*, *activity-transmembrane*, *activity-phosphatidylinositol-phospholipase*, and *growth-factor-binding* (Figure 4.15). By manual annotation I found that the *cytoskeletal-protein-binding* cluster contains pathways involved in actin/myosin binding and muscle contraction; the *activity-transmembrane-cluster* contains pathways involved in ATPase activity and ATP transport; the *activity-phosphatidylinositol-phospholipase* cluster contains pathways involved in phospholipid and fatty acid metabolism; and the *growth-factor-binding* cluster contains pathways involved in cellular adhesion and extracellular matrix integrity. The blue clusters contain pathways enriched with genes with higher scores in LCR than HCR, and include frequently observed words such as *channel activity* and *phosphatase activity* (Figure 4.15). I found that the *channel activity* cluster contains pathways involved in calcium and sodium channel activity; and the *phosphatase activity* cluster contains pathways involved in protein phosphatase activity.

The HCR-LCR comparison at G26 (Figure 4.16) showed two clusters of pathways with stronger selection in HCR, with words of *phospholipid-dephosphorylation* and *transport-acid-anion*, which resembles the same groups of pathways seen in the HCR G26-G5 temporal comparison (Figures 4.13). The blue clusters include words such as *regulation process* and *positive regulation growth development* (Figure 4.16). I found that the *regulation process* cluster contains pathways involved in the regulation of metabolic processes; and the *positive regulation growth development* cluster contains pathways involved in cellular growth and proliferation.

4.4 Discussion

In this study I attempted to identify genomic regions under selection in the HCR-LCR rat model using high-density, whole-genome datasets. I identified genes and pathways under differential selection by line and by time. The majority of the increase in homozygosity between G5 and G26 in both lines is due to lengthening ROHs. The F_{st} analysis shows that the genome average of HCR-LCR differentiation increased by 2-fold from G5 and G26. The AFS analysis shows that the genome wide CLR increased in both lines from G5 to G26, indicating the increase in aberrant local AFS and increased regions experiencing the impact of selective events.

The composite score I developed is an efficient and robust function that takes into account of the different distribution properties of the constituent test statistics. The composite signatures uncovered several physiological pathways, including those function in muscle contraction that seem to be selected in the HCR between G5 and G26, and this observation, if confirmed, offers a potential mechanistic link to the increased exercise capacity in the HCRs. In addition, the composite results provided

further evidence for the importance of the aging-dependent adhesion pathways in the G5 HCR-LCR analysis.

Physical exercise is a stressful event for all complex animals. To sustain muscle contraction during exercise, the demand for adenosine triphosphate (ATP) can increase 1,000-fold compared to the resting state (Baker et al. 2010). In addition, cells must be able to have structural stability in the extracellular matrix to sustain the physiological stress. Taken as a whole, our study suggests that 1) genes in cellular integrity, actin/myosin binding and muscle contraction actin/myosin binding and muscle contraction pathways were swept in HCRs as a consequence of the increased physiological stress beyond the amount that any of the eight inbred rat founder strains can cope with, and 2) genes involved in ATP-production and amino acid/lipid metabolism pathways were affected by selection and this led the HCRs to utilize multiple fuel sources to generate ATP and delay exhaustion compared to LCR during exercise.

4.5 Figures

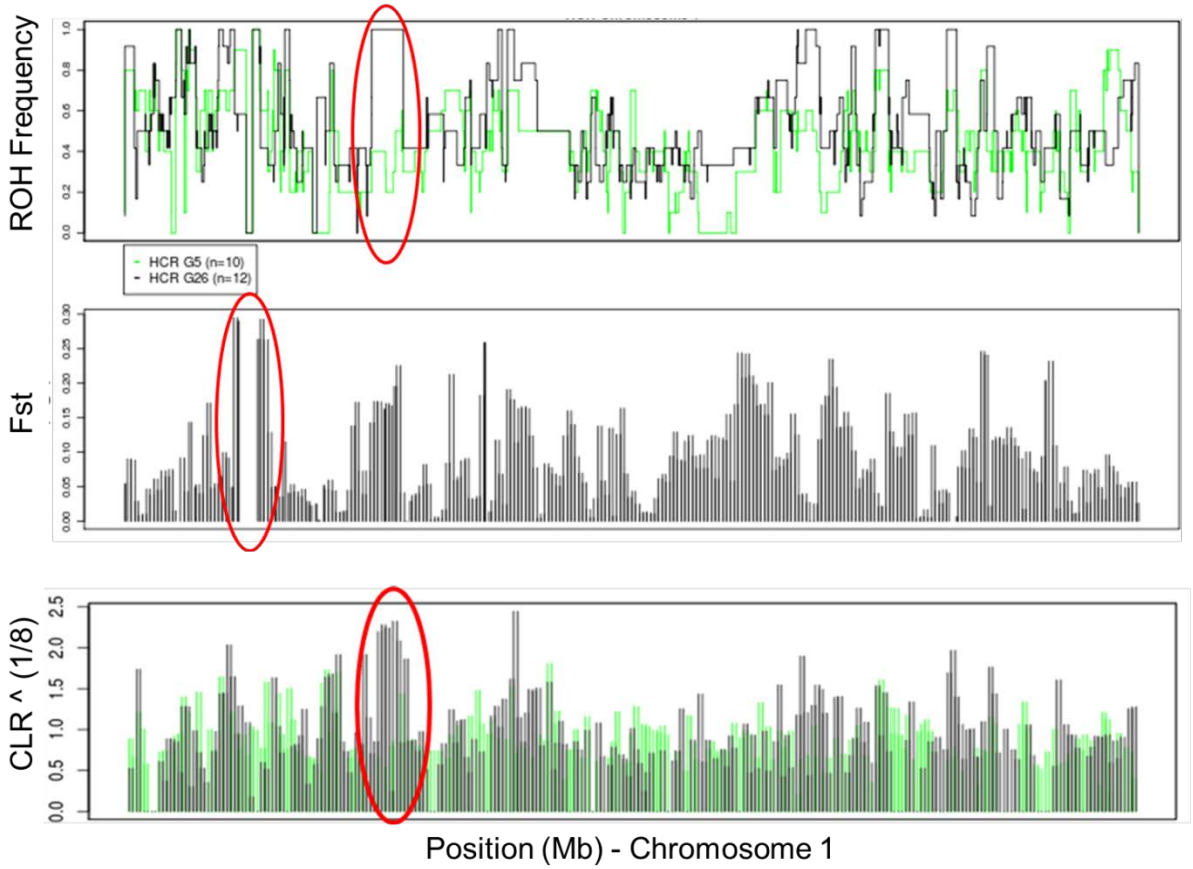

Figure 4.1: Example tracks of the three statistics across Chromosome 1 for HCR G5 and G26.

(TOP) Frequency of ROH intervals across Chromosome 1 for HCRs G5 (green) and G26 (black). Region highlighted in red oval would be a potential top candidate as a temporal selection signature, where the G26 group all possess a long ROH across the region, while the G5 group does not. (MIDDLE) F_{st} values per SNP across Chromosome 1 for HCRs temporal comparison (G5-G26).). Region highlighted in red oval would be a potential top candidate as a temporal selection signature, where the G5 and G26 groups have high levels of population differentiation across a long interval. (BOTTOM) CLR values for 1 Mb windows across Chromosome 1 for HCRs G5 (green) and G26 (black). Region highlighted in red oval would be a potential top candidate as a temporal selection signature, where the G26 group show highly aberrant local AFS, while the G5 group does not.

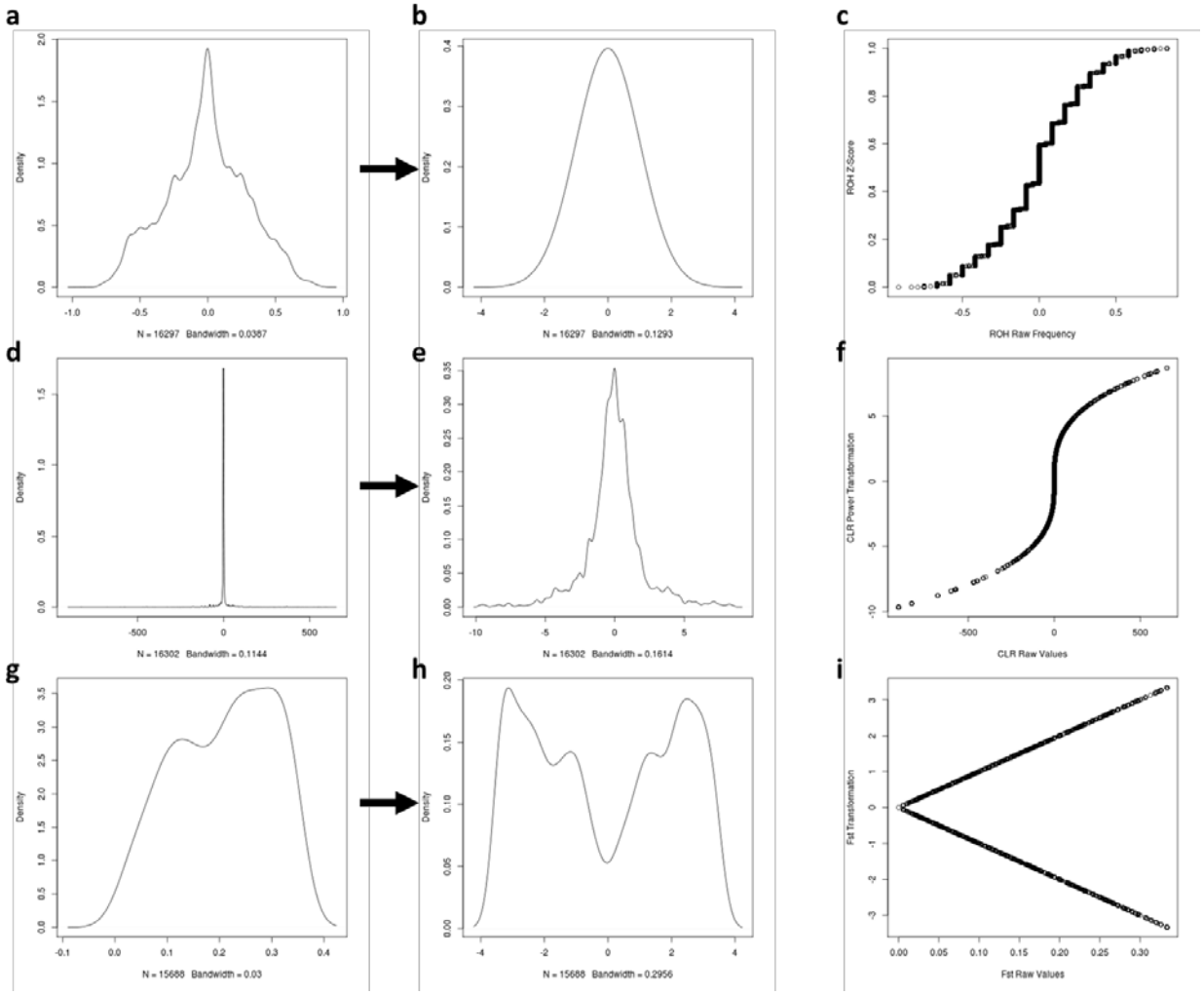

Figure 4.2: Raw and transformed density plots of the three statistics.

Shown are the raw values (a,d,g), transformed values (b,e,h), and scatterplots between the raw and transformed values (c,f,i) for ΔROH (a,b,c), ΔCLR (d,e,f), and F_{st} (g,h,i).

a

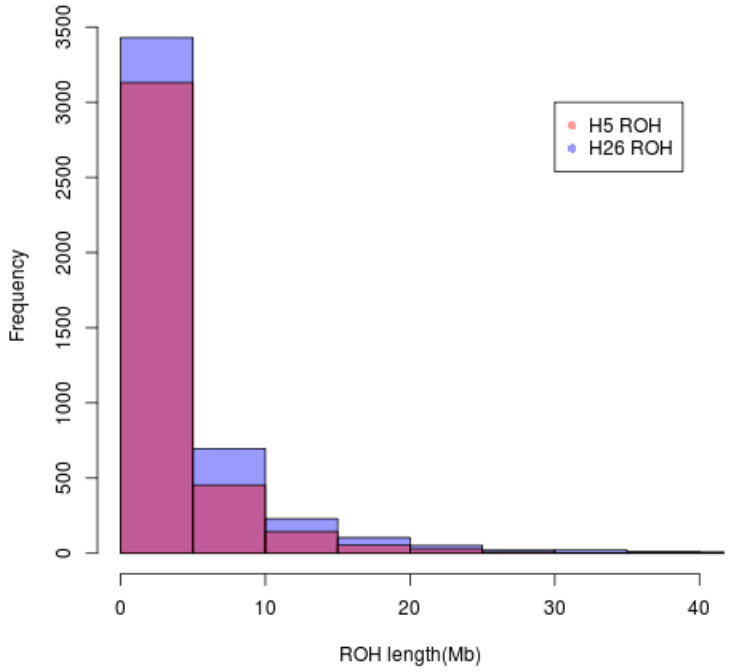

b

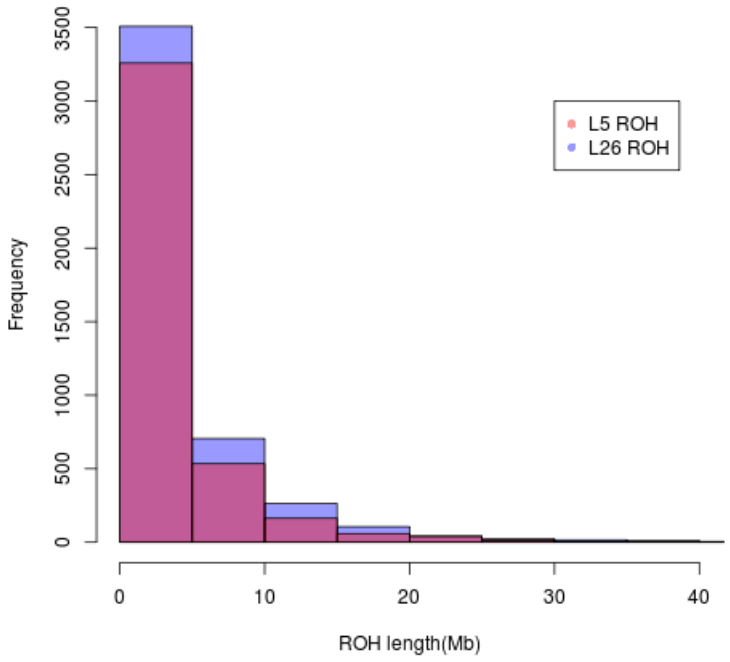

Figure 4.3: Distribution of ROH lengths across (a) HCR and (b) LCR groups.

a

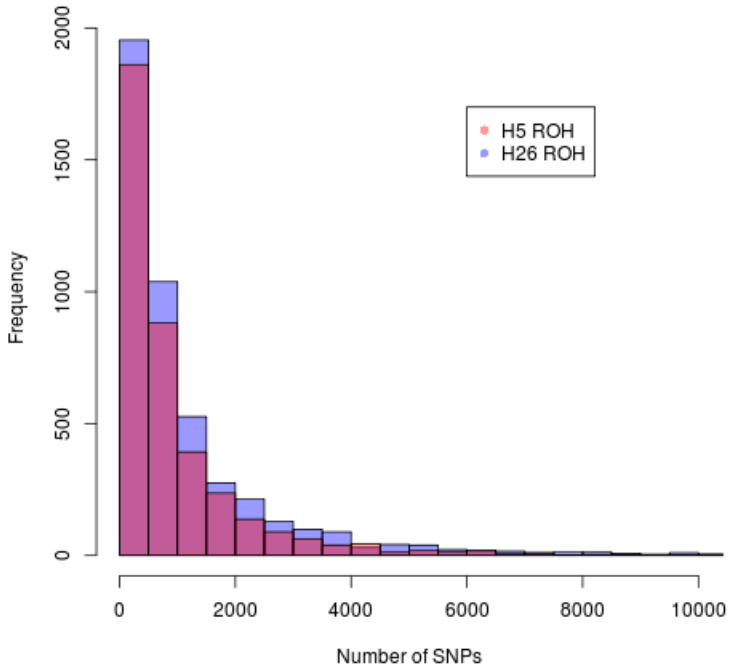

b

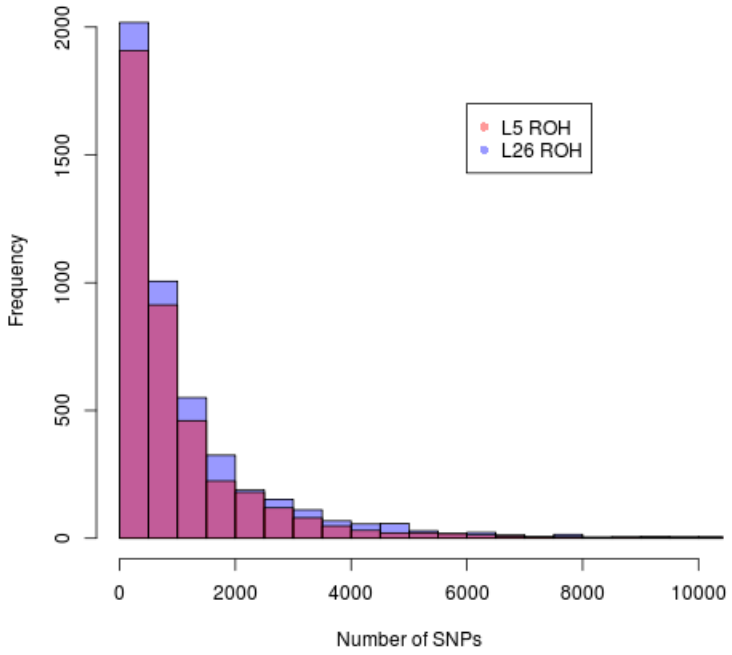

Figure 4.4: Distribution of number of SNPs per ROH for (a) HCR and (b) LCR groups.

a

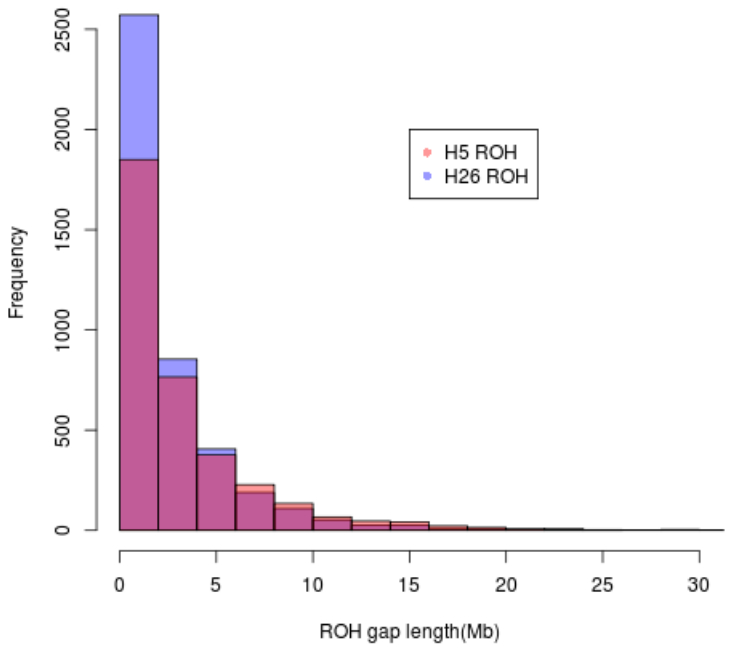

b

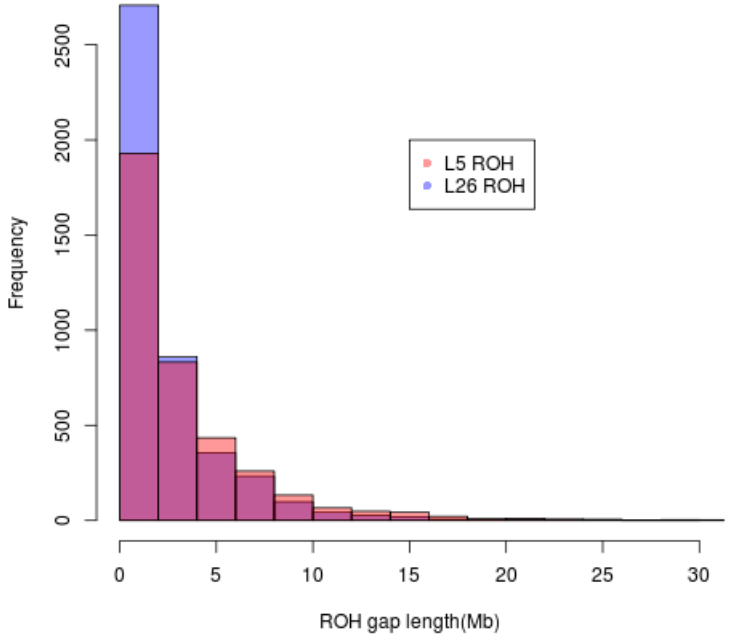

Figure 4.5: Distribution of gap length between ROHs for (a) HCR and (b) LCR groups.

a

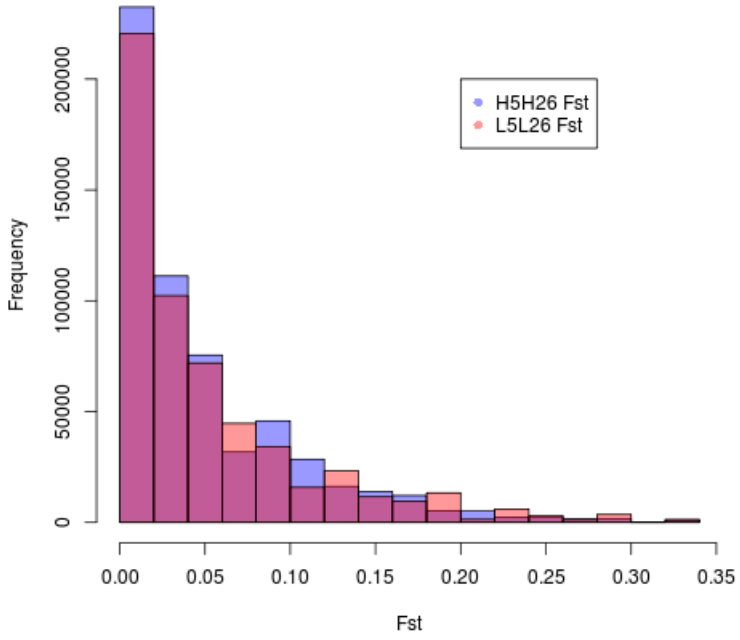

b

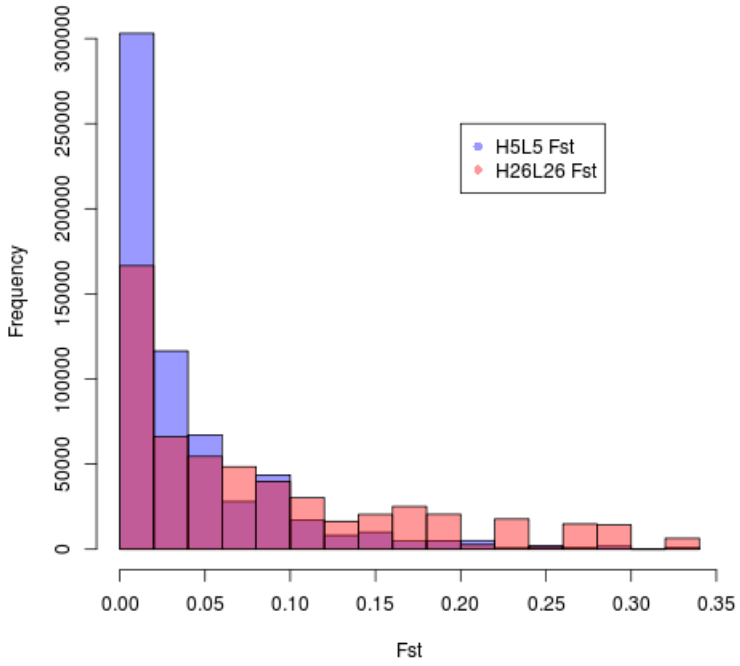

Figure 4.6: Distribution of F_{st} values for (a) temporal and (b) between-line comparisons.

a

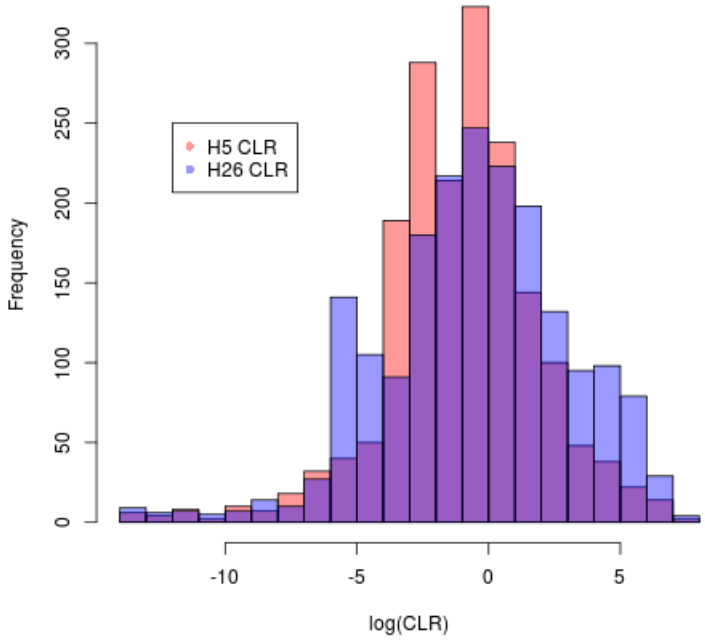

b

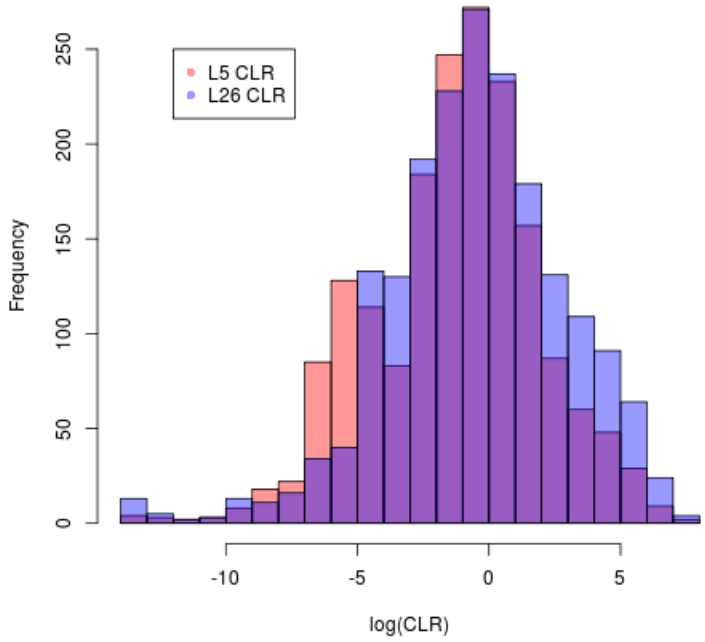

Figure 4.7: Distribution of log(CLR) values per 1 Mb window for (a) HCR and (b) LCR groups.

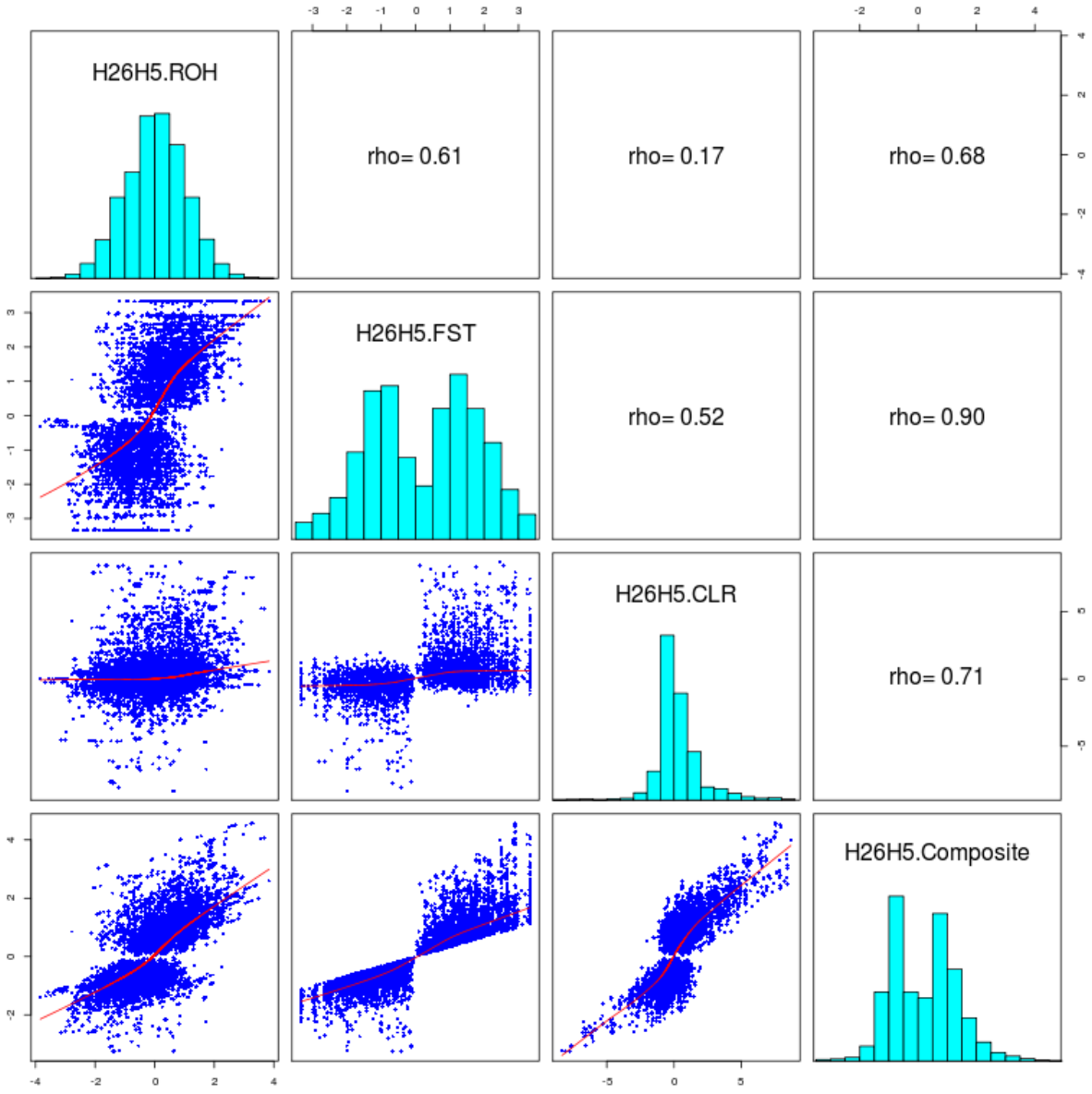

Figure 4.8 Scatterplot and correlation between test statistic scores among HCR G26-G5 comparisons for overlapping genes, and histograms for each respective statistic.

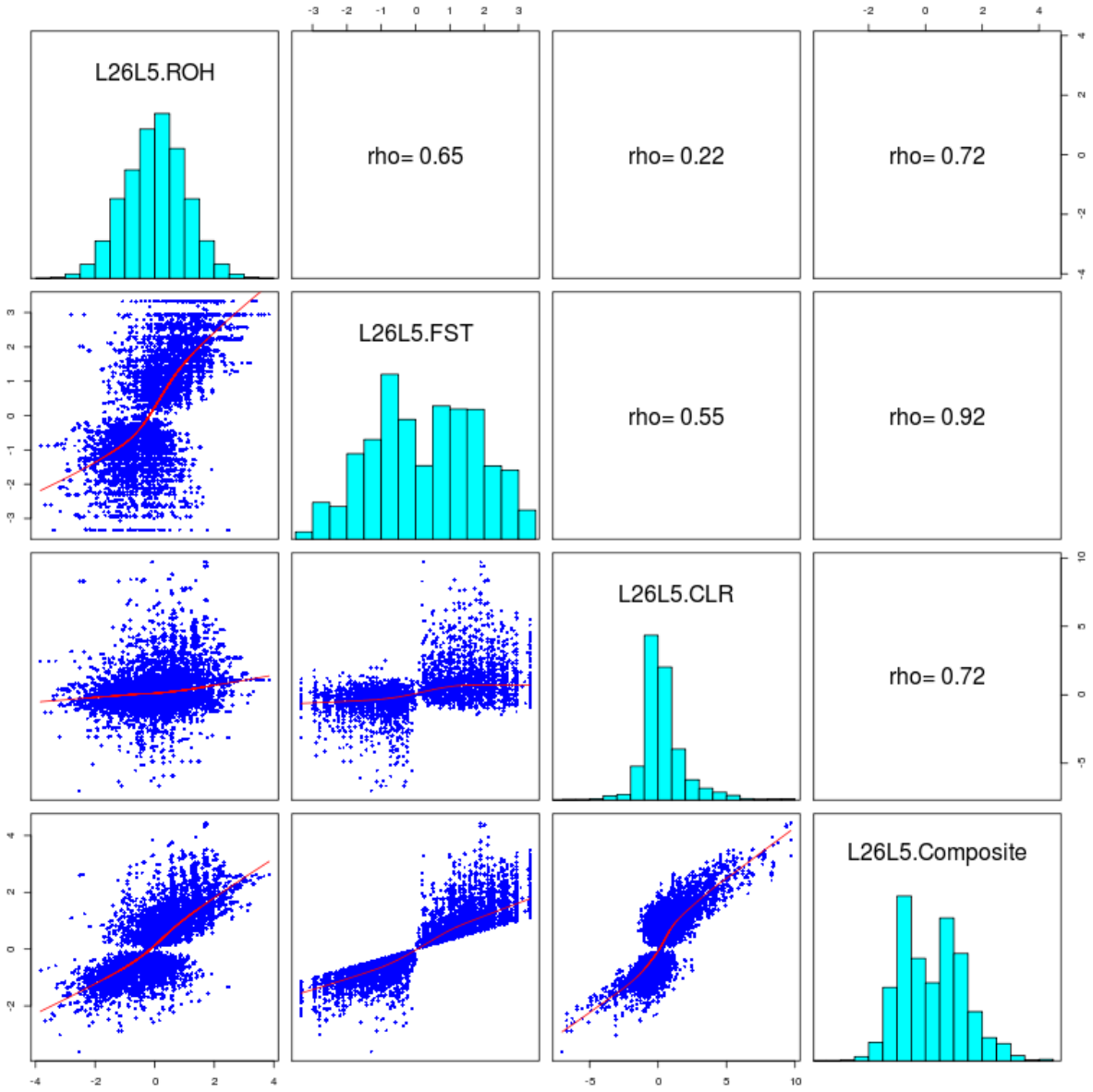

Figure 4.9 Scatterplot and correlation between test statistic scores among LCR G26-G5 comparisons for overlapping genes, and histograms for each respective statistic.

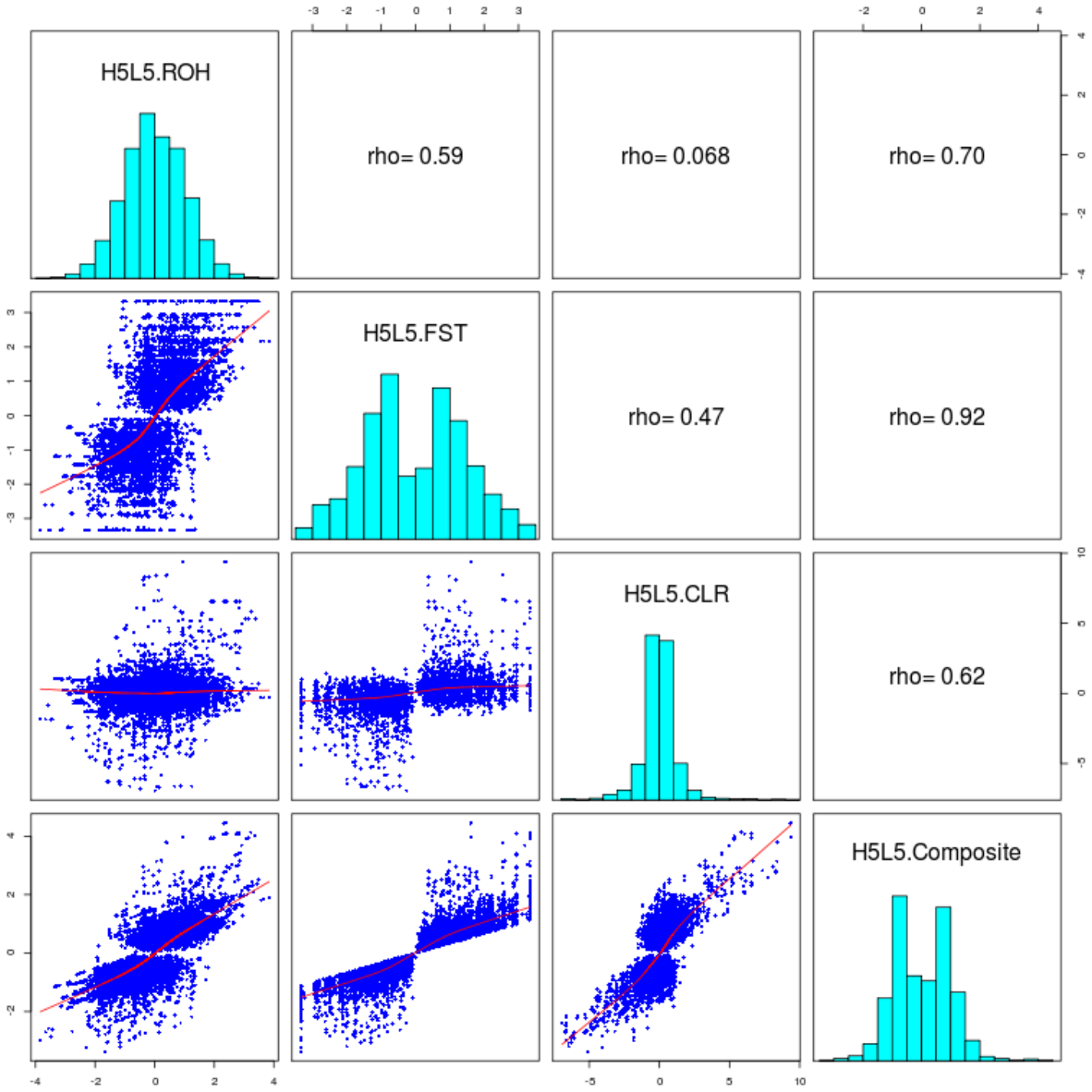

Figure 4.10 Scatterplot and correlation between test statistic scores among G5 HCR-LCR comparisons for overlapping genes, and histograms for each respective statistic.

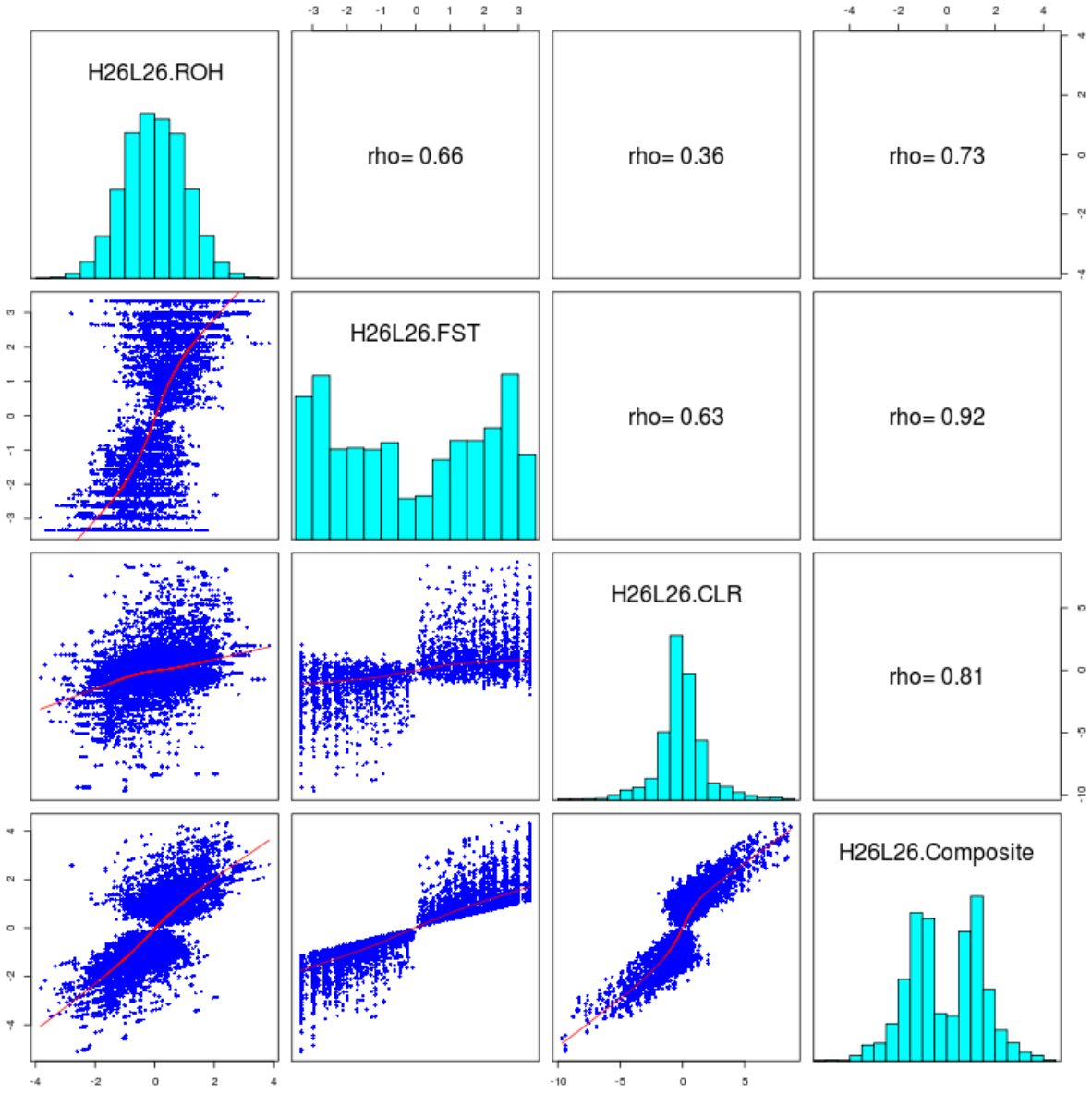

Figure 4.11 Scatterplot and correlation between test statistic scores among G26 HCR-LCR comparisons for overlapping genes, and histograms for each respective statistic.

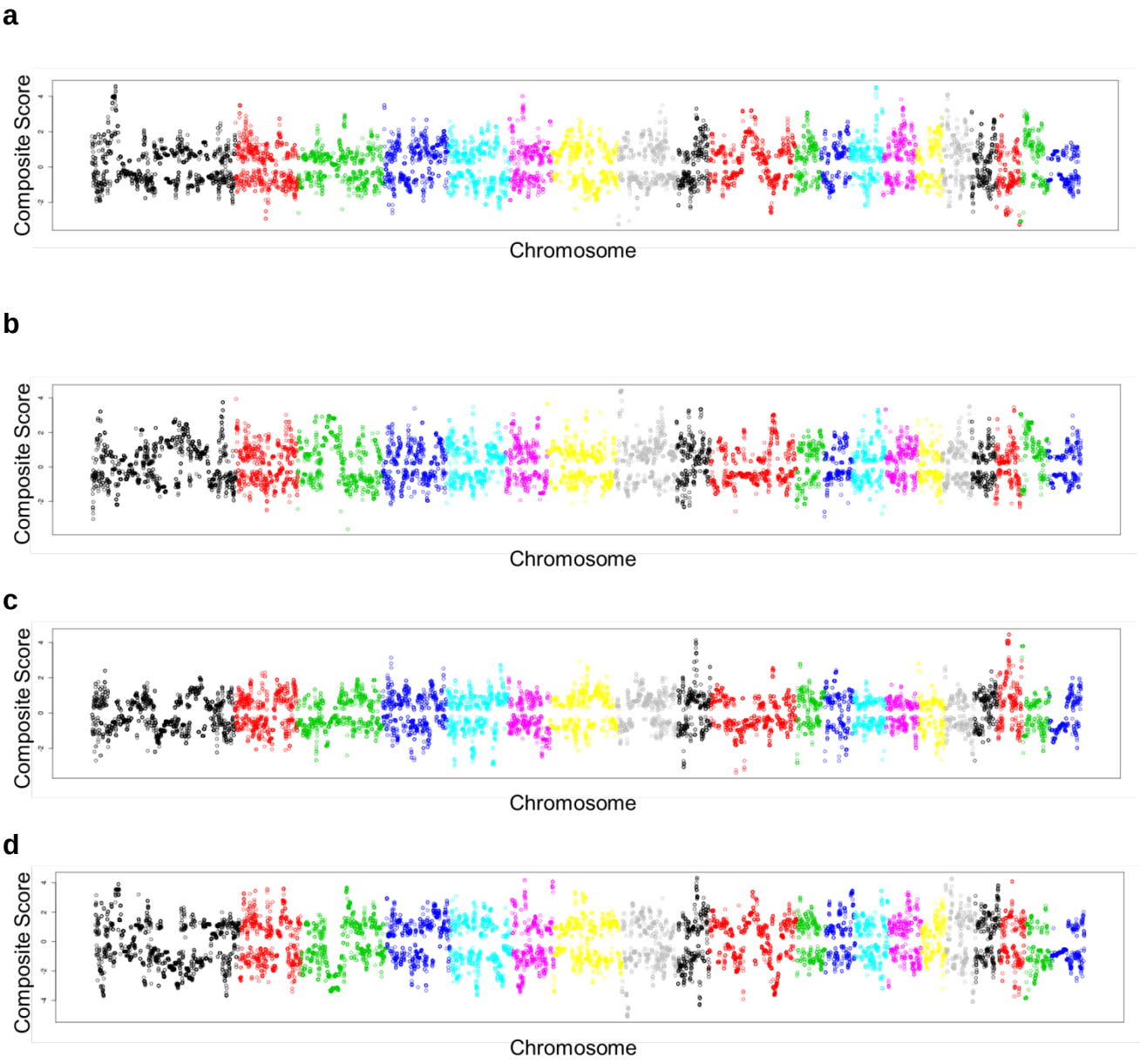

Figure 4.12: Manhattan plot of Composite Scores of Every Gene for HCR G26-G5 (a), LCR G26-G5 (b), G5 HCR-LCR (c), and G26 HCR-LCR (d)

Shown are the composite scores for every gene across all 20 autosomes. Adjacent chromosomes are colored differently for separation.

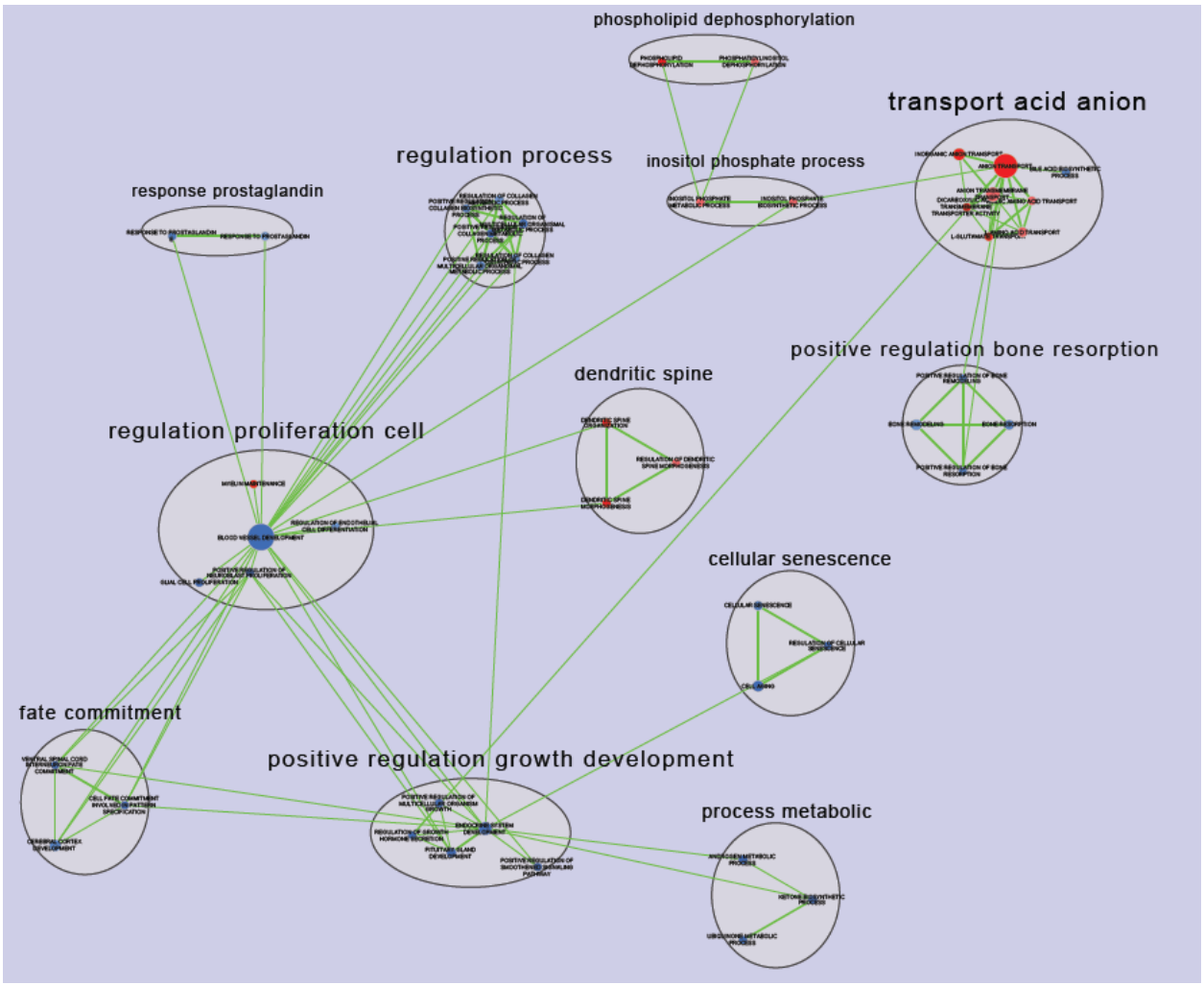

Figure 4.13: *EnrichmentMap* output for HCR G26-G5 LRpath results from the composite analysis.

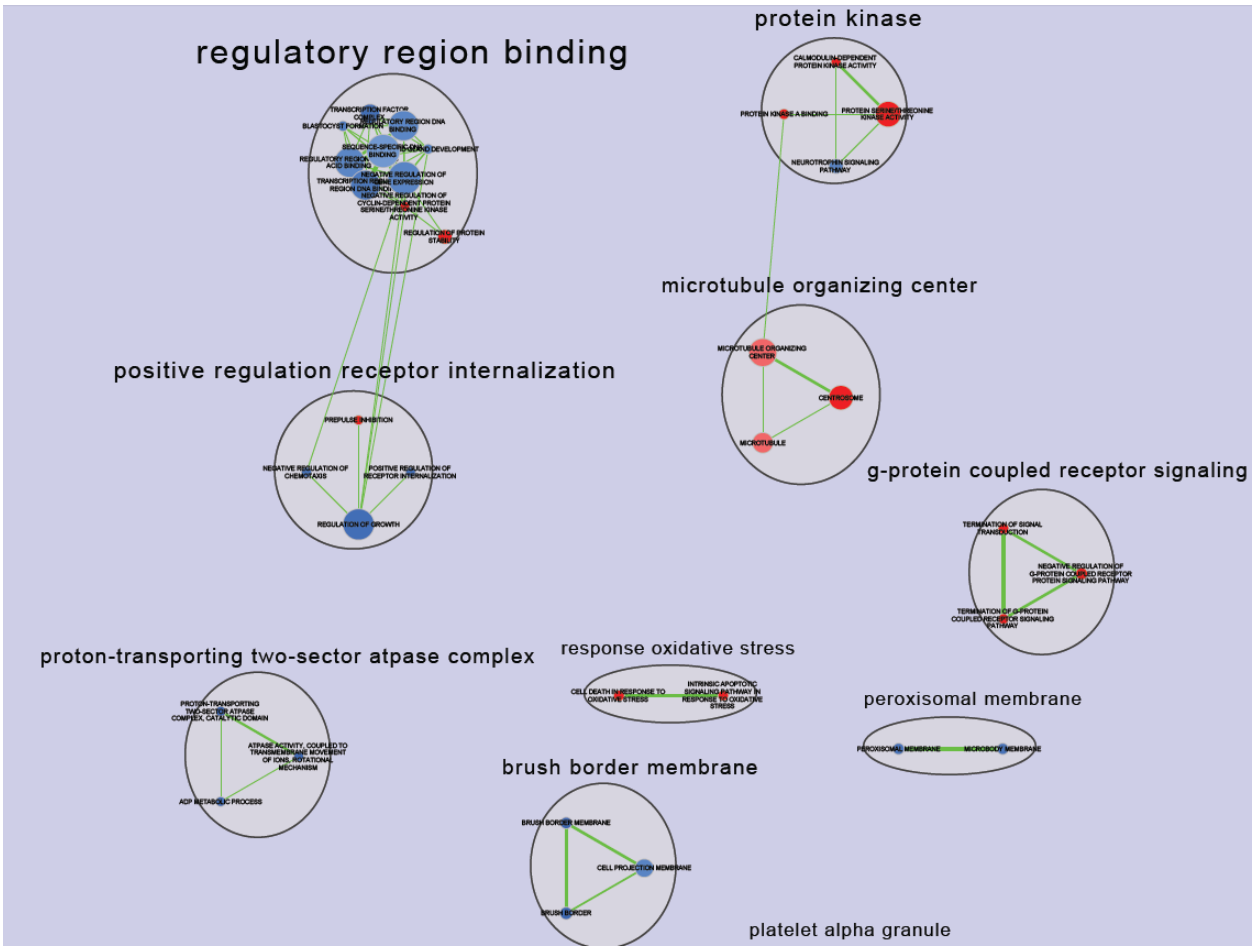

Figure 4.14: *EnrichmentMap* output for LCR G26-G5 LRpath results from the composite analysis.

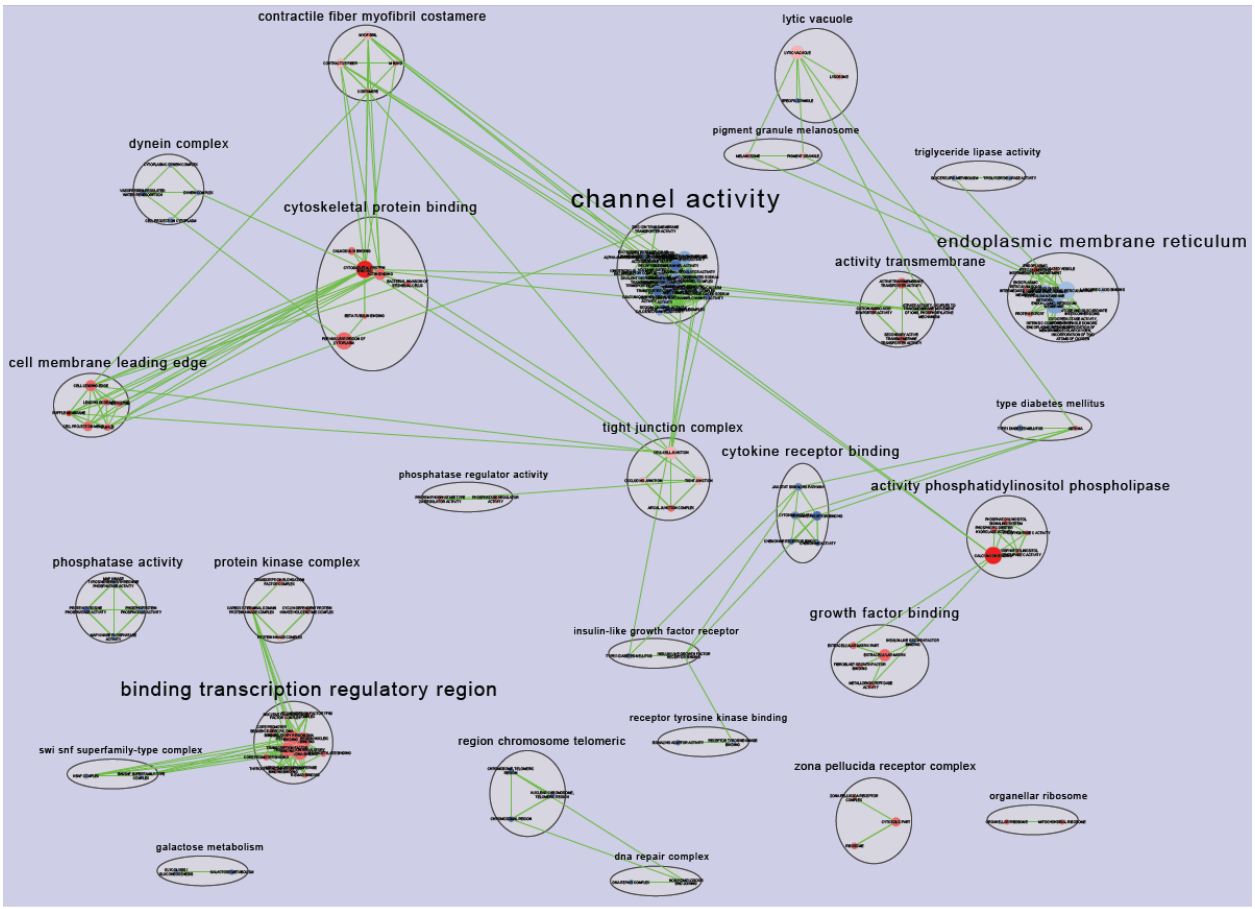

Figure 4.15: *EnrichmentMap* output for G5 HCR-LCR LRpath results from the composite analysis.

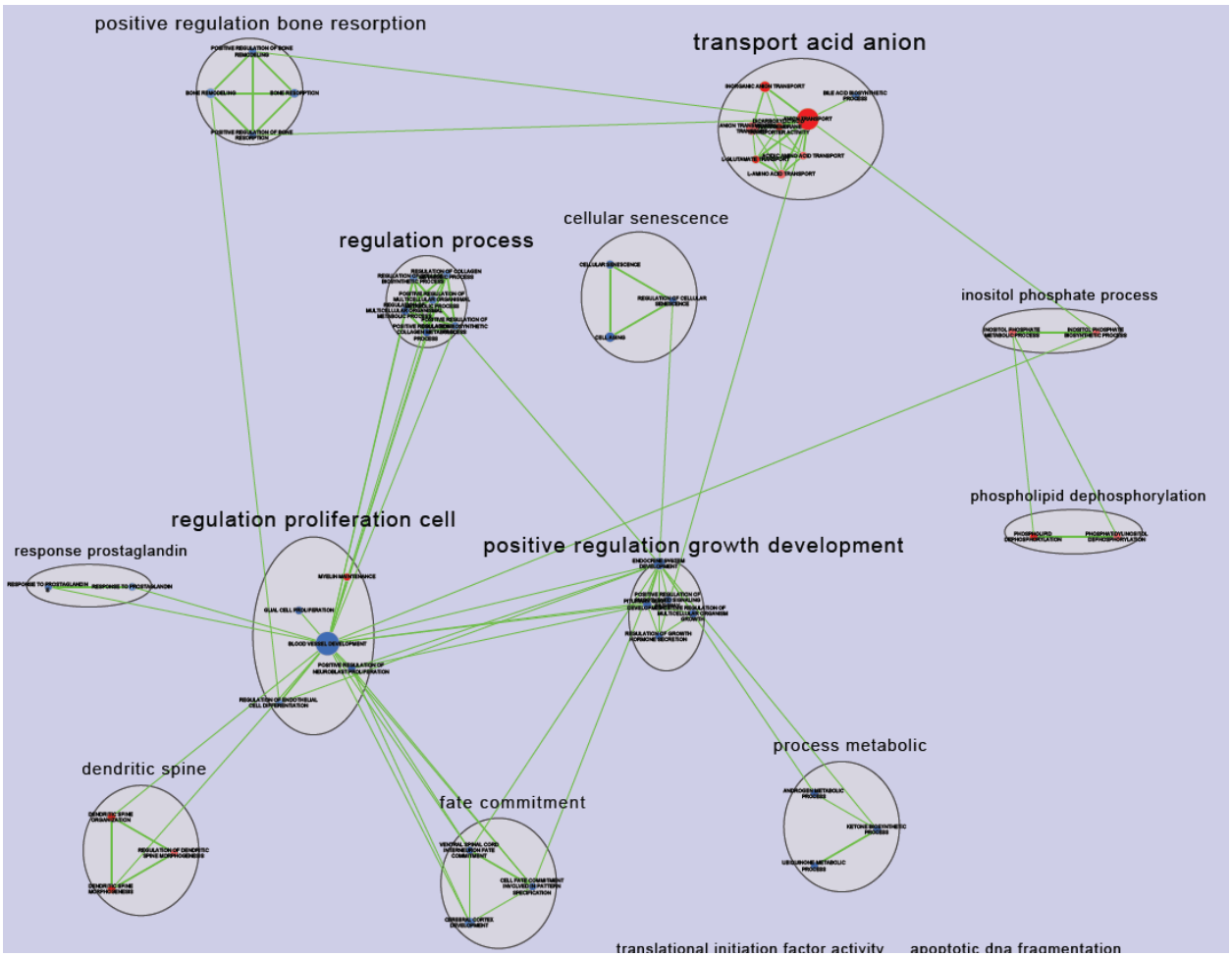

Figure 4.16: *EnrichmentMap* output for G26 HCR-LCR LRpath results from the composite analysis.

4.6 Tables

Name	P-Value	Direction
regulation of actin filament depolymerization	4.44E-06	up
myosin filament	6.47E-06	up
actin filament depolymerization	7.30E-06	up
regulation of protein depolymerization	2.08E-05	up
regulation of protein complex disassembly	3.15E-05	up
photoreceptor activity	3.73E-05	up
zymogen granule	1.31E-04	up
suckling behavior	3.71E-04	up
cellular response to estradiol stimulus	4.48E-04	up
zymogen granule membrane	4.70E-04	up
negative regulation of protein complex disassembly	5.66E-04	up
negative regulation of actin filament depolymerization	6.11E-04	up
actin cytoskeleton	6.56E-04	up
actin filament capping	6.69E-04	up
cytoplasmic part	6.80E-04	up
cellular response to estrogen stimulus	7.70E-04	up
protein depolymerization	8.20E-04	up
endocardial cushion morphogenesis	8.84E-04	up
protein complex disassembly	8.93E-04	up
prostate glandular acinus development	9.15E-04	up

Table 4.1: Significant (p<0.0001) LRpath pathway results for composite HCR G26-G5 analysis

Name	P-Value	Direction
termination of signal transduction	1.16E-04	up
positive regulation of apoptotic signaling pathway	1.50E-04	up
termination of G-protein coupled receptor signaling pathway	2.65E-04	up
prepulse inhibition	3.05E-04	up
protein serine/threonine kinase activity	3.43E-04	up
calmodulin-dependent protein kinase activity	5.72E-04	up

Table 4.2: Significant (p<0.0001) LRpath pathway results for composite LCR G26-G5 analysis

Gene	Name	Chromosome	Start (Mb)	End (Mb)	H5-L5 Rank	H26-L26 Rank
SPAG16	Sperm Associated Antigen 16	9	68.8532	69.7383	70	71
VWC2L	Von Willebrand Factor C Domain Containing Protein 2-Like	9	69.7389	69.9447	37	99
BARD1	BRCA1 associated RING domain 1	9	70.1202	70.1986	100	44
ATIC	5-Aminoimidazole-4-Carboxamide Ribonucleotide Formyltransferase/IMP Cyclohydrolase	9	70.6767	70.6969	5	9
FN1	Fibronectin 1	9	70.7022	70.7712	81	93
MREG	Melanoregulin	9	71.3036	71.3580	37	28
XRCC5	X-ray repair cross-complementing protein 5	9	71.4725	71.5819	48	37
IGFBP2	Insulin-Like Growth Factor Binding Protein 2	9	71.9669	71.9942	97	47
SPATA4	Spermatogenesis Associated 4	16	0.7230	0.7323	25	32
PRELID2	PRELI Domain Containing 2	18	35.0600	35.1542	22	96
GRXCR2	Glutaredoxin, Cysteine Rich 2	18	35.1796	35.1941	28	68
SH3RF2	SH3 Domain Containing Ring Finger 2	18	35.2429	35.3445	55	19

Table 4.3: 12 overlapping genes between the top 100 genes from the G5 and G26 HCR-LCR composite analyses

Name	P-Value	Direction
translation factor activity, nucleic acid binding	2.24E-04	up
hyperosmotic salinity response	2.51E-04	down
ion channel complex	2.98E-04	down
DNA replication initiation	4.08E-04	up
negative regulation of cytokine-mediated signaling pathway	4.73E-04	down
calcium ion binding	4.82E-04	up
homophilic cell adhesion	5.37E-04	up
One carbon pool by folate	6.59E-04	down
endoplasmic reticulum-Golgi intermediate compartment	7.09E-04	up
transcription factor TFIID complex	7.82E-04	up
mitochondrial DNA metabolic process	8.54E-04	down
mitochondrial genome maintenance	8.82E-04	down
regulation of membrane potential	9.52E-04	down

Table 4.4: Significant (p<0.0001) LRpath pathway results for composite G5 HCR-LCR analysis

Name	P-Value	Direction
protein O-linked glycosylation	1.78E-04	up
cell aging	4.17E-04	down
ketone biosynthetic process	6.20E-04	down
regulation of glycogen metabolic process	6.52E-04	up
inorganic anion transport	6.88E-04	up
phototransduction, visible light	8.98E-04	down
calcium ion binding	9.72E-04	down

Table 4.5: Significant (p<0.0001) LRpath pathway results for composite G26 HCR-LCR analysis

CHAPTER 5

F2-Based QTL Mapping

5.1 Introduction

After ~30 generations, the HCR and LCR rats have diverged in both phenotypes and genotypes (Chapter 2). If I were to perform a direct HCR-versus-LCR genetic comparison, numerous loci, distributed throughput the genome, would be apparently associated with every trait that is different between the two lines as a result of "population stratification", whereby the true functional variants "driven apart" by selection would have been hidden amidst a far larger number of neutral differences that have accumulated in the two lines due to random genetic drift. In order to uncover the causal loci, we have crossed HCR and LCR for two generations to create a mapping population of >600 F2 animals that carry random genomic mosaics of the HCR and LCR grandparent genomes, such that most neutral variants are no longer linked to the functional alleles at causal loci and will no longer co-segregate (i.e., be linked with) the phenotypes. Such a "Mendelian Randomization" process makes it possible to identify quantitative trait loci (QTLs) by linkage or association analysis.

Several previous studies have successfully utilized intercross F2 populations of divergently selected outbred animals to map causative genetics variants, including studies of divergently selected body weight in chickens (Wahlberg et al. 2009), tameness/aggressiveness in rats (Albert et al. 2009), and alcohol preference in rats

(Foroud et al. 2000, Bice et al. 2009). My study will follow the general analytical strategies developed in these previous studies, while exploiting new approaches that could account for the complex pedigree structure present in our lines.

5.2 Materials and Methods

5.2.1 "F2" intercross and phenotyping

We performed the F2 intercross in two batches. For the first batch, we randomly selected 4 males and 4 females from 8 different families in G26 of each line to form 8 HCR-LCR reciprocal pairs, which generated 79 F1 rats (with litter size ranging from 4 to 11). All F1's were phenotyped for maximal running distance, total run time, and vertical work done. From the F1's, 20 males and 20 females were randomly selected to form pairs between different F1 families (i.e., avoiding brother-sister mating), ranging from 2 to 6 animals per F1 family. These 20 mating pairs generated 154 F2 rats. For the second batch, we selected 9 males and 9 females from G28 of each line to form 18 mating pairs, which generated 163 F1 rats, of which 97 were phenotyped for the maximal running distance trait. Out of the 97 phenotyped F1 animals, 43 males and 43 females were selected across the 18 families with a comparable representation of the four HCR/LCR parentage combinations, as the following: 11 pairs of HCR-mom male with HCR-mom female, 12 pairs of HCR-mom male with LCR-mom female, 10 pairs of LCR-mom male with HCR-mom female, and 10 pairs of LCR-mom male with LCR-mom female. This generated 491 F2 rats. The two batches together yielded 645 F2 rats. Phenotyping for running performance (described later and in Figure 5.1) and vertical work followed the same protocols as described in Chapter 2. Additionally, for all 491 F2

animals in the second batch we measured lean mass (g), fat mass (g), fluid mass (g) , fasting blood glucose (mg/dL), heart mass (g), and EDL muscle mass (g) at 16-20 weeks of age. Body composition measures (lean, fat, and fluid mass) were determined via NMR using an Optics Minispec LF90 II instrument (Bruker Optics, Billerica, MA, USA) following previously published protocols. Blood glucose after a 4-hour fast was determined using the Accu-Chek Aviva system (Roche Diagnostics, Basel, Switzerland). At the time of dissection, heart and EDL muscles were weighed immediately upon harvesting. Heritability for all measured phenotypes was calculated using *SOLAR* (Almasy and Blangero 1998).

5.2.2 SNP content design for the Affymetrix Axiom genotyping array

I designed a custom panel of ~700K SNPs to be used for genotyping on the Affymetrix Axiom platform. My goal was to select the most informative SNPs for tracking genomic segments in the HCR-LCR rats, both for the segregation of linked markers in the F2-intercross population and for identifying ancestral segments originating from the eight original inbred founders. To start, we combined DNA variants discovered in two whole-genome sequencing (WGS) datasets. First, we sequenced four DNA pools as described in Chapter 4, for n=10 animals each (five of each sex), representing HCR and LCR rats from generations (G) 5 and 26. I aligned the reads to the rat reference genome sequence rn34 (Gibbs et al. 2004) using BWA (Li and Durbin 2009) and detected variants using the GATK Unified Genotyper (DePristo et al. 2011). At the average read depth ~37X (9.25X per pool) I discovered ~9 million single nucleotide variants (SNVs). Applying quality control criteria to the four pools separately I developed four lists of high-confidence variant sites, one for each pool, containing from

6.81 to 7.53 million SNVs. Second, I accessed publicly available SOLiD WGS sequencing data for the eight founder lines (Baud et al. 2014, Baud et al. 2014), previosuly sequenced using liver-derived genomic DNA from one animal per line. I downloaded the variant site list containing >6.4 million SNVs from (https://www.ebi.ac.uk/arrayexpress/experiments/E-MTAB-2332/) on 5/20/2013. The file is named *HS_Rats_SNPs.txt*, and includes variant calls for the eight founder lines that were mapped to the rn34 genome build – the same as used in analyzing the pooled sequencing data described above . By selecting SNVs not monomorphic across the eight lines and not heterozygous in any of the eight lines I obtained a list of ~6.23 million SNVs. These five lists had an overlap of 2,399,171 SNVs.

In order to increase ancestry informativeness I kept SNVs with the minor allele that appeared only once or twice among the eight founders. This reduced the list to 1,484,806 SNVs. To place a higher value on coding variants, I extracted coding variants from the five variant lists described above and from a previously designed high-density Affymetrix SNP genotyping array called RATDIV (Baud et al. 2013). By adding 41,667 coding SNVs back to the master list I increased the SNV count to 1,526,473.

After receiving our target SNV list, the Affymetrix team scored the feasibility of designing a genotyping assay for each submitted SNV, while allowing a higher selection priority for a subset of user-designated high-value SNVs. I submitted the master list of 1,526,473 SNVs, while designating a high-value subset of 862,284 SNVs with the following overlapping categories: 9,703 exonic SNVs, 846,701 that appeared in only one of the eight founders, and 20,341 SNVs with opposing alleles fixed in the HCR and LCR pools, i.e., those with a large HCR-LCR differentiation. The bioinformatics

team at Affymetrix evaluated all the submitted variants and classified them as Recommended, Not Recommended, and Neutral. To create the final panel I included all of the 601,477 Recommended SNVs. At this point the design can accommodate another ~100K SNVs, and I selected 105,980 additional SNVs from the Neutral catagory that are exonic (3,442), with allele count of one out of eight founders (4,403), or with oppositely fixed alleles (98,170, selected out of 177,638 such variants by their rank in the feasibility score). The final list included 707,457 SNVs, of which 625,291 were eventually accommodated on the chip when the probe space were assigned. The 625,291 SNVs were mostly chosen by their feasibility scores. The distribution of these SNVs in the rat genome is not uniform due to the variable density of available variants as discovered by WGS (Figure 5.2). As a result, gaps of >10Mb exist on Chr 2, 4, 6, 19, and X, with the largest gap of >60Mb on Chr 4 (Figure 5.3). These coverage gaps do not cause major concerns because these genomic regions do not seem to contain many variants and thus are less likely to be involved in artificial selection and QTL mapping.

5.2.3 Sample selection for genotyping

We genotyped a total of 672 samples across seven 96-well plates. Plate 1 included 17 batch 1 F1 samples and 79 F2 samples. This subset of F1 samples were genotyped to perform parent-child relatedness quality control, but since they do not represent all the F1's, they are not used in a linkage analysis. Plates 2-6 were all F2 samples (96*5 =480). Plate 7 included 63 F2 samples and 33 non-intercross HCR-LCR samples that need to be genotyped for another project. The non-intercross samples were genotyped previously and can be used to test genotype concordance between the new design and the RATDIV 800K SNP array. Genotyping experiments were performed

in one batch at the U-M DNA Genotyping and Sequencing Core using standard instruments, protocols, and reagents provided by Affymetrix.

5.2.4 Genotype data QC

To perform quality control on the SNP genotype data, I ran the *Best Practices Workflow* in the *Affymetrix Axiom Analysis Suite* version 1.1. The Affymetrix software first performs sample quality control by removing samples with <97% SNP call rate (4 F2 samples were removed in this step), followed by SNP quality control by classifying all of the SNPs into six groups based on the raw data clustering patterns and the resulting genotype calling quality; “PolyHighResolution” are SNPs with 3 distinct genotype clusters (n= 381,883); “NoMinorHom” are SNPs with only 2 distinct genotype clusters (n=70,465); “MonoHighResolution” are SNPs with only 1 genotype cluster (n= 100,198); “Off-Target Variant” are SNPs with 4 clusters, potentially due to 1) samples with genetic mismatch that do now allow hybridization, 2) 3rd/4th allele, or 3) indels (n= 5,091); “CallRateBelowThreshold” are SNPs that fell below 97% call rate (n= 21,918); “Other” are SNPs that fall into a catch-all category (could indicate much lower quality probes) (n= 45,736).

Since our rat system has a typical haplotype length of > 2 Mb (Chapter 2), there are enough SNPs in the highest quality group for association analysis. I therefore only extracted the SNPs in the “PolyHighResolution” class, which produce high-confidence genotype calls with three distinguishable genotype clusters. I then filtered the data using *PLINK*, first removing SNPs with per-SNP missing rate > 0.1 (geno 0.1), then removing samples with per-sample genotype missing rate > 0.03 (mind 0.03). These criteria removed 0 SNPs and 0 samples, yielding a final data set of 381,883 SNPs and 668 samples. To confirm that the genetic relatedness of the genotyped samples is

consistent with the known breeding scheme, I used *PLINK* to calculate the rate that a given pair of animals sharing zero (Z0) or one allele (Z1) across all the genotyped loci. This is done for all pairs of animals for the two batches separately. The Z0-Z1 plots are used to infer genetic relatedness.

5.2.5 QTL mapping

Using the final dataset of 616 F2 samples and 381,883 SNPs I performed association analysis for the running phenotype using three methods, (1) a conventional, single-SNP linear regression model, (2) the same method but using family ID (for the 63 F2 families) as a covariate, and (3) a single-SNP mixed-model association algorithm that accounts for the actual F2 population structure (*EMMAX*) (Kang et al. 2010). For *EMMAX*, I first calculated the kinship matrix for all pairs of animals using the genotype data, and then performed the association for the maximal running distance phenotype. In addition to association analysis, *EMMAX* also implements restricted maximum likelihood (REML) to calculate narrow-sense heritability.

5.3 Results

5.3.1 "F2" Intercross of HCR-LCR

To create a QTL mapping population with randomly mixed HLR-LCR genomes, we performed "F2" intercross experiments using 28 HCR-LCR pairs and obtained 242 F1 animals (described in Methods). From the phenotyped F1 population we set up 63 mating pairs and produced 645 F2 animals. The term "F1" or “F2” is applied loosely in this context because our crosses were not based on inbred lines. We use F0, F1, and F2 to denote the generations.

The running phenotype of F1 animals fell in an intermediate range between that of their HCR and LCR parents; and the F2 animals exhibited larger variations than F1 (Figure 5.1). This pattern is consistent with a model in which most neutral alleles no longer co-segregate with the phenotypes; and at functional loci (i.e., those responsible for the phenotypic differences between HCRs and LCRs), F1's tend to be heterozygous and F2's carry a wider assortment of genotypes that include both heterozygotes and homozygotes.

The Castle-Wright estimator of the effective number of QTLs is calculated as 4-10 using the trait value distributions of our F1 and F2 animals (Castle 1921, Wright 1968). Caution should be taken as the calculation is based on simplifying assumptions such as unlinked loci of equal effects that have no interaction. Only the actual linkage or association studies can reveal the number and impact of QTL underlying the trait in question.

Importantly, the h^2 of the maximal running distance in the F0-F2 pedigree remained high, calculated by *SOLAR* to be 0.60 ± 0.05 (Almasy and Blangero 1998). This is comparable to the h^2 estimate from the actual genotype data over all SNPs using *EMMAX*, which is 0.55. The h^2 for vertical work calculated using *SOLAR* is also high (0.61 ± 0.05), while the h^2 for average body weight is much lower (0.03 ± 0.04). In addition, we phenotyped five other physiological measures in a subset of F2 animals, including heart/body mass ratio (n=380), extensor digitorum longus *(EDL)* mass/body mass ratio (n=387), percent body fat (n=490), percent lean body mass (n=490), and fasting glucose level (n=490). *Using SOLAR,* we observed strong heritability values for the first three phenotypes, and lower values for the last two (lean body mass and fasting

glucose level)*:* 0.42 ± 0.11, 0.36 ± 0.10, 0.48 ± 0.10, 0.16 ± 0.07*, and 0.18* ± 0.07*,* respectively*.* These results indicate that the running capacity and related traits are clearly influenced by genetic factors, confirming that it is feasible to use the F2's as a mapping population in genetic analysis.

5.3.2 Genotyping data collection and QC

The *Best Practices Workflow* from the Affymetrix software removed four individuals with low call rate (<97%) among our samples, all of which were F2 samples from Plate 1, leaving us with 668 total samples. Next, extracting just the "*PolyHighResolution*" class of SNPs left us with 381,883 SNPs. To clean up the data further for QTL mapping, I used *PLINK* to remove SNPs with genotyping rate < 90% (geno 0.1) and then remove samples with genotyping rate < 97% (mind 0.03). It turns out that neither filter removed any SNP or sample, confirming the stringency of the Affymetrix filtering. After extracting only the F2 animals I was left with 616 samples for downstream analysis.

To confirm the expected relatedness, I separated the two intercross batches and created Z0-Z1 plots for all pairs of animals (Figure 5.4). In Batch 1 there was a clear separation of the parent-child pairs, sib pairs, and second-to-higher degree (2+) relative pairs. For Batch 2 we did not genotype any F1 parents, and still saw a clear separation of the sib pairs and the 2+ relative pairs. This result verified that the study maintained accurate sample tracking and the genotype data are reliable.

5.3.3 QTL Mapping by association analysis

I performed a conventional, single-SNP linear regression analysis, followed by two methods to adjust for the impact of familial relatedness among the F2 samples: first,

using F2 family ID as a covariate, and second, using a single-SNP mixed-model. The initial linear model produced more significant p-values than both adjustment methods (Figures 5.5). The logarithm of p-values are highly correlated between the initial analysis and *EMMAX* analysis (ρ=0.38), and less correlated between the analysis with family ID as a covariate and *EMMAX* analysis (ρ =0.24) (Figure 5.6). The QQ-plot shows that this is due to heavily inflated p-values from the linear model, presumably due to not accounting for familial structure (Figure 5.7). Both of the linear regression analyses, with and without accounting for population structure, produced the same top SNP (Chr6: 94,770,157, genome build rn5), which falls under an intergenic region on Chromosome 6 (Figure 5.8). This SNP is not likely a true positive because it is not in LD with any of the adjacent SNPs and therefore not supported by other associated SNP in the vicinity.

In the *EMMAX* results, Chromosome 18p12 has a region of significant association (Figure 5.9). This region of ~1 Mb contains four genes; *Desmocollin* 3 (*Dsc3)*, *Desmocollin* 2 (*Dsc2)*, *Desmoglein 4 (Dsg4)*, and *Kelch-Like Family Member 14* (*Klhl14*). To test if there are additional association signals in the 18p12 associated region, I performed a conditional analysis by using the top SNP (Chr18: 12,529,014 genome build rn5) as a covariate and re-running *EMMAX*. This resulted in the disappearance of all the association signals in 18p12, although the same false-positive SNP on Chromosome 6 described above remains significant (Figure 5.10).

Three of the genes in the QTL region, *Dsc3*, *Dsc2, Dsg4* have direct roles in cell-cell adhesion and desmosome formation (Kljuic et al. 2003, Whittock and Bower 2003, Oshiro et al. 2005, Chen et al. 2008, Resnik et al. 2011, Fang et al. 2014). I therefore

further interrogated these candidates in the pooled WGS data from Chapter 4. I zoomed into the gene regions from the start and end sites for these three genes in the four sequenced pools (HCR G26, LCR G26, HCR G5, LCR G5), to look for 1) oppositely fixed alleles and 2) coding variants. In *Dsc3* (chr18:11,831,071-11,865,107, genome build rn5) there were 81 SNVs, including 3 synonymous coding variants and 1 non-synonymous coding variant (Figure 5.11). Interestingly, for the non-synonymous coding variant (Chr18:11,864,899, genome build rn5), the both lines at G5 are fixed or nearly fixed for the reference allele; however at G26, about half of HCRs have the alternative allele, while the LCRs are all fixed for the reference allele. For this variant, the reference allele is a 'T', while the alternative allele is a 'C', and it is only conserved in mice. The alternative allele results in a missense mutation; changing a Leucine (CTC) to a Proline (CCC), and is annotated as having MODERATE impact by Variant Effector Predictor (McLaren et al. 2010). In *Dsc2* (chr18: 11,902,185-11,933,989, genome build rn5) there were 126 SNVs, including 3 synonymous coding variants and 2 non-synonymous coding variant (Figure 5.12). The 2 non-synonymous coding variants (Chr18: 11,916,469 & Chr18: 11,924,343 genome build rn5) did not show much allelic differences between the two lines across time points. In *Dsg4* (chr18: 12,173,507-12,209,833, genome build rn5) there were 52 SNVs, with no coding variants discovered by sequencing (Figure 5.13). None of these three genes are significantly differentially expressed between HCR-LCR in the transcriptomic data (Chapter 3) for the main effect, although *Dsc3* is mildly differentially expressed for Edge 4 (HCR-LCR for Young Exhausted animals) (p-value= 0.04, fold-change = 1.2).

5.4 Discussion

The strong heritability for the running phenotype in the HCR and LCR lines as reported in Chapter 2 is recapitulated in the F0-F1-F2 population, suggesting that causal variants not only continue to segregate in both HCRs and LCRs but also persist in the F2 population. This observation provided direct evidence that the trait under selection is highly heritable, and provided justification for intercross-based QTL mapping. In addition, the heritability for weight, vertical work, heart/body ratio, EDL/body ratio, and percent body fat suggests that the model can be used for simultaneous QTL mapping for multiple traits.

In the F2 generation of the intercross, the running distance distribution is wider than in F1, but did not reach the full range seen in F0. The fact that none of the F2 animals performed as well as their HCR grandparents, and very few performed as poorly as their LCR grandparents, strongly suggests that multiple genetic loci are involved. Single-SNP association analysis using *EMMAX* identified a cluster of significant SNPs in an 1 Mb region on 18p12 (Figure 5.7b). Interestingly, *Desmocollin* 3 (*Dsc3)*, *Desmocollin* 2 (*Dsc2)*, and *Desmoglein 4 (Dsg4)* have direct roles in cell-cell adhesion and desmosome formation (Kljuic et al. 2003, Whittock and Bower 2003, Oshiro et al. 2005, Chen et al. 2008, Resnik et al. 2011, Fang et al. 2014). In addition, I also found a non-synonymous variant in *Dsc3* with increased alternative allele frequency in HCRs at G26, but not in LCRs, which remain fixed for the reference allele (Chapter 4, and Figure 5.11). *Dsc3* also showed higher expression in young HCR compared to young LCR after exercise (Chapter 3). These factors make *Dsc3* an appealing candidate to further characterize.

Desmosomes are intercellular junctions that provide strong adhesion between muscle cells and are important in resisting mechanical stress, thus their primary function is maintaining proper cell and tissue integrity (Garrod and Chidgey 2008). These genes could be one of the primary drivers that conferred the incredible running performance in the high runners via increased tissue integrity in both skeletal and cardiac muscles. Interestingly, in a recent study of the DNA sequencing data of supercentenarians (110 years or older), one supercentenarian was found to possess a pathogenic mutation in *Dsc2* that disrupts a splice site (Gierman et al. 2014). It's not clear at this time how my QTL hits is related to the link between aerobic exercise capacity and the metabolic, physiological, and longevity phenotypes that diverged between HCR and LCR. At the time of writing this chapter, I have completed the initial steps for QTL mapping in the f2 population, and have shown several promising candidates that need to be refined, validated, and further interrogated for potential mechanism.

5.6 Figures

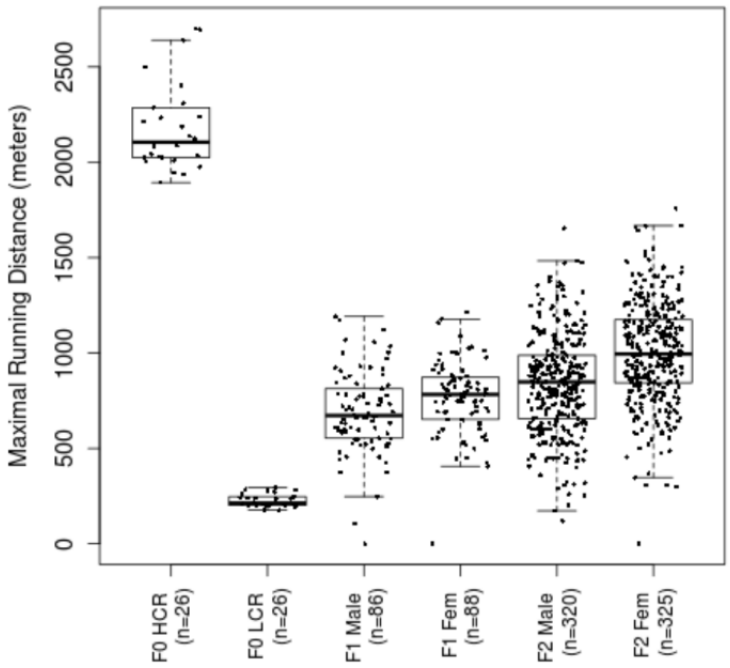

Figure 5.1: Distribution of running performance for animals of the F2 intercross experiment.

Shown are boxplots of the best running distance by generation and by sex.

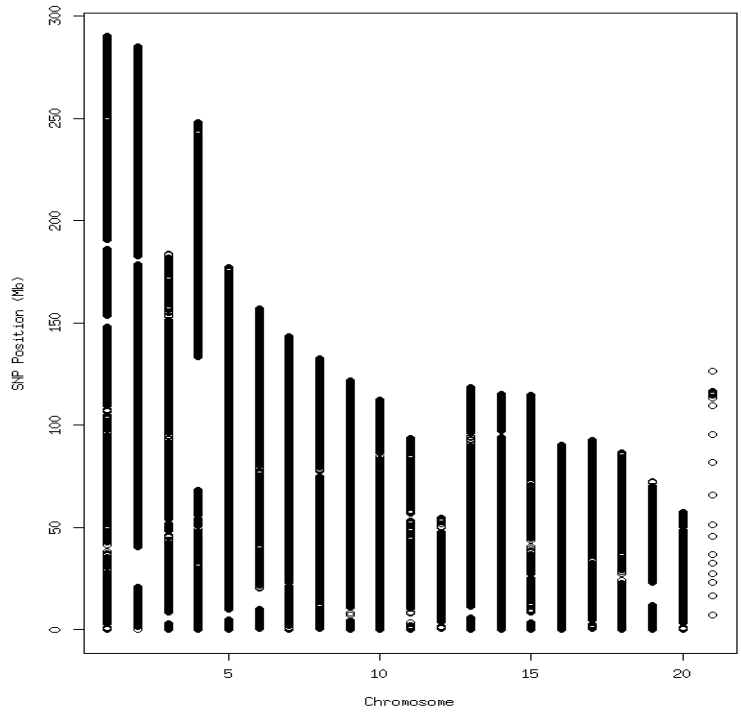

Figure 5.2: Coverage of the ~625K SNPs.

Show is the coverage across the Chromosomes 1-20 and Chromosome X (x-axis) by our custom SNP array. Y-axis represents the position across the chromosomes in Mb.

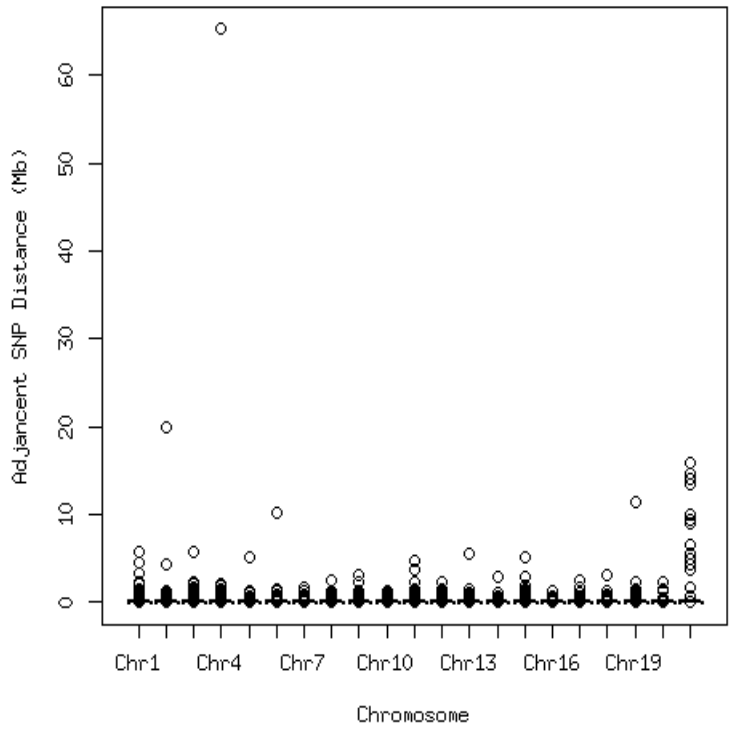

Figure 5.3: Intermarker distance (in Mb, y-axis) for each chromosome (x-axis) for the ~625K SNPs.

There are a few >10Mb SNP gaps on Chromosomes 2, 4, 6, 19, and X. The large gap on Chromosome 4 (>60Mb) is in a gene/polymorphism desert.

a

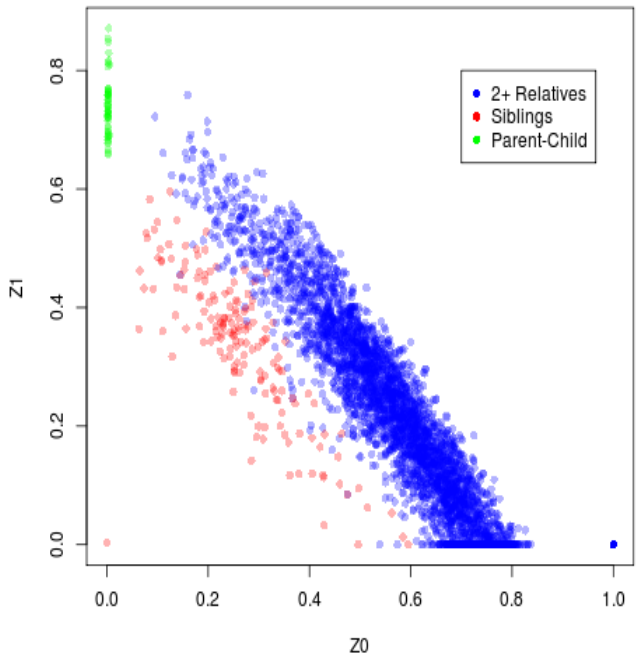

b

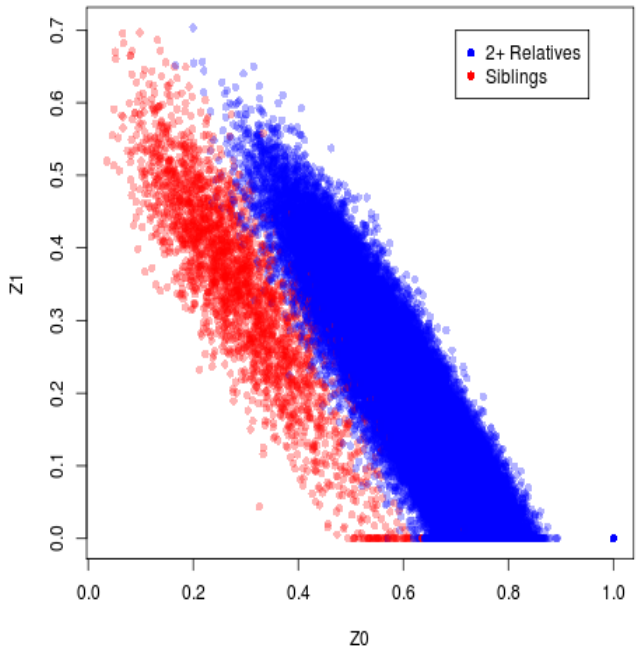

Figure 5.4: Z0-Z1 relatedness plot for all pairwise comparisons among (a) batch 1 and (b) batch 2 samples.

In batch 1, we genotyped 17 F1 samples, which serve to check for parent-child relatedness.

a

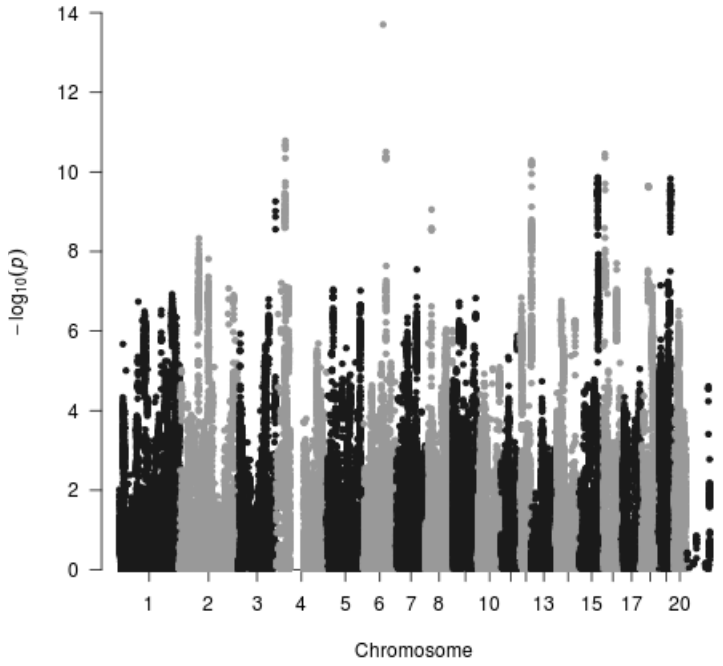
14
12
10
8
6
4
2
0
$-\log_{10}(p)$
1
2
3
4
5
6
7
8
10
13
15
17
20
Chromosome

b

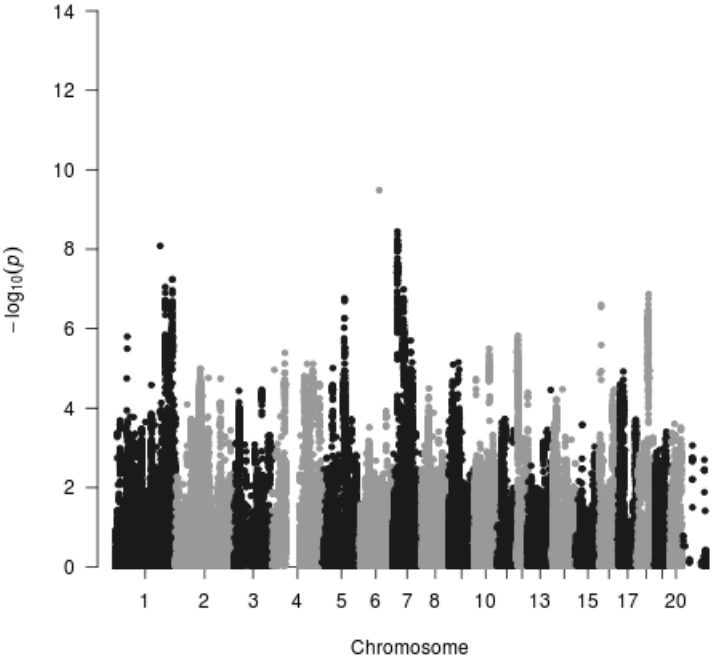
14
12
10
8
6
4
2
0
$-\log_{10}(p)$
1
2
3
4
5
6
7
8
10
13
15
17
20
Chromosome

c

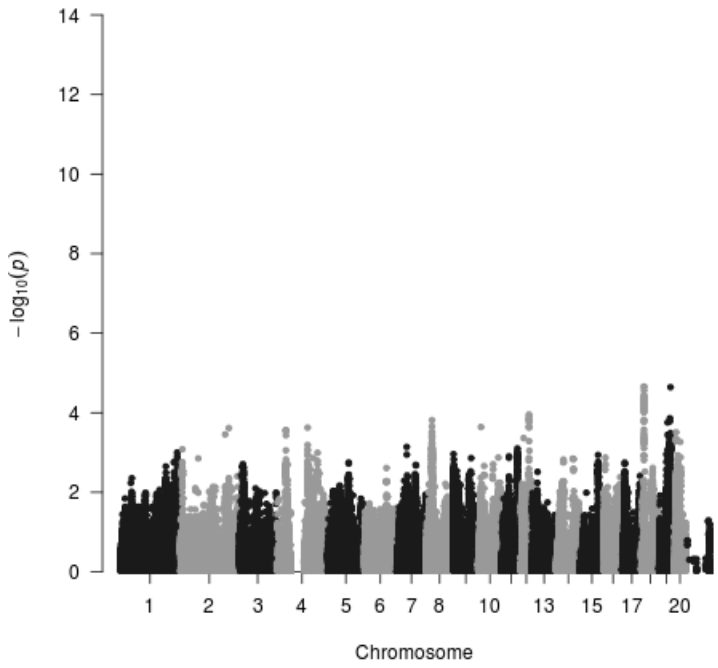

Figure 5.5: GWAS results for linear model (a), linear model with family ID as covariate (b), and EMMAX (b) across 381K SNPs in 616 F2 samples for the maximal running distance trait.

a

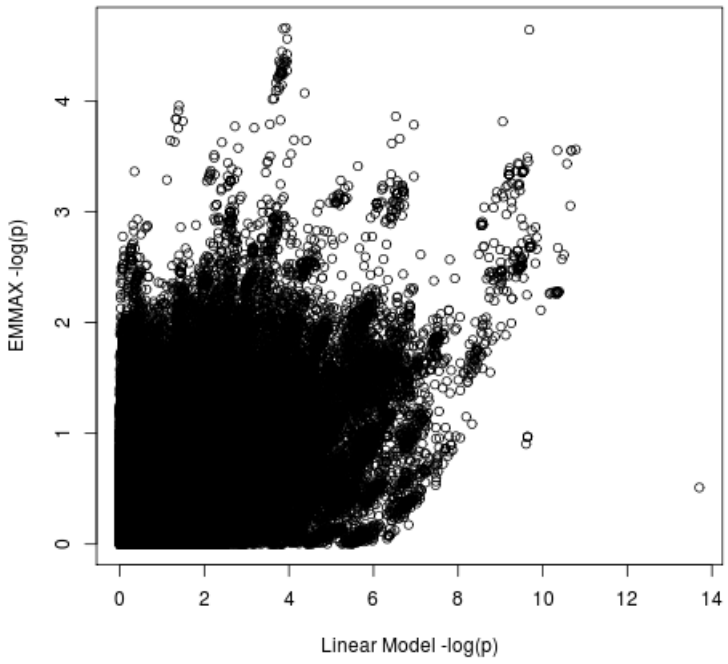

b

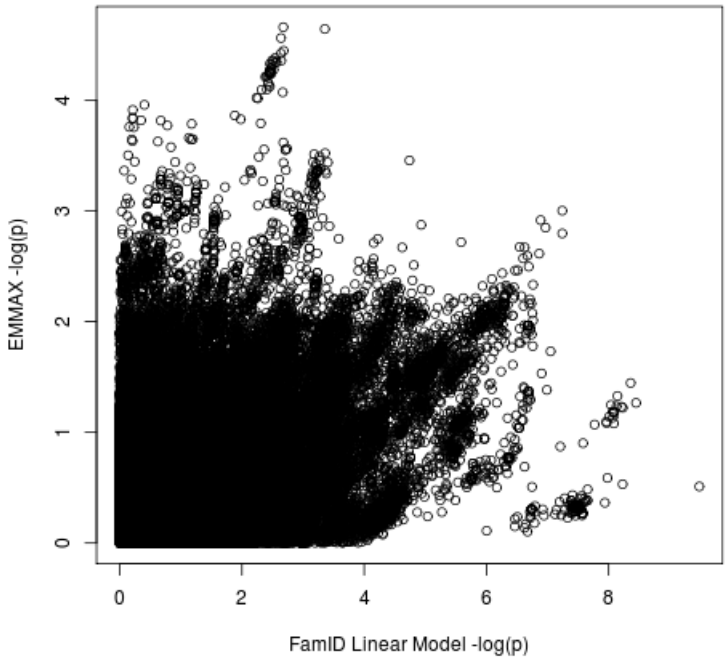

Figure 5.6: Scatterplot of GWAS results for linear model (x-axis) without covariates (a) and with family ID as covariate (b) versus EMMAX (y-axis) across 381K SNPs in 616 F2 samples for the maximal running distance trait.

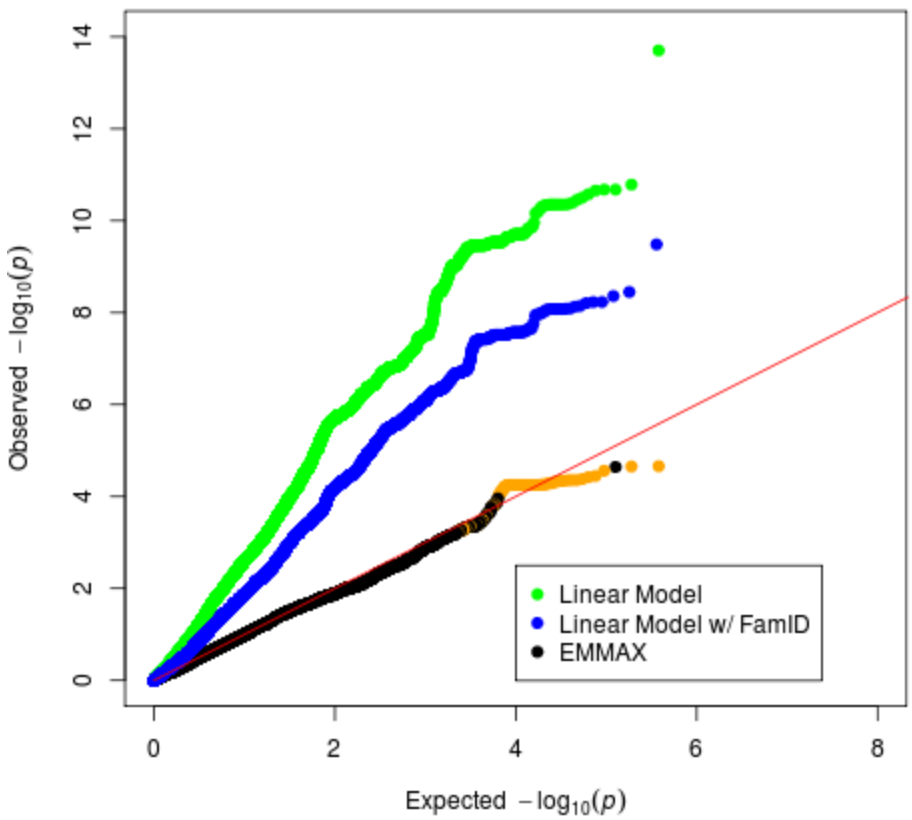

Figure 5.7: QQ-plot of GWAS p-values for linear model (green), linear model with family ID as covariate (blue), and EMMAX (black) across 381K SNPs in 616 F2 samples for the maximal running distance trait.

For the EMMAX QQ-plot, the 84 SNPs in the Chromosome 18 QTL region are shown in orange.

a

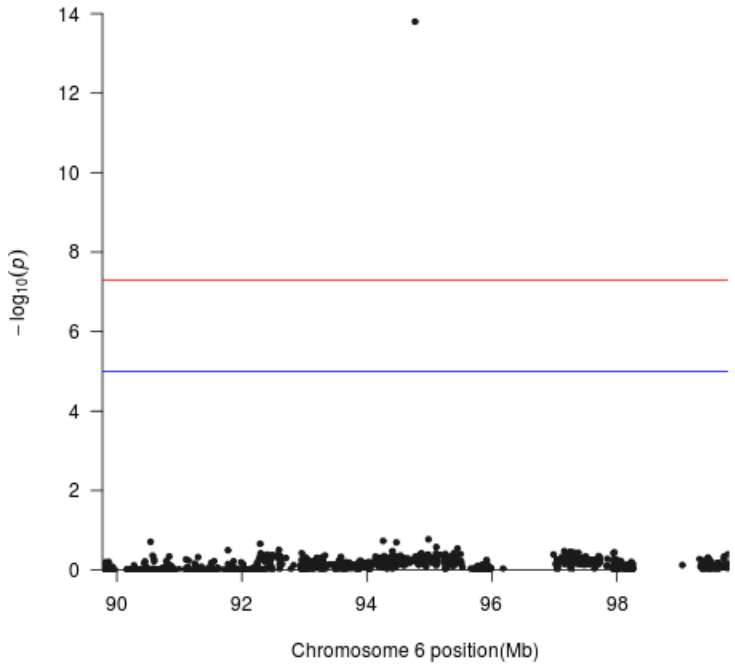
14
12
10
8
6
4
2
0
$-\log_{10}(p)$
90
92
94
96
98
Chromosome 6 position(Mb)

b

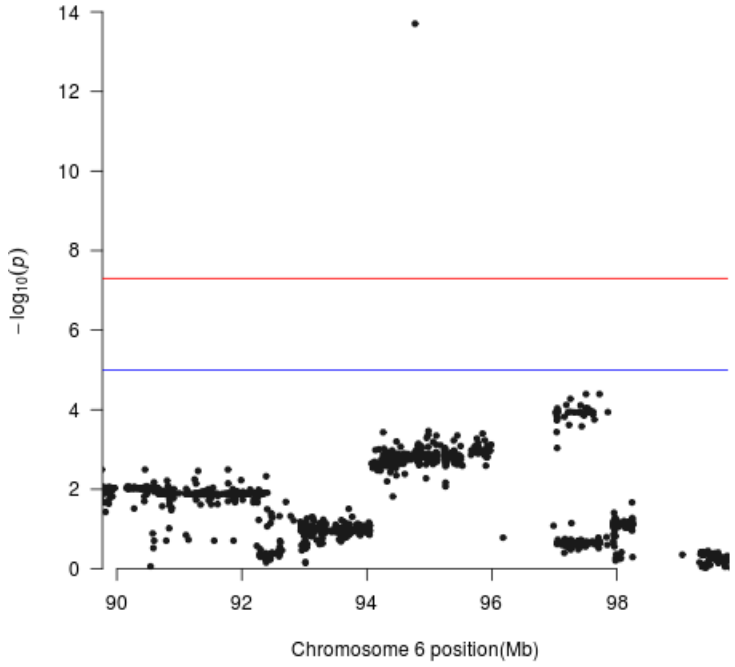
14
12
10
8
6
4
2
0
$-\log_{10}(p)$
90
92
94
96
98
Chromosome 6 position(Mb)

c

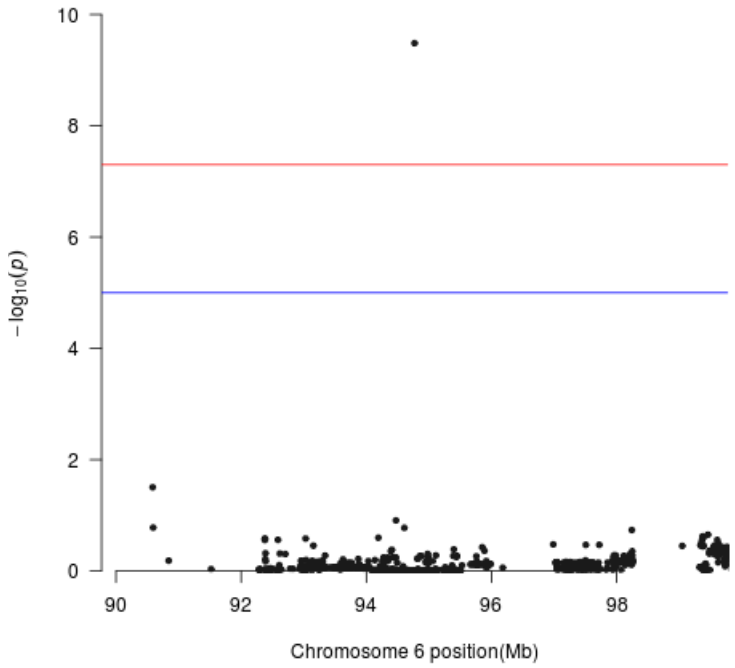

Figure 5.8: Manhattan zoom plot of 5 Mb up- and down-stream from the most significant SNP (Chr6: 94770157).

The EMMAX conditional analysis (a) using the original top SNP (Chr18:12,529,014**)** as a covariate resulted in the SNP on Chromosome 6 to become the most significant signature. This is the same top SNP as for the linear model with (b) and without family id as covariate (c).

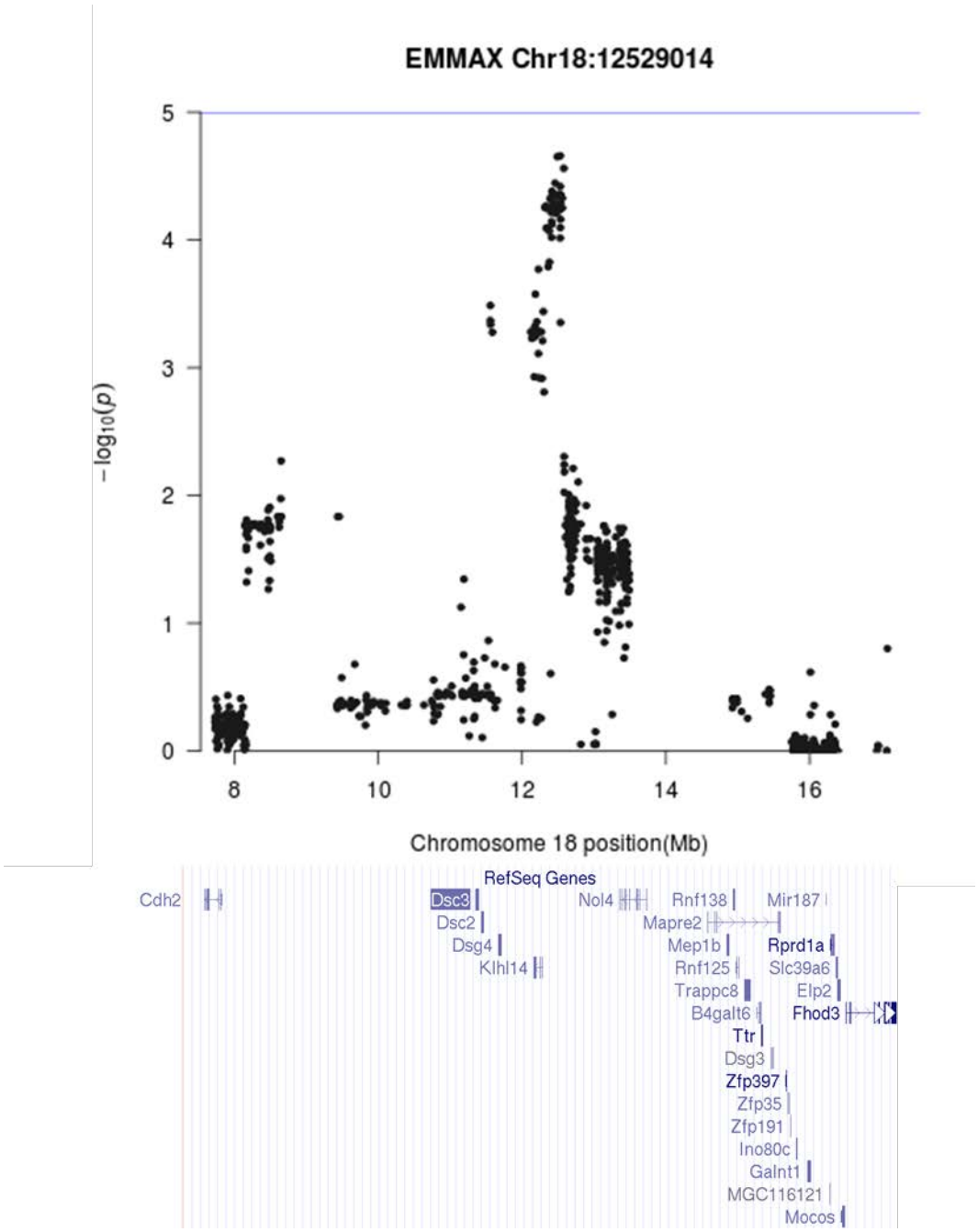

Figure 5.9: Manhattan zoom plot of 5 Mb up- and down-stream from the most significant SNP (Chr18: 12529014) with genes within the region below.

a

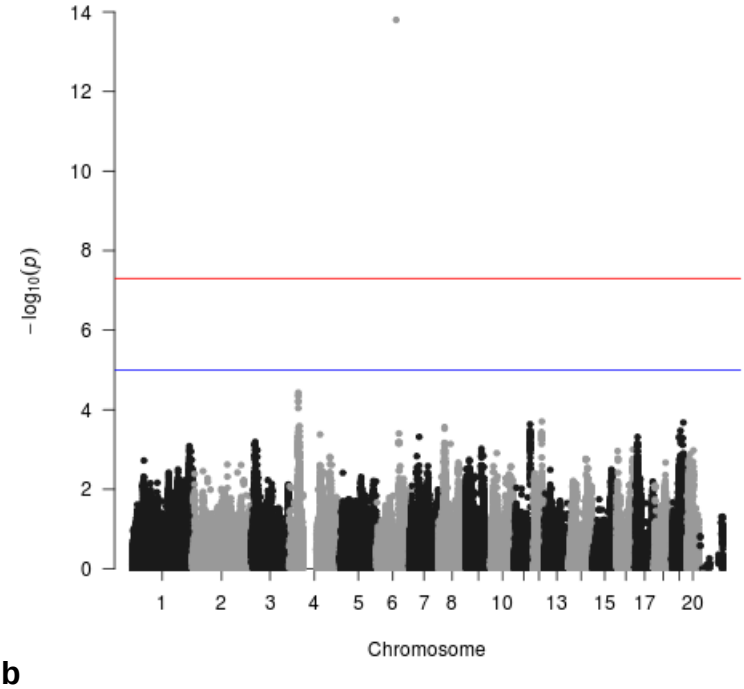

b

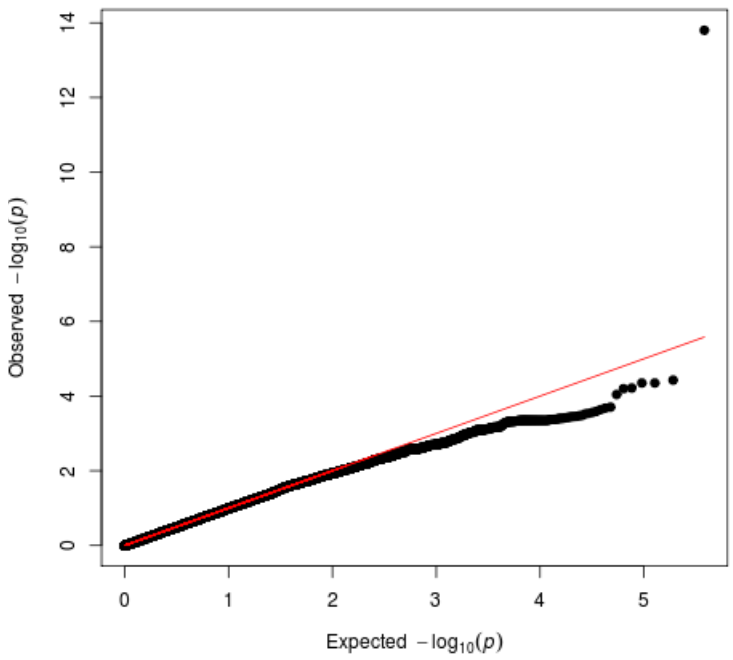

Figure 5.10: (a) Conditional GWAS results and (b) QQ-plot for EMMAX across 381K SNPs in 616 F2 samples for the maximal running distance trait with the top SNP (Chr18: 12529014) added as covariate.

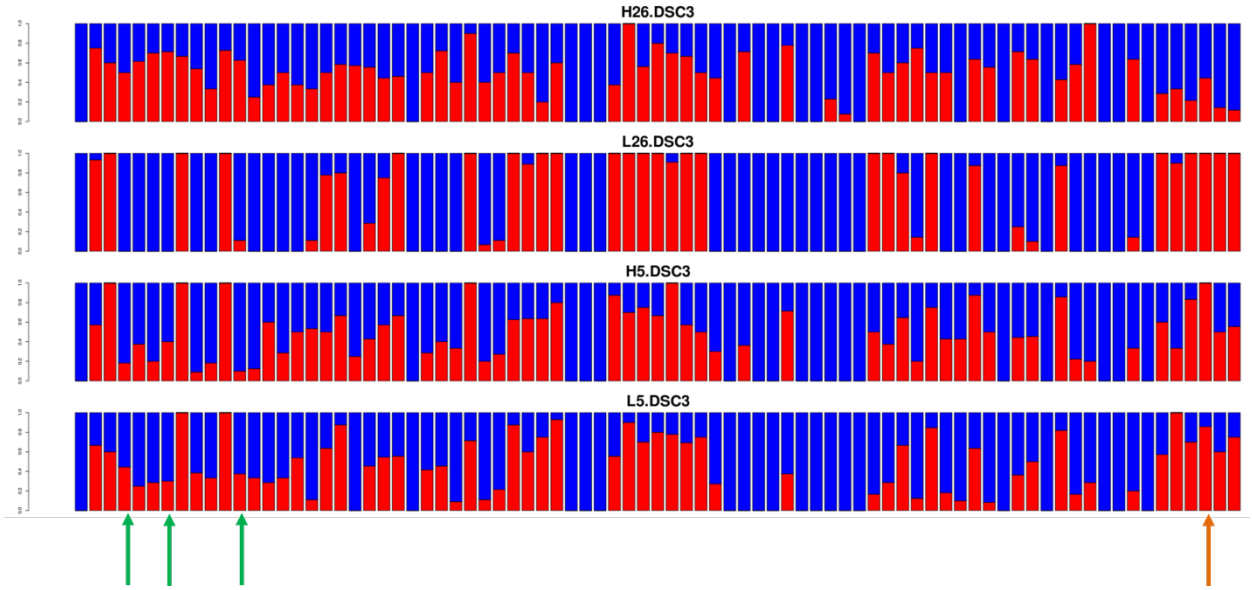

Figure 5.11: Pooled WGS allele counts for the four groups (n=10 each) from Chapter 4 across the *Dsc3* gene.

The four groups sequenced are represented in each of the four tracks. Each column represents the allele count frequency of a single SNV; red represents the proportion of reference alleles and blue represents the proportion of alternative alleles out of each group. The arrows below indicate the synonymous (green) and nonsynonymous (orange) coding variants, while the rest are intronic variants.

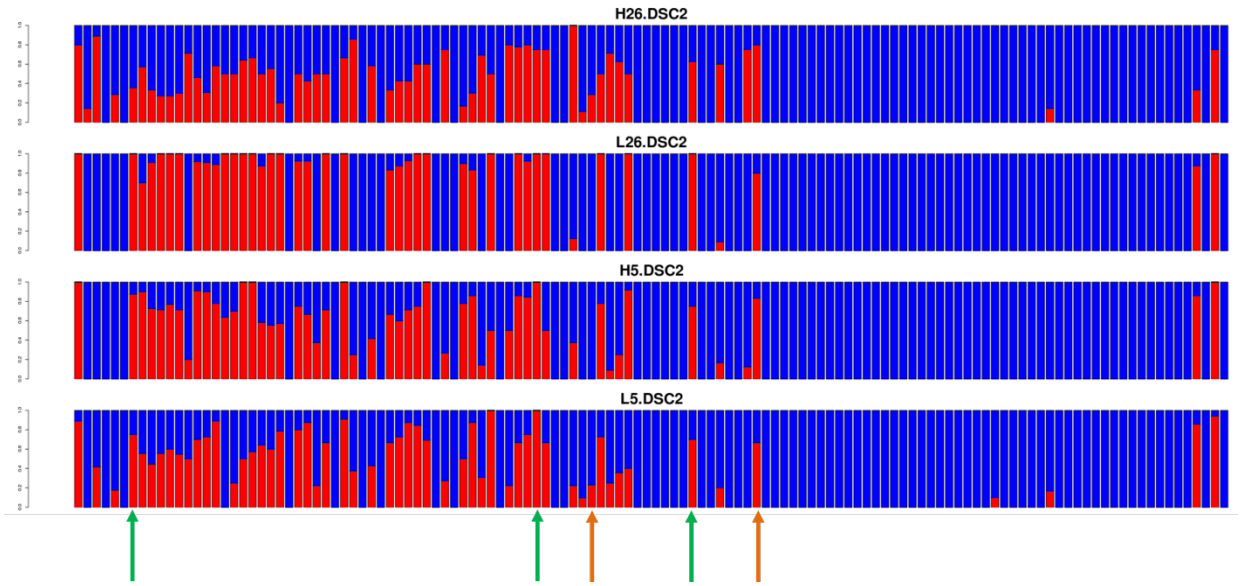

Figure 5.12: Pooled WGS allele counts for the four groups (n=10 each) from Chapter 4 across the *Dsc2* gene.

The four groups sequenced are represented in each of the four tracks. Each column represents the allele count frequency of a single SNV; red represents the proportion of reference alleles and blue represents the proportion of alternative alleles out of each group. The arrows below indicate the synonymous (green) and nonsynonymous (orange) coding variants, while the rest are intronic variants.

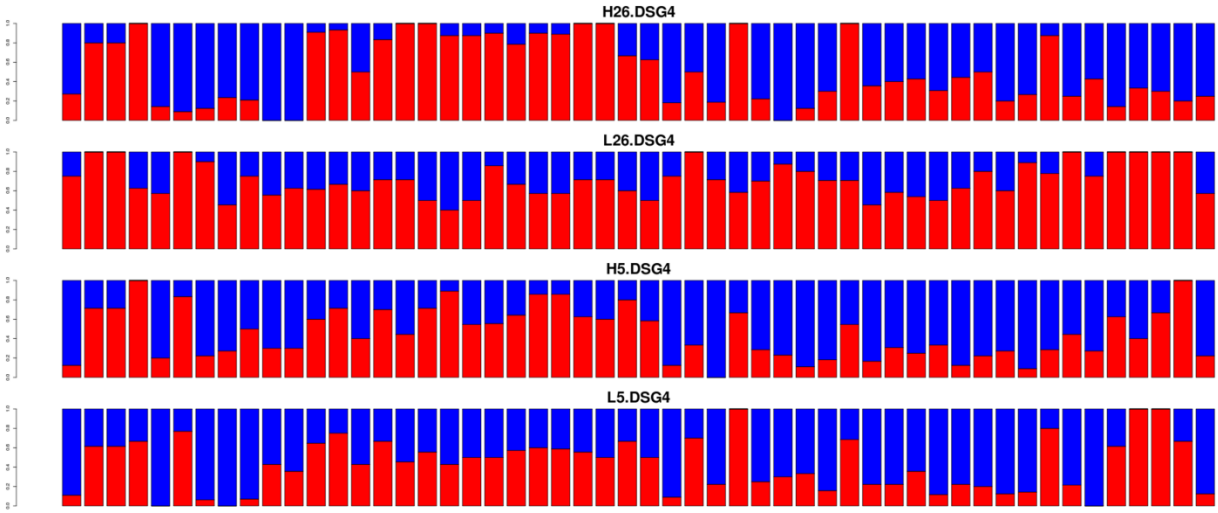

Figure 5.13: Pooled WGS allele counts for the four groups (n=10 each) from Chapter 4 across the *Dsg4* gene.

The four groups sequenced are represented in each of the four tracks. Each column represents the allele count frequency of a single SNV; red represents the proportion of reference alleles and blue represents the proportion of alternative alleles out of each group. There were no coding variants identified by sequencing in this gene.

CHAPTER 6

Conclusions and Future Directions

6.1 Genetic analysis of the pedigrees

While previous studies of HCR/LCR focused on various aspects of their physiology, I conducted the first in-depth genetic analysis and have published the results in an article in *PLoS One*. During the course of 30+ generations of selection the HCRs continue to respond to selection with increased performance. The narrow-sense heritability (h^2) for maximal running distance is 0.47 ± 0.02 in HCRs and 0.43 ± 0.03 in LCRs. These results suggest that causal DNA variants have not been fixed in either line, rather they continue to segregate in both pedigrees. As an initial molecular genetic characterization, we collected genotype data over a genome-wide panel of ~10K single nucleotide polymorphism (SNP) loci for animals in three non-adjacent generations (G5, G14, and G26) in both lines. These data show that at G5, HCRs and LCRs formed two clearly separable clusters, and the two clusters diverged progressively further in G14 and G26. The SNP data also show that genomewide heterozygosity decreased over time, confirming the expected increase of inbreeding levels. However, the rate of increase of inbreeding is slower than random mating, in agreement with the expected benefit of our rotational breeding scheme. A majority of the increase of homozygote genotypes is accounted for by the emergence or expansion of long runs of homozygosity (ROH). Some of these ROH may arise due to selection, while others

reflect random genetic drift. In Chapter 3 I apply ROH as one of the criteria to screen for candidate regions under selection. Taken as a whole, these results suggest that the HCR-LCR system is a novel model system suitable for studying genome evolution under sustained selection, and for dissecting the functional and genetic basis of polygenic traits.

6.2 Selection-, age-, and exercise-dependence of skeletal muscle gene expression patterns

Aerobic capacity in humans is strongly associated with longevity. Similarly, the median lifespan is 23.5 months in LCRs and 30.1 months in HCRs, a 28% difference (a second study showed a 45% difference). It has long been appreciated that biological regulation is affected by inherited genetic variation, naturally occurring aging process, as well as responses to immediate physiological stressors. These factors act jointly but have not been analyzed simultaneously in a single study. I therefore designed a three-factor study, comparing microarray-based gene expression data for both young and old animals, in both HCR and LCR, using tissue collected both at rest and at exhaustion after exercise. This 2-2-2 design consists of a total of eight groups (n=6 each). A principal component analysis (PCA) of the 19,607 measured transcripts shows that the 48 samples fall into eight clusters in the PC1-PC2 space; and they correspond to the eight known groups. Thus, at the global level each of the three factors--line, age, and exercise--has a main effect. I analyzed the main effects for each factor both globally and, in stratified analyses, in each of the four subgroups formed by the combination of the other two factors. For example, I documented the HCR-LCR differences in an overall comparison involving all HCR and all LCR animals, but also in four stratified comparisons involving the old-rest, old-exhausted, young-rest, and young-exhausted

animals. The differences among the four strata reflect the interaction effects among the factors. I analyzed both the main effects and the interaction effects at two levels: individual genes and the functional pathways.

My findings support previous reports that HCRs show higher expression than LCRs in genes involved in mitochondria function, and my data further show that this difference is consistent whether after strenuous exercise or at rest. In addition, I found that old rats consistently show lower expression than young rats in genes involved in extracellular matrix, collagen, and cell adhesion, in both HCRs and LCRs and both after exercise and at rest. Further, aging-effect in LCRs show more significant enrichment for all three pathways compared to HCRs, suggesting that LCRs' lower innate aerobic capacity underlies their faster aging. For the exercise effect, exhausted rats consistently show up-regulation in transcription factor activity compared to rats at rest. These and additional results for interaction effects have been submitted to *Physiological Genomics*.

6.3 High-density SNP array and genome sequencing reveal signatures of selection

To identify genomic regions under selection I combined multiple scan statistics, comparing genomic patterns both among different generations and between the two lines. To increase the density of genomic coverage over the 10K SNP data I collected genotype data using a ~800K SNP panel and analyzed 45 animals (10-12 in each line in G5 and G26). I calculated the fixation index (F_{st}) in 1Mb windows, and detected long runs of homozygosity, using both results to identify regions that are highly differentiated between the two lines and two time points. In addition, I performed whole-genome sequencing on four pools of DNA samples (for HCR/LCR, G5/G26), and estimated

allele frequencies across ~6 million variant sites. Using the between-pool difference in allele frequency spectrum (AFS) in 1 Mb windows I also uncovered another set of signatures of selection. In an effort to combine the selection signatures, I implemented a composite score method that transforms each of the statistics independently in order to preserve the concordant selection signals. The composite score analysis revealed several candidate genes and pathways that will be combined with the multi-omics results in Chapters 3 and 5 to identify the causal mechanisms linking AEC and metabolic health. The manuscript for this chapter is posted to *Biorxiv*.

6.4 F2-based QTL mapping

As HCR and LCR have evolved separately, a direct between-line comparison would be dominated by the effect of population stratification. To create a QTL mapping population with randomized genomes, we performed HCR-LCR intercross and obtained 242 F1 and 645 F2 animals. The running phenotype of F1 fell in an intermediate range between that of their HCR and LCR parents, and the F2 animals exhibited larger variations than the F1 rats. Importantly, the h^2 of the maximal running distance in this population remained high, at 0.60 ± 0.05. In addition, other related metabolic and physiological traits also showed strong heritability. I have designed a custom genotyping array with 625K most informative SNPs based on genome sequencing data of the eight founder lines and our pooled sequencing data. I have genotyped >600 F2 animals and obtained preliminary association results, highlighting, among others, a 1 Mb region on chromosome 18 with three candidate genes with plausible biological relevance for the metabolic phenotype. Combining the multi-omics data from Chapters 3-5 unveils *Dsc3* as a particularly interesting candidate with implications in all three projects.

6.5 Next steps for causal gene identification

Chapter 5 of my dissertation served to establish the basis of using the HCR-LCR model system for gene mapping in an F2 intercross. We now have access to a 625K SNP genotyping array filled with informative ancestral informative markers for our specific genetic background. A potential problem with our current QTL mapping approach is the mapping resolution. To address this, we will take advantage of ancestral haplotype mapping by using the *HAPPY* method (Mott et al. 2000, Valdar et al. 2006). Given that our HCR-LCR lines were derived from the HS rats, which were derived from eight original inbred strains of rats, every animal can have up to eight unique ancestral haplotypes. By analyzing the association between the eight ancestral haplotypes and the observed phenotypes we can take advantage of the historical recombination events over the ~30 generations since the founding of HS and >28 generations of divergent selection. Our preliminary data show that LD in the HCR-LCR lines decreased to $r<0.3$ at about 3 Mb, suggesting that the mapping resolution can be as high as 2-3 cM (Johannesson et al. 2009, Ren et al. 2013). *HAPPY* was successfully applied to HS lines (Solberg et al. 2006, Valdar et al. 2006), and subsequently adopted for QTL fine mapping in projects similar to mine, involving F2 crosses of divergently selected outbred mice for an alcohol preference phenotype (Foroud et al. 2000, Bice et al. 2009).

Once we have identified specific genes with strong confidence as causal factors in the HCR-LCR system, we plan to test the impact of these genes in a transgenic model system. The knock-ins/outs can be done in inbred background strains, or in outbred animals multiple times to average across individual backgrounds.

REFERENCES

Albert, F. W., O. Carlborg, I. Plyusnina, F. Besnier, D. Hedwig, S. Lautenschlager, D. Lorenz, J. McIntosh, C. Neumann, H. Richter, C. Zeising, R. Kozhemyakina, O. Shchepina, J. Kratzsch, L. Trut, D. Teupser, J. Thiery, T. Schoneberg, L. Andersson and S. Paabo (2009). "Genetic architecture of tameness in a rat model of animal domestication." Genetics 182(2): 541-554.

Almasy, L. and J. Blangero (1998). "Multipoint quantitative-trait linkage analysis in general pedigrees." Am J Hum Genet 62(5): 1198-1211.

Almasy, L. and J. Blangero (1998). "Multipoint quantitative-trait linkage analysis in general pedigrees." American Journal of Human Genetics 62(5): 1198-1211.

Baker, J. S., M. C. McCormick and R. A. Robergs (2010). "Interaction among Skeletal Muscle Metabolic Energy Systems during Intense Exercise." Journal of Nutrition and Metabolism 2010: 13.

Barbato, J. C., L. G. Koch, A. Darvish, G. T. Cicila, P. J. Metting and S. L. Britton (1998). "Spectrum of aerobic endurance running performance in eleven inbred strains of rats." J Appl Physiol 85(2): 530-536.

Barrett, J. C., B. Fry, J. Maller and M. J. Daly (2005). "Haploview: analysis and visualization of LD and haplotype maps." Bioinformatics 21(2): 263-265.

Bastiaansen, J. W., A. Coster, M. P. Calus, J. A. van Arendonk and H. Bovenhuis (2012). "Long-term response to genomic selection: effects of estimation method and reference population structure for different genetic architectures." Genetics Selection Evolution 44: 3.

Baud, A., V. Guryev, O. Hummel, M. Johannesson, S. Rat Genome, C. Mapping and J. Flint (2014). "Erratum: Genomes and phenomes of a population of outbred rats and its progenitors." Sci Data 1: 140016.

Baud, A., V. Guryev, O. Hummel, M. Johannesson, S. Rat Genome, C. Mapping and J. Flint (2014). "Genomes and phenomes of a population of outbred rats and its progenitors." Sci Data 1: 140011.

Baud, A., R. Hermsen, V. Guryev, P. Stridh, D. Graham, M. W. McBride, T. Foroud, S. Calderari, M. Diez, J. Ockinger, A. D. Beyeen, A. Gillett, N. Abdelmagid, A. O. Guerreiro-Cacais, M. Jagodic, J. Tuncel, U. Norin, E. Beattie, N. Huynh, W. H. Miller, D. L. Koller, I. Alam, S. Falak, M. Osborne-Pellegrin, E. Martinez-Membrives, T. Canete, G. Blazquez, E. Vicens-Costa, C. Mont-Cardona, S. Diaz-Moran, A. Tobena, O. Hummel, D. Zelenika, K. Saar, G. Patone, A. Bauerfeind, M. T. Bihoreau, M. Heinig, Y. A. Lee, C. Rintisch, H. Schulz, D. A. Wheeler, K. C. Worley, D. M. Muzny, R. A. Gibbs, M. Lathrop, N. Lansu, P. Toonen, F. P. Ruzius, E. de Bruijn, H. Hauser, D. J. Adams, T. Keane, S. S. Atanur, T. J. Aitman, P. Flicek, T. Malinauskas, E. Y. Jones, D. Ekman, R. Lopez-Aumatell, A. F. Dominiczak, M. Johannesson, R. Holmdahl, T. Olsson, D. Gauguier, N. Hubner, A. Fernandez-Teruel, E. Cuppen, R. Mott and J. Flint (2013). "Combined sequence-based and genetic mapping analysis of complex traits in outbred rats." Nat Genet 45(7): 767-775.

Bice, P., W. Valdar, L. Zhang, L. Liu, D. Lai, N. Grahame, J. Flint, T. K. Li, L. Lumeng and T. Foroud (2009). "Genomewide SNP screen to detect quantitative trait loci for alcohol preference in the high alcohol preferring and low alcohol preferring mice." Alcohol Clin Exp Res 33(3): 531-537.

Blair, S. N., J. B. Kampert, H. W. Kohl, 3rd, C. E. Barlow, C. A. Macera, R. S. Paffenbarger, Jr. and L. W. Gibbons (1996). "Influences of cardiorespiratory fitness and other precursors on cardiovascular disease and all-cause mortality in men and women." JAMA 276(3): 205-210.

Blair, S. N., H. W. Kohl, 3rd, R. S. Paffenbarger, Jr., D. G. Clark, K. H. Cooper and L. W. Gibbons (1989). "Physical fitness and all-cause mortality. A prospective study of healthy men and women." JAMA 262(17): 2395-2401.

Bouchard, C., T. Rankinen, Y. C. Chagnon, T. Rice, L. Perusse, J. Gagnon, I. Borecki, P. An, A. S. Leon, J. S. Skinner, J. H. Wilmore, M. Province and D. C. Rao (2000). "Genomic scan for maximal oxygen uptake and its response to training in the HERITAGE Family Study." J Appl Physiol 88(2): 551-559.

Bray, M. S. (2000). "Genomics, genes, and environmental interaction: the role of exercise." J Appl Physiol 88(2): 788-792.
Bray, M. S., J. M. Hagberg, L. Perusse, T. Rankinen, S. M. Roth, B. Wolfarth and C. Bouchard (2009). "The human gene map for performance and health-related fitness phenotypes: the 2006-2007 update." Med Sci Sports Exerc 41(1): 35-73.
Burghardt, P. R., S. B. Flagel, K. J. Burghardt, S. L. Britton, L. Gerard-Koch, S. J. Watson and H. Akil (2011). "Risk-assessment and coping strategies segregate with divergent intrinsic aerobic capacity in rats." Neuropsychopharmacology 36(2): 390-401.
Bye, A., M. A. Hoydal, D. Catalucci, M. Langaas, O. J. Kemi, V. Beisvag, L. G. Koch, S. L. Britton, O. Ellingsen and U. Wisloff (2008). "Gene expression profiling of skeletal muscle in exercise-trained and sedentary rats with inborn high and low VO2max." Physiol Genomics 35(3): 213-221.
Carlborg, O., L. Jacobsson, P. Ahgren, P. Siegel and L. Andersson (2006). "Epistasis and the release of genetic variation during long-term selection." Nat Genet 38(4): 418-420.
Cary, L. A. and J. L. Guan (1999). "Focal adhesion kinase in integrin-mediated signaling." Front Biosci 4: D102-113.
Castle, W. E. (1921). "An Improved Method of Estimating the Number of Genetic Factors Concerned in Cases of Blending Inheritance." Science 54(1393): 223.
Chen, J., Z. Den and P. J. Koch (2008). "Loss of desmocollin 3 in mice leads to epidermal blistering." J Cell Sci 121(Pt 17): 2844-2849.
Church, T. S., Y. J. Cheng, C. P. Earnest, C. E. Barlow, L. W. Gibbons, E. L. Priest and S. N. Blair (2004). "Exercise capacity and body composition as predictors of mortality among men with diabetes." Diabetes Care 27(1): 83-88.
de Magalhaes, J. P., J. Curado and G. M. Church (2009). "Meta-analysis of age-related gene expression profiles identifies common signatures of aging." Bioinformatics 25(7): 875-881.
Deloukas, P., S. Kanoni, C. Willenborg, M. Farrall, T. L. Assimes, J. R. Thompson, E. Ingelsson, D. Saleheen, J. Erdmann, B. A. Goldstein, K. Stirrups, I. R. Konig, J. B. Cazier, A. Johansson, A. S. Hall, J. Y. Lee, C. J. Willer, J. C. Chambers, T. Esko, L. Folkersen, A. Goel, E. Grundberg, A. S. Havulinna, W. K. Ho, J. C. Hopewell, N. Eriksson, M. E. Kleber, K. Kristiansson, P. Lundmark, L. P. Lyytikainen, S. Rafelt, D. Shungin, R. J. Strawbridge, G. Thorleifsson, E. Tikkanen, N. Van Zuydam, B. F. Voight, L. L. Waite, W. Zhang, A. Ziegler, D. Absher, D. Altshuler, A. J. Balmforth, I. Barroso, P. S. Braund, C. Burgdorf, S. Claudi-Boehm, D. Cox, M. Dimitriou, R. Do, A. S. Doney, N. El Mokhtari, P. Eriksson, K. Fischer, P. Fontanillas, A. Franco-Cereceda, B. Gigante, L. Groop, S. Gustafsson, J. Hager, G. Hallmans, B. G. Han, S. E. Hunt, H. M. Kang, T. Illig, T. Kessler, J. W. Knowles, G. Kolovou, J. Kuusisto, C. Langenberg, C. Langford, K. Leander, M. L. Lokki, A. Lundmark, M. I. McCarthy, C. Meisinger, O. Melander, E. Mihailov, S. Maouche, A. D. Morris, M. Muller-Nurasyid, K. Nikus, J. F. Peden, N. W. Rayner, A. Rasheed, S. Rosinger, D. Rubin, M. P. Rumpf, A. Schafer, M. Sivananthan, C. Song, A. F. Stewart, S. T. Tan, G. Thorgeirsson, C. E. van der Schoot, P. J. Wagner, G. A. Wells, P. S. Wild, T. P. Yang, P. Amouyel, D. Arveiler, H. Basart, M. Boehnke, E. Boerwinkle, P. Brambilla, F. Cambien, A. L. Cupples, U. de Faire, A. Dehghan, P. Diemert, S. E. Epstein, A. Evans, M. M. Ferrario, J. Ferrieres, D. Gauguier, A. S. Go, A. H. Goodall, V. Gudnason, S. L. Hazen, H. Holm, C. Iribarren, Y. Jang, M. Kahonen, F. Kee, H. S. Kim, N. Klopp, W. Koenig, W. Kratzer, K. Kuulasmaa, M. Laakso, R. Laaksonen, L. Lind, W. H. Ouwehand, S. Parish, J. E. Park, N. L. Pedersen, A. Peters, T. Quertermous, D. J. Rader, V. Salomaa, E. Schadt, S. H. Shah, J. Sinisalo, K. Stark, K. Stefansson, D. A. Tregouet, J. Virtamo, L. Wallentin, N. Wareham, M. E. Zimmermann, M. S. Nieminen, C. Hengstenberg, M. S. Sandhu, T. Pastinen, A. C. Syvanen, G. K. Hovingh, G. Dedoussis, P. W. Franks, T. Lehtimaki, A. Metspalu, P. A. Zalloua, A. Siegbahn, S. Schreiber, S. Ripatti, S. S. Blankenberg, M. Perola, R. Clarke, B. O. Boehm, C. O'Donnell, M. P. Reilly, W. Marz, R. Collins, S. Kathiresan, A. Hamsten, J. S. Kooner, U. Thorsteinsdottir, J. Danesh, C. N.

Palmer, R. Roberts, H. Watkins, H. Schunkert and N. J. Samani (2013). "Large-scale association analysis identifies new risk loci for coronary artery disease." Nat Genet 45(1): 25-33.
DePristo, M. A., E. Banks, R. Poplin, K. V. Garimella, J. R. Maguire, C. Hartl, A. A. Philippakis, G. del Angel, M. A. Rivas, M. Hanna, A. McKenna, T. J. Fennell, A. M. Kernytsky, A. Y. Sivachenko, K. Cibulskis, S. B. Gabriel, D. Altshuler and M. J. Daly (2011). "A framework for variation discovery and genotyping using next-generation DNA sequencing data." Nat Genet 43(5): 491-498.
Dworkin, I., A. Palsson, K. Birdsall and G. Gibson (2003). "Evidence that Egfr contributes to cryptic genetic variation for photoreceptor determination in natural populations of Drosophila melanogaster." Current Biology 13(21): 1888-1893.
Excoffier, L., G. Laval and S. Schneider (2005). "Arlequin (version 3.0): an integrated software package for population genetics data analysis." Evol Bioinform Online 1: 47-50.
Excoffier, L., P. E. Smouse and J. M. Quattro (1992). "Analysis of molecular variance inferred from metric distances among DNA haplotypes: application to human mitochondrial DNA restriction data." Genetics 131(2): 479-491.
Fang, W. K., L. D. Liao, F. M. Zeng, P. X. Zhang, J. Y. Wu, J. Shen, L. Y. Xu and E. M. Li (2014). "Desmocollin2 affects the adhesive strength and cytoskeletal arrangement in esophageal squamous cell carcinoma cells." Mol Med Rep 10(5): 2358-2364.
Farid, A., M. Makarechian and C. Strobeck (1987). "Inbreeding under a Cyclical Mating System." Theoretical and Applied Genetics 73(4): 506-515.
Flint, J., W. Valdar, S. Shifman and R. Mott (2005). "Strategies for mapping and cloning quantitative trait genes in rodents." Nat Rev Genet 6(4): 271-286.
Foroud, T., P. Bice, P. Castelluccio, R. Bo, L. Miller, A. Ritchotte, L. Lumeng, T. K. Li and L. G. Carr (2000). "Identification of quantitative trait loci influencing alcohol consumption in the high alcohol drinking and low alcohol drinking rat lines." Behav Genet 30(2): 131-140.
Foroud, T., H. J. Edenberg, A. Goate, J. Rice, L. Flury, D. L. Koller, L. J. Bierut, P. M. Conneally, J. I. Nurnberger, K. K. Bucholz, T. K. Li, V. Hesselbrock, R. Crowe, M. Schuckit, B. Porjesz, H. Begleiter and T. Reich (2000). "Alcoholism susceptibility loci: confirmation studies in a replicate sample and further mapping." Alcohol Clin Exp Res 24(7): 933-945.
Garrod, D. and M. Chidgey (2008). "Desmosome structure, composition and function." Biochim Biophys Acta 1778(3): 572-587.
Gibbs, R. A., G. M. Weinstock, M. L. Metzker, D. M. Muzny, E. J. Sodergren, S. Scherer, G. Scott, D. Steffen, K. C. Worley, P. E. Burch, G. Okwuonu, S. Hines, L. Lewis, C. DeRamo, O. Delgado, S. Dugan-Rocha, G. Miner, M. Morgan, A. Hawes, R. Gill, Celera, R. A. Holt, M. D. Adams, P. G. Amanatides, H. Baden-Tillson, M. Barnstead, S. Chin, C. A. Evans, S. Ferriera, C. Fosler, A. Glodek, Z. Gu, D. Jennings, C. L. Kraft, T. Nguyen, C. M. Pfannkoch, C. Sitter, G. G. Sutton, J. C. Venter, T. Woodage, D. Smith, H. M. Lee, E. Gustafson, P. Cahill, A. Kana, L. Doucette-Stamm, K. Weinstock, K. Fechtel, R. B. Weiss, D. M. Dunn, E. D. Green, R. W. Blakesley, G. G. Bouffard, P. J. De Jong, K. Osoegawa, B. Zhu, M. Marra, J. Schein, I. Bosdet, C. Fjell, S. Jones, M. Krzywinski, C. Mathewson, A. Siddiqui, N. Wye, J. McPherson, S. Zhao, C. M. Fraser, J. Shetty, S. Shatsman, K. Geer, Y. Chen, S. Abramzon, W. C. Nierman, P. H. Havlak, R. Chen, K. J. Durbin, A. Egan, Y. Ren, X. Z. Song, B. Li, Y. Liu, X. Qin, S. Cawley, K. C. Worley, A. J. Cooney, L. M. D'Souza, K. Martin, J. Q. Wu, M. L. Gonzalez-Garay, A. R. Jackson, K. J. Kalafus, M. P. McLeod, A. Milosavljevic, D. Virk, A. Volkov, D. A. Wheeler, Z. Zhang, J. A. Bailey, E. E. Eichler, E. Tuzun, E. Birney, E. Mongin, A. Ureta-Vidal, C. Woodwark, E. Zdobnov, P. Bork, M. Suyama, D. Torrents, M. Alexandersson, B. J. Trask, J. M. Young, H. Huang, H. Wang, H. Xing, S. Daniels, D. Gietzen, J. Schmidt, K. Stevens, U. Vitt, J. Wingrove, F. Camara, M. Mar Alba, J. F. Abril, R. Guigo, A. Smit, I. Dubchak, E. M. Rubin, O. Couronne, A. Poliakov, N. Hubner, D. Ganten, C. Goesele, O. Hummel, T. Kreitler, Y. A. Lee, J. Monti, H. Schulz, H. Zimdahl, H. Himmelbauer, H. Lehrach, H. J. Jacob, S. Bromberg, J. Gullings-Handley, M. I. Jensen-Seaman, A. E. Kwitek, J. Lazar, D. Pasko, P. J. Tonellato,

S. Twigger, C. P. Ponting, J. M. Duarte, S. Rice, L. Goodstadt, S. A. Beatson, R. D. Emes, E. E. Winter, C. Webber, P. Brandt, G. Nyakatura, M. Adetobi, F. Chiaromonte, L. Elnitski, P. Eswara, R. C. Hardison, M. Hou, D. Kolbe, K. Makova, W. Miller, A. Nekrutenko, C. Riemer, S. Schwartz, J. Taylor, S. Yang, Y. Zhang, K. Lindpaintner, T. D. Andrews, M. Caccamo, M. Clamp, L. Clarke, V. Curwen, R. Durbin, E. Eyras, S. M. Searle, G. M. Cooper, S. Batzoglou, M. Brudno, A. Sidow, E. A. Stone, J. C. Venter, B. A. Payseur, G. Bourque, C. Lopez-Otin, X. S. Puente, K. Chakrabarti, S. Chatterji, C. Dewey, L. Pachter, N. Bray, V. B. Yap, A. Caspi, G. Tesler, P. A. Pevzner, D. Haussler, K. M. Roskin, R. Baertsch, H. Clawson, T. S. Furey, A. S. Hinrichs, D. Karolchik, W. J. Kent, K. R. Rosenbloom, H. Trumbower, M. Weirauch, D. N. Cooper, P. D. Stenson, B. Ma, M. Brent, M. Arumugam, D. Shteynberg, R. R. Copley, M. S. Taylor, H. Riethman, U. Mudunuri, J. Peterson, M. Guyer, A. Felsenfeld, S. Old, S. Mockrin, F. Collins and C. Rat Genome Sequencing Project (2004). "Genome sequence of the Brown Norway rat yields insights into mammalian evolution." Nature 428(6982): 493-521.

Gierman, H. J., K. Fortney, J. C. Roach, N. S. Coles, H. Li, G. Glusman, G. J. Markov, J. D. Smith, L. Hood, L. S. Coles and S. K. Kim (2014). "Whole-genome sequencing of the world's oldest people." PLoS One 9(11): e112430.

Grossman, S. R., I. Shlyakhter, E. K. Karlsson, E. H. Byrne, S. Morales, G. Frieden, E. Hostetter, E. Angelino, M. Garber, O. Zuk, E. S. Lander, S. F. Schaffner and P. C. Sabeti (2010). "A composite of multiple signals distinguishes causal variants in regions of positive selection." Science 327(5967): 883-886.

Gulati, M., D. K. Pandey, M. F. Arnsdorf, D. S. Lauderdale, R. A. Thisted, R. H. Wicklund, A. J. Al-Hani and H. R. Black (2003). "Exercise capacity and the risk of death in women: the St James Women Take Heart Project." Circulation 108(13): 1554-1559.

Hansen, C. and K. Spuhler (1984). "Development of the National Institutes of Health genetically heterogeneous rat stock." Alcohol Clin Exp Res 8(5): 477-479.

Haus, J. M., J. A. Carrithers, S. W. Trappe and T. A. Trappe (2007). "Collagen, cross-linking, and advanced glycation end products in aging human skeletal muscle." J Appl Physiol (1985) 103(6): 2068-2076.

Hedrich, H. J., M. Adams and International Council for Laboratory Animal Science. (1990). Genetic monitoring of inbred strains of rats : a manual on colony management, basic monitoring techniques, and genetic variants of the laboratory rat. Stuttgart ; New York, Gustav Fischer Verlag.

Howlett, R. A., N. C. Gonzalez, H. E. Wagner, Z. Fu, S. L. Britton, L. G. Koch and P. D. Wagner (2003). "Selected contribution: skeletal muscle capillarity and enzyme activity in rats selectively bred for running endurance." J Appl Physiol (1985) 94(4): 1682-1688.

Howlett, R. A., S. D. Kirkton, N. C. Gonzalez, H. E. Wagner, S. L. Britton, L. G. Koch and P. D. Wagner (2009). "Peripheral oxygen transport and utilization in rats following continued selective breeding for endurance running capacity." J Appl Physiol (1985) 106(6): 1819-1825.

Huang, D. W., B. T. Sherman, Q. Tan, J. Kir, D. Liu, D. Bryant, Y. Guo, R. Stephens, M. W. Baseler, H. C. Lane and R. A. Lempicki (2007). "DAVID Bioinformatics Resources: expanded annotation database and novel algorithms to better extract biology from large gene lists." Nucleic Acids Res 35(Web Server issue): W169-175.

Jacob, H. J. and A. E. Kwitek (2002). "Rat genetics: attaching physiology and pharmacology to the genome." Nat Rev Genet 3(1): 33-42.

James, P. T., N. Rigby and R. Leach (2004). "The obesity epidemic, metabolic syndrome and future prevention strategies." European Journal of Cardiovascular Prevention & Rehabilitation 11(1): 3-8.

Johannesson, M., R. Lopez-Aumatell, P. Stridh, M. Diez, J. Tuncel, G. Blazquez, E. Martinez-Membrives, T. Canete, E. Vicens-Costa, D. Graham, R. R. Copley, P. Hernandez-Pliego, A. D. Beyeen, J. Ockinger, C. Fernandez-Santamaria, P. S. Gulko, M. Brenner, A. Tobena, M. Guitart-Masip, L. Gimenez-Llort, A. Dominiczak, R. Holmdahl, D. Gauguier, T. Olsson, R. Mott, W. Valdar, E. E. Redei, A. Fernandez-Teruel

and J. Flint (2009). "A resource for the simultaneous high-resolution mapping of multiple quantitative trait loci in rats: the NIH heterogeneous stock." Genome Res 19(1): 150-158.
Kang, H. M., J. H. Sul, S. K. Service, N. A. Zaitlen, S. Y. Kong, N. B. Freimer, C. Sabatti and E. Eskin (2010). "Variance component model to account for sample structure in genome-wide association studies." Nat Genet 42(4): 348-354.
Kaprio, J., M. Koskenvuo and S. Sarna (1981). "Cigarette smoking, use of alcohol, and leisure-time physical activity among same-sexed adult male twins." Prog Clin Biol Res 69 Pt C: 37-46.
Kivelä, R., M. Silvennoinen, M. Lehti, Rinnankoski-Tuikka, Rita, T. Purhonen, T. Ketola, K. Pullinen, M. Vuento, N. Mutanen, M. A. Sartor, H. Reunanen, L. G. Koch, S. L. Britton and H. Kainulainen (2010). "Gene expression centroids that link with low intrinsic aerobic exercise capacity and complex disease risk." The FASEB Journal 24(11): 4565-4574.
Kivela, R., M. Silvennoinen, M. Lehti, R. Rinnankoski-Tuikka, T. Purhonen, T. Ketola, K. Pullinen, M. Vuento, N. Mutanen, M. A. Sartor, H. Reunanen, L. G. Koch, S. L. Britton and H. Kainulainen (2010). "Gene expression centroids that link with low intrinsic aerobic exercise capacity and complex disease risk." FASEB J 24(11): 4565-4574.
Kljuic, A., H. Bazzi, J. P. Sundberg, A. Martinez-Mir, R. O'Shaughnessy, M. G. Mahoney, M. Levy, X. Montagutelli, W. Ahmad, V. M. Aita, D. Gordon, J. Uitto, D. Whiting, J. Ott, S. Fischer, T. C. Gilliam, C. A. Jahoda, R. J. Morris, A. A. Panteleyev, V. T. Nguyen and A. M. Christiano (2003). "Desmoglein 4 in hair follicle differentiation and epidermal adhesion: evidence from inherited hypotrichosis and acquired pemphigus vulgaris." Cell 113(2): 249-260.
Koch, L. G. and S. L. Britton (2001). "Artificial selection for intrinsic aerobic endurance running capacity in rats." Physiol Genomics 5(1): 45-52.
Koch, L. G., S. L. Britton and U. Wisloff (2012). "A rat model system to study complex disease risks, fitness, aging, and longevity." Trends Cardiovasc Med 22(2): 29-34.
Koch, L. G., O. J. Kemi, N. Qi, S. X. Leng, P. Bijma, L. J. Gilligan, J. E. Wilkinson, H. Wisloff, M. A. Hoydal, N. Rolim, P. M. Abadir, E. M. van Grevenhof, G. L. Smith, C. F. Burant, O. Ellingsen, S. L. Britton and U. Wisloff (2011). "Intrinsic aerobic capacity sets a divide for aging and longevity." Circ Res 109(10): 1162-1172.
Kokkinos, P., J. Myers, J. P. Kokkinos, A. Pittaras, P. Narayan, A. Manolis, P. Karasik, M. Greenberg, V. Papademetriou and S. Singh (2008). "Exercise capacity and mortality in black and white men." Circulation 117(5): 614-622.
Lakka, T. A., J. M. Venalainen, R. Rauramaa, R. Salonen, J. Tuomilehto and J. T. Salonen (1994). "Relation of leisure-time physical activity and cardiorespiratory fitness to the risk of acute myocardial infarction." N Engl J Med 330(22): 1549-1554.
Leeper, N. J., J. Myers, M. Zhou, K. T. Nead, A. Syed, Y. Kojima, R. D. Caceres and J. P. Cooke (2012). "Exercise capacity is the strongest predictor of mortality in patients with peripheral arterial disease." J Vasc Surg.
Lessard, S. J., D. A. Rivas, Z. P. Chen, B. J. van Denderen, M. J. Watt, L. G. Koch, S. L. Britton, B. E. Kemp and J. A. Hawley (2009). "Impaired skeletal muscle beta-adrenergic activation and lipolysis are associated with whole-body insulin resistance in rats bred for low intrinsic exercise capacity." Endocrinology 150(11): 4883-4891.
Li, H. and R. Durbin (2009). "Fast and accurate short read alignment with Burrows-Wheeler transform." Bioinformatics 25(14): 1754-1760.
Lujan, H. L., S. L. Britton, L. G. Koch and S. E. DiCarlo (2006). "Reduced susceptibility to ventricular tachyarrhythmias in rats selectively bred for high aerobic capacity." Am J Physiol Heart Circ Physiol 291(6): H2933-2941.

McKenna, A., M. Hanna, E. Banks, A. Sivachenko, K. Cibulskis, A. Kernytsky, K. Garimella, D. Altshuler, S. Gabriel, M. Daly and M. A. DePristo (2010). "The Genome Analysis Toolkit: a MapReduce framework for analyzing next-generation DNA sequencing data." Genome Res 20(9): 1297-1303.
McLaren, W., B. Pritchard, D. Rios, Y. Chen, P. Flicek and F. Cunningham (2010). "Deriving the consequences of genomic variants with the Ensembl API and SNP Effect Predictor." Bioinformatics 26(16): 2069-2070.
Merico, D., R. Isserlin, O. Stueker, A. Emili and G. D. Bader (2010). "Enrichment map: a network-based method for gene-set enrichment visualization and interpretation." PLoS One 5(11): e13984.
Morris, A. P., B. F. Voight, T. M. Teslovich, T. Ferreira, A. V. Segre, V. Steinthorsdottir, R. J. Strawbridge, H. Khan, H. Grallert, A. Mahajan, I. Prokopenko, H. M. Kang, C. Dina, T. Esko, R. M. Fraser, S. Kanoni, A. Kumar, V. Lagou, C. Langenberg, J. Luan, C. M. Lindgren, M. Muller-Nurasyid, S. Pechlivanis, N. W. Rayner, L. J. Scott, S. Wiltshire, L. Yengo, L. Kinnunen, E. J. Rossin, S. Raychaudhuri, A. D. Johnson, A. S. Dimas, R. J. Loos, S. Vedantam, H. Chen, J. C. Florez, C. Fox, C. T. Liu, D. Rybin, D. J. Couper, W. H. Kao, M. Li, M. C. Cornelis, P. Kraft, Q. Sun, R. M. van Dam, H. M. Stringham, P. S. Chines, K. Fischer, P. Fontanillas, O. L. Holmen, S. E. Hunt, A. U. Jackson, A. Kong, R. Lawrence, J. Meyer, J. R. Perry, C. G. Platou, S. Potter, E. Rehnberg, N. Robertson, S. Sivapalaratnam, A. Stancakova, K. Stirrups, G. Thorleifsson, E. Tikkanen, A. R. Wood, P. Almgren, M. Atalay, R. Benediktsson, L. L. Bonnycastle, N. Burtt, J. Carey, G. Charpentier, A. T. Crenshaw, A. S. Doney, M. Dorkhan, S. Edkins, V. Emilsson, E. Eury, T. Forsen, K. Gertow, B. Gigante, G. B. Grant, C. J. Groves, C. Guiducci, C. Herder, A. B. Hreidarsson, J. Hui, A. James, A. Jonsson, W. Rathmann, N. Klopp, J. Kravic, K. Krjutskov, C. Langford, K. Leander, E. Lindholm, S. Lobbens, S. Mannisto, G. Mirza, T. W. Muhleisen, B. Musk, M. Parkin, L. Rallidis, J. Saramies, B. Sennblad, S. Shah, G. Sigurethsson, A. Silveira, G. Steinbach, B. Thorand, J. Trakalo, F. Veglia, R. Wennauer, W. Winckler, D. Zabaneh, H. Campbell, C. van Duijn, A. G. Uitterlinden, A. Hofman, E. Sijbrands, G. R. Abecasis, K. R. Owen, E. Zeggini, M. D. Trip, N. G. Forouhi, A. C. Syvanen, J. G. Eriksson, L. Peltonen, M. M. Nothen, B. Balkau, C. N. Palmer, V. Lyssenko, T. Tuomi, B. Isomaa, D. J. Hunter, L. Qi, A. R. Shuldiner, M. Roden, I. Barroso, T. Wilsgaard, J. Beilby, K. Hovingh, J. F. Price, J. F. Wilson, R. Rauramaa, T. A. Lakka, L. Lind, G. Dedoussis, I. Njolstad, N. L. Pedersen, K. T. Khaw, N. J. Wareham, S. M. Keinanen-Kiukaanniemi, T. E. Saaristo, E. Korpi-Hyovalti, J. Saltevo, M. Laakso, J. Kuusisto, A. Metspalu, F. S. Collins, K. L. Mohlke, R. N. Bergman, J. Tuomilehto, B. O. Boehm, C. Gieger, K. Hveem, S. Cauchi, P. Froguel, D. Baldassarre, E. Tremoli, S. E. Humphries, D. Saleheen, J. Danesh, E. Ingelsson, S. Ripatti, V. Salomaa, R. Erbel, K. H. Jockel, S. Moebus, A. Peters, T. Illig, U. de Faire, A. Hamsten, A. D. Morris, P. J. Donnelly, T. M. Frayling, A. T. Hattersley, E. Boerwinkle, O. Melander, S. Kathiresan, P. M. Nilsson, P. Deloukas, U. Thorsteinsdottir, L. C. Groop, K. Stefansson, F. Hu, J. S. Pankow, J. Dupuis, J. B. Meigs, D. Altshuler, M. Boehnke and M. I. McCarthy (2012). "Large-scale association analysis provides insights into the genetic architecture and pathophysiology of type 2 diabetes." Nat Genet 44(9): 981-990.
Mott, R., C. J. Talbot, M. G. Turri, A. C. Collins and J. Flint (2000). "A method for fine mapping quantitative trait loci in outbred animal stocks." Proc Natl Acad Sci U S A 97(23): 12649-12654.
Muncey, A. R., A. R. Saulles, L. G. Koch, S. L. Britton, H. A. Baghdoyan and R. Lydic (2010). "Disrupted sleep and delayed recovery from chronic peripheral neuropathy are distinct phenotypes in a rat model of metabolic syndrome." Anesthesiology 113(5): 1176-1185.
Myers, J., M. Prakash, V. Froelicher, D. Do, S. Partington and J. E. Atwood (2002). "Exercise capacity and mortality among men referred for exercise testing." N Engl J Med 346(11): 793-801.
Nielsen, R., S. Williamson, Y. Kim, M. J. Hubisz, A. G. Clark and C. Bustamante (2005). "Genomic scans for selective sweeps using SNP data." Genome Res 15(11): 1566-1575.
Noland, R. C., J. P. Thyfault, S. T. Henes, B. R. Whitfield, T. L. Woodlief, J. R. Evans, J. A. Lust, S. L. Britton, L. G. Koch, R. W. Dudek, G. L. Dohm, R. N. Cortright and R. M. Lust (2007). "Artificial selection

for high-capacity endurance running is protective against high-fat diet-induced insulin resistance." Am J Physiol Endocrinol Metab 293(1): E31-41.
Nomura, T. and K. Yonezawa (1996). "A comparison of four systems of group mating for avoiding inbreeding." Genetics Selection Evolution 28(2): 141-159.
Novak, C. M., C. Escande, P. R. Burghardt, M. Zhang, M. T. Barbosa, E. N. Chini, S. L. Britton, L. G. Koch, H. Akil and J. A. Levine (2010). "Spontaneous activity, economy of activity, and resistance to diet-induced obesity in rats bred for high intrinsic aerobic capacity." Horm Behav 58(3): 355-367.
Oesper, L., D. Merico, R. Isserlin and G. D. Bader (2011). "WordCloud: a Cytoscape plugin to create a visual semantic summary of networks." Source Code Biol Med 6: 7.
Oshiro, M. M., C. J. Kim, R. J. Wozniak, D. J. Junk, J. L. Munoz-Rodriguez, J. A. Burr, M. Fitzgerald, S. C. Pawar, A. E. Cress, F. E. Domann and B. W. Futscher (2005). "Epigenetic silencing of DSC3 is a common event in human breast cancer." Breast Cancer Res 7(5): R669-680.
Overmyer, K. A., C. R. Evans, N. R. Qi, C. E. Minogue, J. J. Carson, C. J. Chermside-Scabbo, L. G. Koch, S. L. Britton, D. J. Pagliarini, J. J. Coon and C. F. Burant (2015). "Maximal oxidative capacity during exercise is associated with skeletal muscle fuel selection and dynamic changes in mitochondrial protein acetylation." Cell Metab 21(3): 468-478.
Pedersen, B. K. and B. Saltin (2006). "Evidence for prescribing exercise as therapy in chronic disease." Scand J Med Sci Sports 16 Suppl 1: 3-63.
Peltonen, L. and V. A. McKusick (2001). "Genomics and medicine. Dissecting human disease in the postgenomic era." Science 291(5507): 1224-1229.
Perusse, L., A. Tremblay, C. Leblanc and C. Bouchard (1989). "Genetic and environmental influences on level of habitual physical activity and exercise participation." Am J Epidemiol 129(5): 1012-1022.
Prud'homme, D., C. Bouchard, C. Leblanc, F. Landry and E. Fontaine (1984). "Sensitivity of maximal aerobic power to training is genotype-dependent." Med Sci Sports Exerc 16(5): 489-493.
Purcell, S., B. Neale, K. Todd-Brown, L. Thomas, M. A. R. Ferreira, D. Bender, J. Maller, P. Sklar, P. I. W. de Bakker, M. J. Daly and P. C. Sham (2007). "PLINK: A tool set for whole-genome association and population-based linkage analyses." American Journal of Human Genetics 81(3): 559-575.
Queitsch, C., T. A. Sangster and S. Lindquist (2002). "Hsp90 as a capacitor of phenotypic variation." Nature 417(6889): 618-624.
R Development Core Team (2010). R: A language and environment for statistical computing. Vienna, Austria, R Foundation for Statistical Computing.
Randhawa, I. A., M. S. Khatkar, P. C. Thomson and H. W. Raadsma (2014). "Composite selection signals can localize the trait specific genomic regions in multi-breed populations of cattle and sheep." BMC Genet 15: 34.
Ren, Y. Y., K. A. Overmyer, N. R. Qi, M. K. Treutelaar, L. Heckenkamp, M. Kalahar, L. G. Koch, S. L. Britton, C. F. Burant and J. Z. Li (2013). "Genetic analysis of a rat model of aerobic capacity and metabolic fitness." PLoS One 8(10): e77588.
Resnik, N., K. Sepcic, A. Plemenitas, R. Windoffer, R. Leube and P. Veranic (2011). "Desmosome assembly and cell-cell adhesion are membrane raft-dependent processes." J Biol Chem 286(2): 1499-1507.
Sandvik, L., J. Erikssen, E. Thaulow, G. Erikssen, R. Mundal and K. Rodahl (1993). "Physical fitness as a predictor of mortality among healthy, middle-aged Norwegian men." N Engl J Med 328(8): 533-537.
Sartor, M. A., G. D. Leikauf and M. Medvedovic (2009). "LRpath: a logistic regression approach for identifying enriched biological groups in gene expression data." Bioinformatics 25(2): 211-217.
Simoneau, J. A., G. Lortie, M. R. Boulay, M. Marcotte, M. C. Thibault and C. Bouchard (1986). "Inheritance of human skeletal muscle and anaerobic capacity adaptation to high-intensity intermittent training." Int J Sports Med 7(3): 167-171.

Solberg, L. C., W. Valdar, D. Gauguier, G. Nunez, A. Taylor, S. Burnett, C. Arboledas-Hita, P. Hernandez-Pliego, S. Davidson, P. Burns, S. Bhattacharya, T. Hough, D. Higgs, P. Klenerman, W. O. Cookson, Y. Zhang, R. M. Deacon, J. N. Rawlins, R. Mott and J. Flint (2006). "A protocol for high-throughput phenotyping, suitable for quantitative trait analysis in mice." Mamm Genome 17(2): 129-146.

Sui, X., M. J. LaMonte, J. N. Laditka, J. W. Hardin, N. Chase, S. P. Hooker and S. N. Blair (2007). "Cardiorespiratory fitness and adiposity as mortality predictors in older adults." JAMA 298(21): 2507-2516.

Teslovich, T. M., K. Musunuru, A. V. Smith, A. C. Edmondson, I. M. Stylianou, M. Koseki, J. P. Pirruccello, S. Ripatti, D. I. Chasman, C. J. Willer, C. T. Johansen, S. W. Fouchier, A. Isaacs, G. M. Peloso, M. Barbalic, S. L. Ricketts, J. C. Bis, Y. S. Aulchenko, G. Thorleifsson, M. F. Feitosa, J. Chambers, M. Orho-Melander, O. Melander, T. Johnson, X. Li, X. Guo, M. Li, Y. Shin Cho, M. Jin Go, Y. Jin Kim, J. Y. Lee, T. Park, K. Kim, X. Sim, R. Twee-Hee Ong, D. C. Croteau-Chonka, L. A. Lange, J. D. Smith, K. Song, J. Hua Zhao, X. Yuan, J. Luan, C. Lamina, A. Ziegler, W. Zhang, R. Y. Zee, A. F. Wright, J. C. Witteman, J. F. Wilson, G. Willemsen, H. E. Wichmann, J. B. Whitfield, D. M. Waterworth, N. J. Wareham, G. Waeber, P. Vollenweider, B. F. Voight, V. Vitart, A. G. Uitterlinden, M. Uda, J. Tuomilehto, J. R. Thompson, T. Tanaka, I. Surakka, H. M. Stringham, T. D. Spector, N. Soranzo, J. H. Smit, J. Sinisalo, K. Silander, E. J. Sijbrands, A. Scuteri, J. Scott, D. Schlessinger, S. Sanna, V. Salomaa, J. Saharinen, C. Sabatti, A. Ruokonen, I. Rudan, L. M. Rose, R. Roberts, M. Rieder, B. M. Psaty, P. P. Pramstaller, I. Pichler, M. Perola, B. W. Penninx, N. L. Pedersen, C. Pattaro, A. N. Parker, G. Pare, B. A. Oostra, C. J. O'Donnell, M. S. Nieminen, D. A. Nickerson, G. W. Montgomery, T. Meitinger, R. McPherson, M. I. McCarthy, W. McArdle, D. Masson, N. G. Martin, F. Marroni, M. Mangino, P. K. Magnusson, G. Lucas, R. Luben, R. J. Loos, M. L. Lokki, G. Lettre, C. Langenberg, L. J. Launer, E. G. Lakatta, R. Laaksonen, K. O. Kyvik, F. Kronenberg, I. R. Konig, K. T. Khaw, J. Kaprio, L. M. Kaplan, A. Johansson, M. R. Jarvelin, A. C. Janssens, E. Ingelsson, W. Igl, G. Kees Hovingh, J. J. Hottenga, A. Hofman, A. A. Hicks, C. Hengstenberg, I. M. Heid, C. Hayward, A. S. Havulinna, N. D. Hastie, T. B. Harris, T. Haritunians, A. S. Hall, U. Gyllensten, C. Guiducci, L. C. Groop, E. Gonzalez, C. Gieger, N. B. Freimer, L. Ferrucci, J. Erdmann, P. Elliott, K. G. Ejebe, A. Doring, A. F. Dominiczak, S. Demissie, P. Deloukas, E. J. de Geus, U. de Faire, G. Crawford, F. S. Collins, Y. D. Chen, M. J. Caulfield, H. Campbell, N. P. Burtt, L. L. Bonnycastle, D. I. Boomsma, S. M. Boekholdt, R. N. Bergman, I. Barroso, S. Bandinelli, C. M. Ballantyne, T. L. Assimes, T. Quertermous, D. Altshuler, M. Seielstad, T. Y. Wong, E. S. Tai, A. B. Feranil, C. W. Kuzawa, L. S. Adair, H. A. Taylor, Jr., I. B. Borecki, S. B. Gabriel, J. G. Wilson, H. Holm, U. Thorsteinsdottir, V. Gudnason, R. M. Krauss, K. L. Mohlke, J. M. Ordovas, P. B. Munroe, J. S. Kooner, A. R. Tall, R. A. Hegele, J. J. Kastelein, E. E. Schadt, J. I. Rotter, E. Boerwinkle, D. P. Strachan, V. Mooser, K. Stefansson, M. P. Reilly, N. J. Samani, H. Schunkert, L. A. Cupples, M. S. Sandhu, P. M. Ridker, D. J. Rader, C. M. van Duijn, L. Peltonen, G. R. Abecasis, M. Boehnke and S. Kathiresan (2010). "Biological, clinical and population relevance of 95 loci for blood lipids." Nature 466(7307): 707-713.

Thyfault, J. P., R. S. Rector, G. M. Uptergrove, S. J. Borengasser, E. M. Morris, Y. Wei, M. J. Laye, C. F. Burant, N. R. Qi, S. E. Ridenhour, L. G. Koch, S. L. Britton and J. A. Ibdah (2009). "Rats selectively bred for low aerobic capacity have reduced hepatic mitochondrial oxidative capacity and susceptibility to hepatic steatosis and injury." J Physiol 587(Pt 8): 1805-1816.

Utsunomiya, Y. T., A. M. Perez O'Brien, T. S. Sonstegard, C. P. Van Tassell, A. S. do Carmo, G. Meszaros, J. Solkner and J. F. Garcia (2013). "Detecting loci under recent positive selection in dairy and beef cattle by combining different genome-wide scan methods." PLoS One 8(5): e64280.

Valdar, W., J. Flint and R. Mott (2006). "Simulating the collaborative cross: power of quantitative trait loci detection and mapping resolution in large sets of recombinant inbred strains of mice." Genetics 172(3): 1783-1797.

Valdar, W., L. C. Solberg, D. Gauguier, S. Burnett, P. Klenerman, W. O. Cookson, M. S. Taylor, J. N. Rawlins, R. Mott and J. Flint (2006). "Genome-wide genetic association of complex traits in heterogeneous stock mice." Nat Genet 38(8): 879-887.

Valdar, W. S., J. Flint and R. Mott (2003). "QTL fine-mapping with recombinant-inbred heterogeneous stocks and in vitro heterogeneous stocks." Mamm Genome 14(12): 830-838.

Voight, B. F., L. J. Scott, V. Steinthorsdottir, A. P. Morris, C. Dina, R. P. Welch, E. Zeggini, C. Huth, Y. S. Aulchenko, G. Thorleifsson, L. J. McCulloch, T. Ferreira, H. Grallert, N. Amin, G. Wu, C. J. Willer, S. Raychaudhuri, S. A. McCarroll, C. Langenberg, O. M. Hofmann, J. Dupuis, L. Qi, A. V. Segre, M. van Hoek, P. Navarro, K. Ardlie, B. Balkau, R. Benediktsson, A. J. Bennett, R. Blagieva, E. Boerwinkle, L. L. Bonnycastle, K. Bengtsson Bostrom, B. Bravenboer, S. Bumpstead, N. P. Burtt, G. Charpentier, P. S. Chines, M. Cornelis, D. J. Couper, G. Crawford, A. S. Doney, K. S. Elliott, A. L. Elliott, M. R. Erdos, C. S. Fox, C. S. Franklin, M. Ganser, C. Gieger, N. Grarup, T. Green, S. Griffin, C. J. Groves, C. Guiducci, S. Hadjadj, N. Hassanali, C. Herder, B. Isomaa, A. U. Jackson, P. R. Johnson, T. Jorgensen, W. H. Kao, N. Klopp, A. Kong, P. Kraft, J. Kuusisto, T. Lauritzen, M. Li, A. Lieverse, C. M. Lindgren, V. Lyssenko, M. Marre, T. Meitinger, K. Midthjell, M. A. Morken, N. Narisu, P. Nilsson, K. R. Owen, F. Payne, J. R. Perry, A. K. Petersen, C. Platou, C. Proenca, I. Prokopenko, W. Rathmann, N. W. Rayner, N. R. Robertson, G. Rocheleau, M. Roden, M. J. Sampson, R. Saxena, B. M. Shields, P. Shrader, G. Sigurdsson, T. Sparso, K. Strassburger, H. M. Stringham, Q. Sun, A. J. Swift, B. Thorand, J. Tichet, T. Tuomi, R. M. van Dam, T. W. van Haeften, T. van Herpt, J. V. van Vliet-Ostaptchouk, G. B. Walters, M. N. Weedon, C. Wijmenga, J. Witteman, R. N. Bergman, S. Cauchi, F. S. Collins, A. L. Gloyn, U. Gyllensten, T. Hansen, W. A. Hide, G. A. Hitman, A. Hofman, D. J. Hunter, K. Hveem, M. Laakso, K. L. Mohlke, A. D. Morris, C. N. Palmer, P. P. Pramstaller, I. Rudan, E. Sijbrands, L. D. Stein, J. Tuomilehto, A. Uitterlinden, M. Walker, N. J. Wareham, R. M. Watanabe, G. R. Abecasis, B. O. Boehm, H. Campbell, M. J. Daly, A. T. Hattersley, F. B. Hu, J. B. Meigs, J. S. Pankow, O. Pedersen, H. E. Wichmann, I. Barroso, J. C. Florez, T. M. Frayling, L. Groop, R. Sladek, U. Thorsteinsdottir, J. F. Wilson, T. Illig, P. Froguel, C. M. van Duijn, K. Stefansson, D. Altshuler, M. Boehnke and M. I. McCarthy (2010). "Twelve type 2 diabetes susceptibility loci identified through large-scale association analysis." Nat Genet 42(7): 579-589.

Wahlberg, P., O. Carlborg, M. Foglio, X. Tordoir, A. C. Syvanen, M. Lathrop, I. G. Gut, P. B. Siegel and L. Andersson (2009). "Genetic analysis of an F(2) intercross between two chicken lines divergently selected for body-weight." BMC Genomics 10: 248.

Whittock, N. V. and C. Bower (2003). "Genetic evidence for a novel human desmosomal cadherin, desmoglein 4." J Invest Dermatol 120(4): 523-530.

Wikgren, J., G. G. Mertikas, P. Raussi, R. Tirkkonen, L. Ayravainen, M. Pelto-Huikko, L. G. Koch, S. L. Britton and H. Kainulainen (2012). "Selective breeding for endurance running capacity affects cognitive but not motor learning in rats." Physiol Behav 106(2): 95-100.

Windig, J. J. and L. Kaal (2008). "An effective rotational mating scheme for inbreeding reduction in captive populations illustrated by the rare sheep breed Kempisch Heideschaap." Animal 2(12): 1733-1741.

Wisloff, U., S. M. Najjar, O. Ellingsen, P. M. Haram, S. Swoap, Q. Al-Share, M. Fernstrom, K. Rezaei, S. J. Lee, L. G. Koch and S. L. Britton (2005). "Cardiovascular risk factors emerge after artificial selection for low aerobic capacity." Science 307(5708): 418-420.

Wright, S. (1965). "The Interpretation of Population-Structure by F-Statistics with Special Regard to Systems of Mating." Evolution 19(3): 395-420.

Wright, S. (1968). Evolution and the genetics of populations; a treatise. Chicago,, University of Chicago Press.